



University of Liège - Faculty of Applied Sciences

The first-passage time as an analysis tool for the reliability of stochastic oscillators

Thesis submitted in partial fulfillment of the requirements
for the degree of
Doctor of Philosophy in Applied Sciences by

Hélène Vanvinckenroye

June 2018

Members of the Doctoral Jury

Prof. Jean-Claude GOLINVAL (President)
Structural Dynamics, University of Liège

Prof. Vincent DENOËL (Advisor)
Structural Engineering, University of Liège

Dr. Ir. Thomas ANDRIANNE
Wind Tunnel Laboratory, University of Liège

Prof. Vincent DE VILLE DE GOYET
Bureau d'Etudes Greisch, Liège
Structural Engineering, University of Liège

Prof. Ioannis KOUGIOUMTZOGLOU
Nonlinear stochastic dynamics,
Columbia University in the city of New York

Dr. Ir. Jiří NÁPRSTEK
The Czech Academy of Sciences,
Department of Dynamics, Prague

Abstract

Because some systems spend most of their time in transient regimes, it is important to focus on a relevant representation of their transient response. The question “How much time ?” is addressed in this work through the *first-passage* problem. The first-passage time is the time required for a system, leaving a given initial configuration, to reach a certain state for the first time. When the excitation is a stochastic process, the first-passage time is a random variable and the determination of its statistics is an attractive approach for assessing the reliability of a transient system exposed to uncertainty. Although the number of engineering results seen from this angle is very limited today, the first-passage problem has been widely studied in physics and mathematics and presents a high potential for a wide range of engineering problems.

Since many physical problems can be described by a stochastic Mathieu equation, this work provides a frame for the first-passage time of this category of oscillators as an analysis tool in engineering applications.

The first step is the determination of a closed-form expression for the average first-passage time of the linear, undamped Mathieu oscillator under parametric and external white noise excitations. Given by the solution of the Pontryagin equation, the approximate expression is obtained using an asymptotic expansion. The solution highlights the groups of parameters influencing the first-passage time which is presented in a universal map. Three regimes –the incubation, additive and multiplicative regimes– are identified in the map with their typical features.

Next, the complexity of the model is progressively increased, considering for example a damped oscillator or the variance of the first-passage time. The features of the three regimes are re-identified and a new map is determined.

An attempt at fitting our simple model to the complex dynamics of a tower crane oscillating in a turbulent wind flow has proven very satisfactory. This indicates that the three elementary regimes (incubation, additive and multiplicative) are also present in other problems than those circumscribed by the hypotheses of the Mathieu oscillator.

The first-passage maps are calculated using an appropriate algorithm and it is shown that there exists an equivalent linear Mathieu oscillator so that the theoretical model may be used to understand and predict the tower crane behavior. The identification of this map with the analytical model developed before, as well as the observation of the three regimes, serves as a demonstration of the applicability of the first-passage time as an identification tool or a reliability assessment tool in engineering applications.

Finally, a Galerkin scheme is developed to provide a robust and versatile method of resolution of the Backward-Kolmogorov equation governing the first-passage time complete distribution of nonlinear systems under evolutionary excitation.

Acknowledgments

Pour commencer, je souhaite exprimer toute ma gratitude envers Vincent Denoël, mon promoteur. Vincent, merci pour tes qualités tant humaines que scientifiques. Ton enthousiasme et ton énergie ont grandement contribué à la réalisation de cette thèse. Merci également pour la très grande qualité de ton expertise scientifique.

I would also like to express my gratitude to the members of the committee for accepting the revision of my thesis and for their participation to the defense. I wish you an enjoyable reading of this manuscript. Thomas, thank you for your help in the experimental part of my work. Thanks for our nice talks, scientific or not. Ioannis, I am very grateful for the opportunity you gave me to share a few months of my research with you. This experience has been inspiring, both from a scientific and a personal point of view.

Puisque la soumission de ce manuscrit est une étape clé de la fin de mon doctorat, je voudrais remercier les personnes grâce à qui j'étais heureuse de venir travailler chaque matin. Christophe, Nicolas, Renaud, François, et tant d'autres, merci pour l'agréable environnement de travail auquel vous avez contribué.

J'adresse également mes remerciements à mes parents, frères et sœurs, qui me soutiendront toujours même s'ils ne me comprendront peut-être jamais. Votre amour inconditionnel fait chaud au cœur !

Finalement, je voudrais remercier David et Maurine. Cette thèse existe en partie grâce à vous. Pour tout, merci.

This research was performed thanks to the support of the National Fund for Scientific Research of Belgium (FRIA, F.R.S.-FNRS).

Contents

Abstract	i
Acknowledgements	iii
I Introduction	1
I.1 Motivation	2
I.2 The Mathieu oscillator	3
I.3 Non-stationary dynamics	4
I.4 Outline of this work	7
I.5 Personal contributions	7
I.6 Theoretical background	9
II Analytical determination of the first-passage time in a reference case	15
II.1 Introduction	16
II.2 Pontryagin equation	18
II.3 Analysis and discussion	22
II.4 Conclusion	28
III Analytical determination of the first-passage time in more general conditions	29
III.1 Second order solution of the average first-passage time	30
III.1.1 Pontryagin equation	31
III.1.2 Analysis and discussion	33
III.2 Damped oscillator	34
III.2.1 Pontryagin equation	35
III.2.2 Analysis and discussion	35
III.3 Variance of the first-passage time	40
III.3.1 Pontryagin equation	40
III.3.2 Analysis and discussion	42
III.4 Conclusion	48

IV	Some applications of the first-passage time	51
IV.1	Introduction	52
IV.2	Application 1: The pendulum under horizontal and vertical excitations of its support	52
IV.3	Application 2: Cable vibrations under acceleration of one anchorage	55
IV.4	Algorithmic establishment of the first-passage time map from experimental data	60
IV.4.1	Introduction	60
IV.4.2	The algorithm	60
IV.5	Application 3: A tower crane under gusty winds	62
IV.5.1	A mathematical model of a tower crane	62
IV.5.2	Experimental investigations	65
IV.5.3	Results	68
IV.5.4	Discussion	69
IV.6	Application 4: A pre-stressed steel strip	72
IV.7	Conclusion	77
V	A numerical approach for the first-passage time of more complex systems:	
	The Galerkin scheme	79
V.1	Introduction	80
V.2	Markovian modeling of the response energy	80
V.3	Amplitude-based energy envelope	83
V.3.1	Backward-Kolmogorov equation	83
V.3.2	Galerkin projection scheme	84
V.3.3	Special case: Undamped oscillator	87
V.3.4	The first-passage time distribution and its statistical moments	89
V.3.5	Numerical examples	90
V.4	Potential energy envelope	95
V.4.1	Backward-Kolmogorov equation and Galerkin scheme for a Duffing nonlinear oscillator	95
V.4.2	Numerical examples	96
V.5	Conclusion	97
VI	Conclusion	99
VI.1	Contributions of this work	100
VI.2	Limitations of the study and perspectives	102
	Bibliography	104
A	List of Publications	117

CONTENTS

vii

B	Second order and boundary layer solutions	119
C	Damped oscillator	123
D	Pseudo-code for the computation of the average first-passage times map	125
E	Comparison Galerkin vs analytical	129

Chapter I

Introduction

-
- I.1 Motivation
 - I.2 The Mathieu oscillator
 - I.3 Non-stationary dynamics
 - I.4 Outline of this work
 - I.5 Personal contributions
 - I.6 Theoretical background
-

I.1 Motivation

The first motivation of this thesis was the study of tower cranes that are left free to rotate in gusty winds. Depending on the wind conditions and the environment, a tower crane can respond with large oscillations that can lead to dramatic failures. The increasing number of recorded incidents over the past few years [1, 2] might be understood as a need for progress on crane performances and received little interest from the scientific community until now. Out-of-service wind velocities criteria are proposed by [3, 4] while the stochastic response under turbulent wind conditions was the object of experimental testing assessing the risk of autorotation of the crane in a given environment [5, 6, 7, 3], as illustrated in Figure I.1 (a). In current practice, the reliability of a given configuration is typically assessed by measuring the rotation of a reduced scale model of the crane in its urban environment in a wind tunnel under different wind conditions and for a certain duration of time. This method requires repetition of the test for every new configuration and does not contribute to the understanding of the problem since no general safety rules are established. An analytical modeling of the stochastically excited system is an evident step to a deeper apprehension of the phenomenon and the development of guiding rules for the placement of a tower crane on a working site.

As a heritage of deterministic dynamics, systems are usually studied with the scope to determine the stability zones, the amplitude of the limit cycle oscillations [8] or steady state solutions [9, 10, 11, 12]. However, these objectives lose interest in undamped or even very slightly damped systems like tower cranes, since a steady-state configuration takes too long to develop. Moreover, it is possible to demonstrate [13] that any large value of the position or velocity, as large as desired (!), is encountered with probability **one** in the case of an undamped system. This mathematical fact therefore suggests to reconsider the practical questions related to the possible large rotations of a crane from a different standpoint since any large amplitude could be reached by waiting sufficiently long enough (in case dissipation is negligible).

This was the motivation to study a more general problem known as the *first-passage* problem that addresses the important question

How much time?

The first-passage time is the time required for an excited system, leaving a known initial condition, to reach a certain state for the first time. In deterministic dynamics, this concept is central in the description of transient regimes, for instance to estimate the time required for a deterministic system to reach its steady-state, under a stationary excitation [14]. When the excitation is a stochastic process, the first-passage time is a random variable and can be characterized by its probability density function. While this concept has received little interest from the engineering community until now, it has been widely studied in physics

and mathematics. Determining first-passage time statistics is an attractive approach for assessing the reliability of transient systems exposed to uncertainty and presents a high potential for a wide range of engineering applications, and for developing, eventually, robust optimization and design frameworks.

The number of practical or experimental applications where the results are seen from the angle of time is very limited. Some examples of the possible application of first-passage times in engineering are the following ones. First, dispersion of pollutant releases is the object of massive experimental and numerical research [15, 16, 17, 18]. A first-passage approach in the problem of pollutant dispersion would consist in determining the time it takes for a pollutant to reach a given concentration at a given place. Second, a bridge deck flutter instability in turbulent flow [19] is another problem in which first-passage times are of outmost concern since a sufficiently long first-passage time would make a site operation possible. In these applications, the question of first-passage time is central and offers an alternative answer to the risk assessment with a good understanding of the influence of problem parameters of a system/structure's transient response. More examples follow next.

Because a lot of systems (like the tower crane) can be described by a Mathieu equation, and in order to offer a general analysis, this work focuses on the first-passage time of a single-degree-of-freedom Mathieu oscillator.

I.2 The Mathieu oscillator

Using the appropriate non-dimensionalization, the governing equation of the tower crane, as well as a large number of other applications [20], can be cast under the format of the linear Mathieu equation

$$\ddot{x}(t) + 2\xi\dot{x}(t) + [1 + u(t)]x(t) = w(t) \quad (\text{I.2.1})$$

where $x(t)$ is the state variable as a function of time t , ξ is the damping coefficient, $w(t)$ is an external force and $u(t)$ is a parametric excitation since it multiplies the coordinate x . Equation (I.2.1) develops in various forms, from deterministic to stochastic, depending on the non-deterministic nature of the parameters of the problem and of the excitations.

The tower crane is a typical example of a structural element governed by the Mathieu equation. As another example, the deflection of a horizontal cable subjected to a motion of one anchorage is described by a similar Mathieu equation [21]. Beside, interest has been shown for the energy of a pendulum submitted to wave excitations in [22, 23, 24]. Such a system is also governed by the Mathieu equation and finds a direct application in the extraction of energy from waves and heave, as also discussed earlier by [25, 26]. In the same way, capsizing and rolling motions of ships under stochastic wave excitation can also be assimilated

to similar oscillators and are studied by Moshchuk and Troesch in [27, 28]. The pendulum excited by its support and the cable vibrations are presented as numerical examples, while the tower crane is the object of an experimental investigation in Chapter IV.

The Mathieu oscillator has been first studied in its most simple case under a deterministic harmonic and parametric excitation, viz. $u(t) = \lambda \cos(\nu t)$ and $w(t) = 0$ [29, 1, 30], and, in some instances, including nonlinearities [31, 8]. In those works, it is shown that, assuming no damping and depending on the frequency content and magnitude of the excitation, the oscillator describes small or large oscillations or eventually complete rotations (in the nonlinear case). These three regimes are described in [1] and illustrated in Figure I.2. In the amplitude-frequency plane, higher energy lobes are observed for a frequency of the parametric excitation close to the fundamental frequency ν_0 of the pendulum or an irreducible fraction of it, as illustrated in Figure I.1 (b). An experimental analysis of the instability is performed in [32]. Other authors developed analytical solutions of the deterministic problem [33, 34] including the different stable regions thanks to the harmonic balance method, the perturbation method and the critical velocity criterion [35, 36, 37].

Notable works study the transition from deterministic to stochastic excitations including the evolution of unstable regions [38]. Besides, Gitterman studies the stability of the pendulum under deterministic and stochastic excitations of its support [39, 29]. Narrow band and random phase excitations are investigated by Alevras and Yurchenko in [40, 41] through a numerical path integration. Higher energy lobes are observed, similarly to the deterministic case (see Figure I.1 (b)) and an increasing stochasticity of the excitation leads to larger lobes of lower intensity. Mallick presents an analytical method providing an expression for the asymptotic probability distribution function of the energy of a pendulum [42]. Other estimations of the system stability are proposed in [43, 44, 45, 46, 47] based on its Liapunov exponents and on approximate solutions of the moment equations.

I.3 Non-stationary dynamics

The first-passage approach is an analysis tool for transient responses of non-stationary problems. The analysis of such systems can be done in different ways. First, Monte Carlo simulations [48, 49, 50, 1, 51, 52] provide for instance realizations and statistics of the generalized coordinates in transient and, eventually, stationary regimes. Figure I.3 presents three realizations of the energy H of an oscillator departing from small initial energy H_0 and reaching a larger energy level $H_0 + \Delta H$. Such Monte Carlo simulations are known to be versatile and accurate, although highly time consuming.

Secondly, the analysis of transient responses can be done by resolution of

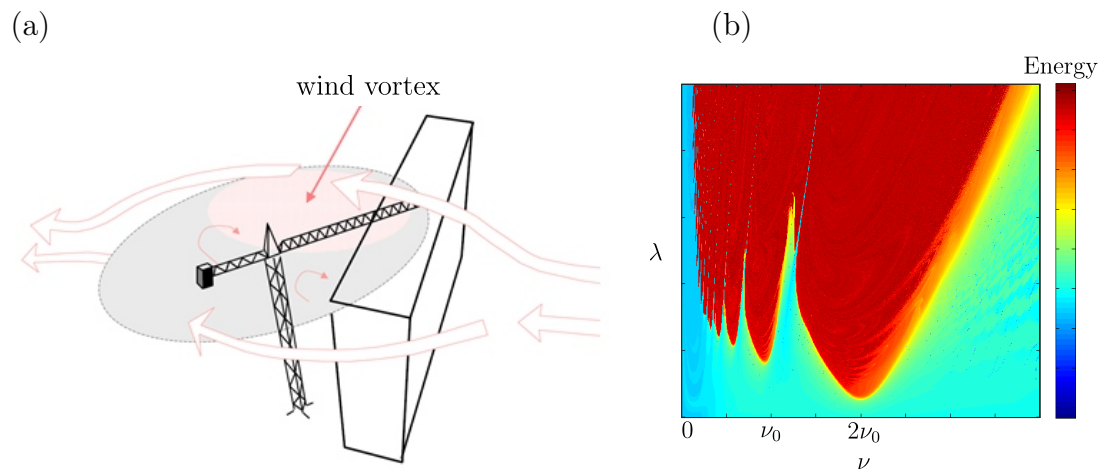


Figure I.1: (a) Rotation of a tower crane in gusty wind conditions [5] (b) Energy of the pendulum in the steady-state under harmonic parametric excitation [1].

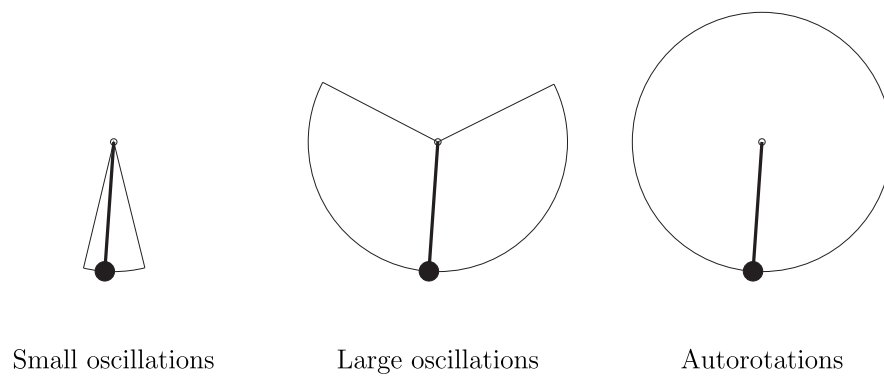


Figure I.2: The three regimes of oscillations that a pendulum may exhibit under horizontal and vertical excitations of its support. [1].

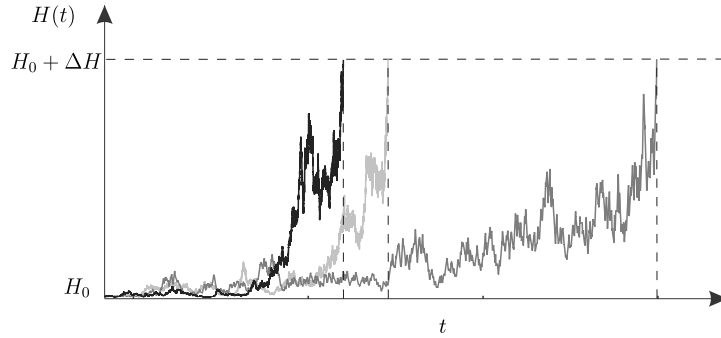


Figure I.3: Three realizations of the energy H of a stochastic oscillator (Equation (I.2.1)) from $H_0 = 10^{-5}$ to $H = 10^{-2}$ with $\xi = 0$ and white noise excitations of intensities $S_u = 0.01$ and $S_w = 0.5 \times 10^{-5}$.

stochastic differential equations [53, 54, 55, 56]. As a non-exhaustive list, the transition probability density function, the cumulative distribution of the first-passage time, and its statistical moments are respectively the solutions of the Fokker-Planck, Kolmogorov [57, 58, 59, 60, 61] and generalized Pontryagin equations [13, 62, 63]. These stochastic equations can be solved via use of numerical [64, 65, 42] or semi-analytical methods [66, 67] such as the path integration method [68, 69, 70], the Galerkin scheme [71, 72], the perturbation method [73], the smooth particle hydrodynamics method [74], high dimensional finite elements/differences [75, 76, 77, 78, 79], the Poisson distribution based assumption [80] or other approximate techniques. Comparisons of approached and numerical solutions for the first-passage times and the associated, so-called, reliability function, are widely available [69, 71, 65, 81].

While many stochastic oscillators are studied by means of approached solutions [82, 83, 84, 85], explicit solutions are available in some very limited cases only [86, 13, 87, 49, 88]. Indeed, analytical methods are usually not able to determine the complete distribution of the first-passage time and are limited to its first few statistical moments. In particular, the mean first-passage time provides a first apprehension of the phenomenon while the variance reflects the spread of the first-passage times. It also provides a valuable information as to the sample distribution of the mean first-passage time, as it depends on the parent distribution of this random variable. With this respect, confidence intervals of observed mean first-passage times basically depend on the spread of this random variable.

As highlighted by this literature review, the first-passage problem has been widely studied from a mathematical point of view, but received little attention for engineering applications. Consequently, this work presents the first-passage time as a new manner of considering transient engineering problems for conceptual design purposes.

I.4 Outline of this work

The first-passage problem is addressed step by step, starting from a simple model and progressively increasing its complexity.

Chapter II focuses on the stochastic version of the undamped, externally and parametrically excited oscillator and provides an approximate but closed-form solution for the average first-passage time of the single-degree-of-freedom system submitted to broadband parametric and forced excitations. The expression is obtained as the first order solution of an asymptotic expansion. Although the model is too simple to capture the full complexity of realistic problems such as those related to colored excitations, nonlinearities or multi-degrees-of-freedom structures, the closed-form solution lays the foundation for the analysis of more complex systems. Three different regimes corresponding to different behaviours of the system from a first-passage time point of view are identified.

In Chapter III, the different assumptions of the model of Chapter II are released one by one and a new formulation of the first-passage time is determined in each case. The influence of each simplification on the first-passage problem is described in detail. In this context, one successively observes the second order term of the asymptotic expansion, the damped oscillator, the variance of the first-passage time, nonlinearities and non-stationary excitations. The study of each assumption individually enables the development of a new solution and the assessment of its influence on the first-passage time while limiting the induced complexity.

As it is expected that the theoretical model of Chapters II and III can be fitted or adjusted to many (more complex) engineering problems, Chapter IV presents different applications of the first-passage time to physical systems. Oscillations of a pendulum and cable vibrations are presented as numerical examples where the first-passage time can be applied. A pre-stressed steel strip and a tower crane oscillating in a turbulent wind flow serve as an experimental demonstration of the first-passage approach.

Finally, Chapter V develops a numerical method for the first-passage time distribution and the reliability function of nonlinear systems under external evolutionary excitations. Two distinct definitions of the energy are employed and their influence on the accuracy of the solution is detailed. A specific scheme is developed for the undamped oscillator.

I.5 Personal contributions

The main contributions of this thesis are the following:

- The analytical determination of the average first-passage time in the reference case.

The average first-passage time of a linear undamped oscillator under stationary white noise excitations is obtained by resolution of the Pontryagin equation. An asymptotic expansion method is used and a closed-form expression for the first-order solution is developed. No analytical solution was known until now combining both parametric and forced excitations.

- The universal map and the three regimes.

The solution highlights the groups of parameters influencing the first-passage time which is presented in a universal map. The incubation, additive and multiplicative regimes are evidenced in the map with their typical features. This is a totally novel way of considering the first-passage problem.

- Influence of damping on the three regimes.

A closed-form solution of the average first-passage time is developed for the damped oscillator. Making use of the universal map, the three regimes are re-identified and the influence of damping on their features is characterized.

- Spread of the distribution of the first-passage time.

A closed form solution of the coefficient of variation of the first-passage time is determined. It provides a clear estimation of the spread of the distribution of the first-passage time. Once more, typical features are identified in the different regimes.

- Algorithmic establishment of the universal map based on experimental data

An efficient and original algorithm is developed to reconstruct the first-passage universal map based on measured time series.

- Experimental observation of the first-passage time.

The first-passage time of a tower crane under gusty winds is measured and its universal map is calculated. The identification of this map with the analytical model developed before serves as a demonstration of the applicability of the first-passage time as an identification tool or a reliability assessment tool in engineering applications.

- Development of a Galerkin resolution scheme for the distribution of the first-passage time of nonlinear systems under external evolutionary excitation.

A Galerkin scheme is developed to provide a robust and versatile method of resolution of the Backward-Kolmogorov equation governing the first-passage time probability density function. Consequently, one offers here an accurate solution for the complete distribution of the first-passage time

of nonlinear, damped oscillators submitted to an external evolutionary excitation. The combination of nonlinearities and evolutionary excitation has never been done before and is therefore a new contribution.

- Development of a specific scheme for the distribution of the first-passage time of an undamped oscillator

While the Galerkin scheme of a damped oscillator has been widely studied, no specific scheme is dedicated to the undamped oscillator until now. A specific formulation is proposed with analytical development of a pertinent basis of eigenfunctions. This new basis presents a particular interest due to its lower computational complexity and its use might be extended to slightly damped systems.

I.6 Theoretical background

This section provides a theoretical background on stochastic differential equations concerning the first-passage problem.

I.6.1 Definitions

Let \mathcal{D} be a closed domain in the phase plane and an initial condition $\mathbf{x}_0 \in \mathcal{D}$. The first-passage time of a system through the boundary of the domain $\partial\mathcal{D}$ is defined as

$$t_f = \inf \{t > 0 \mid \mathbf{x}(t) \in \partial\mathcal{D} \ \& \ \mathbf{x}(0) = \mathbf{x}_0\} \quad (\text{I.6.1})$$

Under stochastic excitations, the first-passage time is a random variable and can be characterized by its probability density function (pdf) p_f , or its cumulative density function (cdf) P_f . The complement of the cdf P is called the reliability function, or survival probability, and provides the probability that the system does not leave the domain \mathcal{D} over the time interval $[0, t]$

$$P(t; \mathbf{x}_0) = \text{prob}(t_f > t) = 1 - P_f(t; \mathbf{x}_0), \quad (\text{I.6.2})$$

An equivalent definition can be provided by the probability of the first-passage time t_f being greater than t . Consequently, the probability density function of the first-passage time is given by

$$p_f(t; \mathbf{x}_0) = \frac{\partial P_f(t; \mathbf{x}_0)}{\partial t} = -\frac{\partial P(t; \mathbf{x}_0)}{\partial t}. \quad (\text{I.6.3})$$

The cumulative probability of the first-passage time $P_f(t; \mathbf{x}_0)$ can be expressed as a function of the transition probability function $p(\mathbf{x}, t \mid \mathbf{x}_0, t_0 = 0)$

$$P_f(t; \mathbf{x}_0) = \int_{\mathcal{D}} p(\mathbf{x}, t \mid \mathbf{x}_0, 0) d\mathbf{x}. \quad (\text{I.6.4})$$

I.6.2 Stochastic differential equations

Let us consider a system represented in the n -dimensional state-space \mathbf{x} by its Itô formulation [13, 89, 87, 62]

$$d\mathbf{x} = \mathbf{a}(\mathbf{x}, t)dt + \mathbf{b}(\mathbf{x}, t)d\mathbf{B}, \quad (\text{I.6.5})$$

where \mathbf{x} and $\mathbf{a}(\mathbf{x}, t)$ are vectors of dimension $n \times 1$, \mathbf{B} is a $m \times 1$ vector of m Brownian motions characterized by the $m \times m$ power spectrum matrix \mathbf{S} and $\mathbf{b}(\mathbf{x}, t)$ is a $n \times m$ matrix. Equivalently, (I.6.5) can be expressed with indices as

$$dx_i = a_i(\mathbf{x}, t)dt + b_{i,j}(\mathbf{x}, t)dB_j, \quad i = 1, \dots, n; \quad j = 1, \dots, m. \quad (\text{I.6.6})$$

Change of variables and Wong-Zakai correction terms

The N -dimensional transformation $\mathbf{F}(\mathbf{x}, t)$ of the n -dimensional variable \mathbf{x} given by (I.6.5) is governed by the stochastic equation [13, 89, 90, 53]

$$d\mathbf{F} = \left(\frac{\partial \mathbf{F}}{\partial t} + \frac{\partial \mathbf{F}}{\partial \mathbf{x}} \mathbf{a}(\mathbf{x}, t) + \frac{1}{2} \text{Tr} \left\{ \mathbf{J}(\mathbf{x}, t) \frac{\partial}{\partial \mathbf{x}} \frac{\partial^T \mathbf{F}}{\partial \mathbf{x}} \right\} \right) dt + \frac{\partial \mathbf{F}}{\partial \mathbf{x}} \mathbf{b}(\mathbf{x}, t) d\mathbf{B}, \quad (\text{I.6.7})$$

that can also be expressed with indices for $k = 1, \dots, N$ as

$$dF_k = \left(\begin{aligned} & \frac{\partial F_k}{\partial t} + \sum_{i=1}^n a_i(\mathbf{x}, t) \frac{\partial F_k}{\partial x_i} + \underbrace{\frac{1}{2} \sum_{i=1}^n \sum_{j=1}^n J_{ij}(\mathbf{x}, t) \frac{\partial^2 F_k}{\partial x_i \partial x_j}}_{\text{WZ correction}} \\ & + \sum_{i=1}^n \sum_{j=1}^m b_{ij}(\mathbf{x}, t) \frac{\partial F_k}{\partial x_i} dB_j, \end{aligned} \right) dt \quad (\text{I.6.8})$$

where

$$\mathbf{J}(\mathbf{x}, t) = \mathbf{b}(\mathbf{x}, t) \mathbf{S} \mathbf{b}^T(\mathbf{x}, t) \quad (\text{I.6.9})$$

is a $n \times n$ diffusion matrix. The first, second and fourth terms of Equation (I.6.8) result from the usual transformation of Equation (I.6.5) with change of variable, while the third term is a supplementary term, called the Wong-Zakai correction, due to the peculiar property of the Brownian motion that typically appears in stochastic differential equations.

Fokker-Planck or Forward Kolmogorov equation

The transition pdf $p = p(\mathbf{x}, t | \mathbf{x}_0, 0)$ is given by the solution of the Fokker-Planck, or Forward Kolmogorov equation [89, 62, 13]

$$\frac{\partial p}{\partial t} = \mathcal{L}\{p\}, \quad (\text{I.6.10})$$

where $\mathcal{L}\{p\}$ is the Fokker-Planck or Forward-Kolmogorov operator defined as

$$\mathcal{L}\{p\} = \frac{1}{2} \mathbf{Tr} \left\{ \left[\frac{\partial}{\partial \mathbf{x}} \frac{\partial^T}{\partial \mathbf{x}} (\mathbf{J}(\mathbf{x}, t)p) \right] \right\} - \frac{\partial (\mathbf{a}(\mathbf{x}, t)p)}{\partial \mathbf{x}}, \quad (\text{I.6.11})$$

that can also be expressed with indices as

$$\mathcal{L}\{p\} = \sum_{i=1}^n \sum_{j=1}^n \frac{1}{2} \frac{\partial^2 (J_{ij}(\mathbf{x}, t)p)}{\partial x_i \partial x_j} - \sum_{i=1}^n \frac{\partial (a_i(\mathbf{x}, t)p)}{\partial x_i}. \quad (\text{I.6.12})$$

In many practical problems, the initial state is fixed, so that the initial condition is given by

$$p(\mathbf{x}, 0 \mid \mathbf{x}_0, 0) = \delta(\mathbf{x} - \mathbf{x}_0). \quad (\text{I.6.13})$$

The boundary condition imposes that the state \mathbf{x} reached in any final time t must be finite, i.e.

$$\lim_{\mathbf{x} \rightarrow \infty} p(\mathbf{x}, t \mid \mathbf{x}_0, 0) = 0. \quad (\text{I.6.14})$$

Backward Kolmogorov equation

The cumulative density function $P_f = P_f(t; \mathbf{x}_0)$ is given by the solution of the Backward Kolmogorov equation [89, 62, 13]

$$\frac{\partial P_f}{\partial t} = \mathcal{L}^* \{P_f\}, \quad (\text{I.6.15})$$

where $\mathcal{L}^* \{P\}$ is the Backward-Kolmogorov operator defined as

$$\mathcal{L}^* \{P_f\} = \frac{1}{2} \mathbf{Tr} \left\{ \left[\mathbf{J}(\mathbf{x}_0, t) \frac{\partial}{\partial \mathbf{x}_0} \frac{\partial^T}{\partial \mathbf{x}_0} P_f \right] \right\} + \mathbf{a}(\mathbf{x}_0, t) \frac{\partial P_f}{\partial \mathbf{x}_0}, \quad (\text{I.6.16})$$

that can also be expressed with indices as

$$\mathcal{L}^* \{P_f\} = \sum_{i=1}^n \sum_{j=1}^n \frac{J_{ij}(\mathbf{x}_0, t)}{2} \frac{\partial^2 P_f}{\partial x_{0,i} \partial x_{0,j}} + \sum_{i=1}^n a_i(\mathbf{x}_0, t) \frac{\partial P_f}{\partial x_{0,i}}. \quad (\text{I.6.17})$$

The initial condition is given by the fact that the first-passage time of a system, departing from a point inside the domain, is strictly positive with probability one

$$P_f(0; \mathbf{x}_0) = 0 \quad \forall \mathbf{x}_0 \in \mathcal{D}, \quad (\text{I.6.18})$$

and the boundary condition imposes that the first-passage time is equal to zero if the initial condition is on the limit of the domain

$$P_f(t; \mathbf{x}_0) = 1 \quad \text{if } \mathbf{x}_0 \in \partial\mathcal{D}. \quad (\text{I.6.19})$$

The reliability function $P(t; \mathbf{x}_0)$ given by (I.6.2) is governed by the same equation as (I.6.15), but replacing P_f by P and changing the initial and boundary conditions by

$$P(0; \mathbf{x}_0) = 1 \quad \forall \mathbf{x}_0 \in \mathcal{D}, \quad (\text{I.6.20})$$

and

$$P(t; \mathbf{x}_0) = 0 \quad \text{if } \mathbf{x}_0 \in \partial\mathcal{D}. \quad (\text{I.6.21})$$

It is observed that Equation (I.6.16) is a function of the initial condition \mathbf{x}_0 . This is a typical feature of the so-called ‘‘Backward’’-Kolmogorov operator, since it is defined as a function of the initial state. The target state, defined by the limit of the domain $\partial\mathcal{D}$ is introduced into the problem via the boundary condition (I.6.19).

Generalized Pontryagin equation

The statistical moments of the first-passage time, defined as [91, 89, 62, 86]

$$M_k = \mathcal{E} \{t_f^k\} \quad (\text{I.6.22})$$

where $\mathcal{E} \{ \}$ is the statistical expectation, and k is the concerned order, are given by the solution of the generalized Pontryagin equation

$$\frac{\partial M_k}{\partial t} + \mathcal{L}^* \{M_k\} = -M_{k-1} \quad \forall k \geq 1 \quad \text{with } M_0 = 1, \quad (\text{I.6.23})$$

where $\mathcal{L}^* \{ \}$ is the Backward Kolmogorov operator defined in (I.6.16) and (I.6.17). When the system characteristics $\mathbf{a}(\mathbf{x}, t)$ and $\mathbf{b}(\mathbf{x}, t)$ are independent of time, the system is autonomous, i.e. its evolution does not depend on the origin of time. In this case, the first-passage time is autonomous too and Equation (I.6.23) becomes

$$\mathcal{L}^* \{M_k\} = -M_{k-1} \quad \forall k \geq 1 \quad \text{with } M_0 = 1. \quad (\text{I.6.24})$$

For $k = 1$, the average first-passage time $M_1 = \mu_f$ is given by the solution of

$$\mathcal{L}^* \{\mu_f\} = -1, \quad (\text{I.6.25})$$

which is called the Pontryagin equation [86, 91, 88]. The boundary conditions are given by

$$M_k(\mathbf{x}_0) = 0, \quad \forall \mathbf{x}_0 \in \partial\mathcal{D} \quad \text{and} \quad |M_k(\mathbf{x}_0 = 0)| < \infty. \quad (\text{I.6.26})$$

The first condition translates the fact that the first-passage time is deterministic and equal to zero for trajectories starting on the boundary, $\partial\mathcal{D}$. The second condition expresses that the time (and its statistical moments) required to reach the boundary starting from $\mathbf{x}_0 = 0$ is finite. This condition is rather qualitative and its applicability is limited to simple analytical closed form expressions. An equivalent quantitative condition is given in [86, 89] depending on the boundary class of the problem, which is determined through the diffusion exponent α_l , drift exponent β_l and character value c_l . For one-dimensional processes, those coefficients are given by the following limits:

$$\begin{cases} J(x, t) & \rightarrow \mathcal{O}(|x - x_l|^{\alpha_l}), \quad \alpha_l \geq 0, & x \rightarrow x_l \\ a(x, t) & \rightarrow \mathcal{O}(|x - x_l|^{\beta_l}), \quad \beta_l \geq 0, & x \rightarrow x_l \\ \frac{2a(x, t)(x - x_l)^{\alpha_l - \beta_l}}{J(x, t)} & \rightarrow c_l, & x \rightarrow 0 \end{cases} \quad (\text{I.6.27})$$

where x_l is the left boundary for the initial state corresponding to the root of J and $\mathcal{O}(|\cdot|)$ denotes the order of $|\cdot|$. The functions $a(x)$ and $J(x)$ correspond to the vector and matrix of equations (I.6.5) and (I.6.9) that become scalars in the one-dimensional case. For entrance and repulsively natural boundary classes, the second condition (I.6.26) can be replaced by the quantitative condition

$$\mathcal{O}(|a(x_0, t)M'_k(x_0)|) \sim \mathcal{O}(|M'_{k-1}(x_0)|), \quad x_0 \rightarrow x_l. \quad (\text{I.6.28})$$

Similarly to the Backward-Kolmogorov equation (I.6.16), the generalized Pontryagin equation (I.6.23) is a function of the initial condition \mathbf{x}_0 and the target state is introduced via the boundary condition (I.6.26).

One-dimensional stochastic processes

In the case of a one-dimensional Brownian motion ($n = m = 1$), x , $a(x, t)$, $b(x, t)$ and $dB(t)$ are scalars. Equations (I.6.8), (I.6.9), (I.6.12) and (I.6.17) considerably simplify and become

$$dF = \left(\frac{\partial F}{\partial t} + a(x, t) \frac{\partial F}{\partial x} + \underbrace{\frac{1}{2} J(x, t) \frac{\partial^2 F}{\partial x^2}}_{\text{WZ correction}} \right) dt + b(x, t) \frac{\partial F}{\partial x} dB, \quad (\text{I.6.29})$$

$$J(x, t) = b^2(x, t)S, \quad (\text{I.6.30})$$

$$\mathcal{L}\{p\} = \frac{\partial}{\partial x} \left[\frac{1}{2} \frac{\partial (J(x, t)p)}{\partial x} - a(x, t)p \right] \quad (\text{I.6.31})$$

and

$$\mathcal{L}^*\{P_f\} = \frac{J(x_0, t)}{2} \frac{\partial^2 P_f}{\partial x_0^2} + a(x_0, t) \frac{\partial P_f}{\partial x_0}. \quad (\text{I.6.32})$$

The coefficients $a(x, t)$ and $b(x, t)$ are commonly named the drift and diffusion coefficients and sometimes also noted $m(x, t)$ and $\sigma(x, t)$.

Chapter II

Analytical determination of the first-passage time in a reference case

This chapter determines the *average* first-passage time of an *undamped linear* oscillator under *stationary* parametric and external white noise excitations. An approached closed-form expression is obtained via an asymptotic expansion of the Pontryagin equation and the *first order solution* provides a frame for the analysis of the first-passage problem.

II.1	Introduction
II.2	Pontryagin equation
II.3	Analysis and discussion
II.4	Conclusion

This Chapter is based on the following article:

Vanvinckenroye, H., & Denoël, V. (2017). Average first-passage time of a quasi-Hamiltonian Mathieu oscillator with parametric and forcing excitations. *Journal of Sound and Vibration*, 406, pp. 328–345.

II.1 Introduction

This Chapter provides a first tool for understanding the first-passage time problem and therefore focuses on the average value of the first-passage time instead of the complete distribution.

Since the problem at hand is particularly interesting when the damping and the intensities of the excitations are small –otherwise the steady regime develops fast enough– the considered oscillator actually happens to be a *quasi-Hamiltonian* system for which the total internal energy $H(t)$ evolves on a slow time scale [42]. The energy balance of the Mathieu equation (I.2.1), obtained by time integration of the power fluxes, yields

$$\frac{\dot{x}^2}{2} + \frac{x^2}{2} + \int (2\xi\dot{x}^2 + u x \dot{x}) dt = \int w \dot{x} dt. \quad (\text{II.1.1})$$

This indeed shows that the total internal energy (referred to as *the Hamiltonian*, by extension, in the sequel) defined by

$$H = \frac{x^2}{2} + \frac{\dot{x}^2}{2}, \quad (\text{II.1.2})$$

composed of potential and kinetic energies, is slowly varying, since $\dot{H} = \text{ord}(\varepsilon)$ if $\{\xi, u, w\} = \text{ord}(\varepsilon)$. This is also illustrated in Figure II.1 which shows, in the phase-plane (x, \dot{x}) , three fragments of one realization of the Mathieu oscillator (I.2.1) subjected to parametric and external δ -correlated white noises¹ u and w of intensities $S_u = 10^{-2}$ and $S_w = 10^{-4}$, while the damping ratio is set to $\xi = 0.01$. It is seen that the trajectories are nearly tangent to the ellipses of constant energy, which indicates that the Hamiltonian varies by only a small quantity over one period of revolution of the unperturbed dynamical system. These observations support the quasi-Hamiltonian nature of the system, which is, in this case, a consequence of the smallness of ξ , S_u and S_w .

The first-passage problem of quasi-Hamiltonian systems has been studied in the literature in the undamped configuration ($\xi = 0$) and without external forcing term ($w = 0$). The stochastic parametric excitation $u(t)$ has first been considered to be a δ -correlated process [92] and more recently an Ornstein-Uhlenbeck process [43]. In the latter case, Potapov also proposes an estimation of the problem stability based on its Liapunov exponents, an approach that is also followed in [93] for quasi non-integrable Hamiltonian systems under Gaussian and Poisson white noises through the averaged Itô equation.

Still considering the undamped configuration ($\xi = 0$) and without external forcing ($w = 0$), the stochastic differential equation governing the Hamiltonian

¹A δ -correlated white noise is defined by an autocorrelation function of the form $R_x(\Delta t) = \mathcal{E}[x(t)x(t + \Delta t)] = S_x\delta(\Delta t)$, where $\delta(\cdot)$ is the Dirac-function. S_x is called the intensity of the white noise.

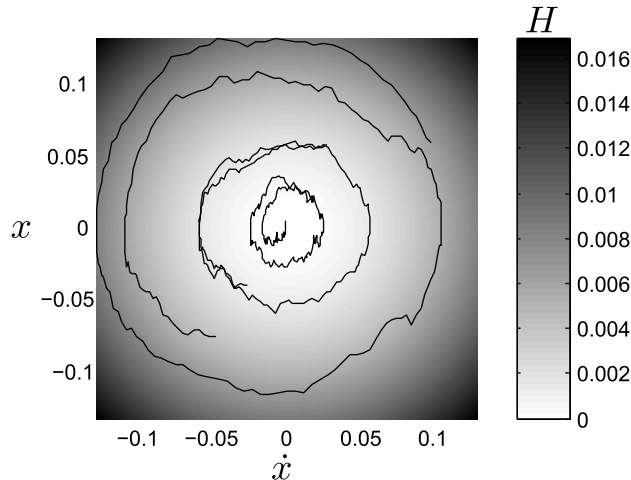


Figure II.1: Fragments of the trajectory of a Mathieu oscillator in the phase plane and contours of the Hamiltonian. Numerical values: $\xi = 0.01$, $S_u = 10^{-2}$ and $S_w = 10^{-4}$.

reads

$$dH = k_1 H dt + k_2 H dB, \quad (\text{II.1.3})$$

with $k_1 = S_u/2$ and $k_2 = \sqrt{S_u/2}$ two parameters depending on the spectral intensity of the parametric excitation u , and dB the increment of a δ -correlated Brownian noise $B(t)$ [49, 86]. This equation can be solved explicitly [49]:

$$H(t) = H_0 \exp \left[k_1 B_t + \left(k_1 - \frac{k_2^2}{2} \right) t \right]. \quad (\text{II.1.4})$$

The first-passage time of the energy level H_c , starting from a lower initial energy H_0 , follows an inverse Gaussian distribution with parameters $\frac{\ln(H_c/H_0)}{k_1 - k_2^2/2}$ and $\frac{\ln(H_c/H_0)^2}{k_2^2}$, so that its mean first-passage time μ_f can be expressed as [49]

$$\mu_f(H_0) = \frac{4}{S_u} \ln \frac{H_c}{H_0}. \quad (\text{II.1.5})$$

It is rather rare that the stochastic differential equation of a (more complex but realistic) problem can take a simple explicit solution as (II.1.4). The complete probability density function of the first-passage time is therefore seldom available. However, the mean first-passage time of a stochastic system through the boundary of a given domain is ruled by the Pontryagin equation (I.6.25).

Many solutions of more or less complex problems in terms of mean first-passage time can be found in the literature [86, 13, 88, 94, 64]. Among them the first-passage time for a stochastic fractional derivative system with power-law

restoring force [64] shows the typical range of difficulties that can be tackled today. An important contribution in the field concerns the works of Khasminskii [95] which consist in the formal development of an asymptotic analysis of the Pontryagin equation. This is precisely the approach that is followed in this work.

Based on this review of the literature, we have identified the first-passage time of an undamped linear system subjected to both parametric and external white noise excitations as a first step into the analysis of the first-passage problem. Considered here as the reference configuration, this problem is solved in closed but approximate form and the solutions are thoroughly discussed in Section II.3. Different variants such as the damped oscillator or the mean square first-passage time are studied in Chapter III.

II.2 Pontryagin equation

The system considered here is governed by

$$\ddot{x}(t) + [1 + u(t)]x(t) = w(t) \quad (\text{II.2.1})$$

where $u(t)$ and $w(t)$ are Brownian δ -correlated white noises of small intensities S_u and S_w . Formally this problem is represented in the state-space $\mathbf{x} = (x, \dot{x}) = (q, p)$ by its Itô formulation (I.6.5) for Markov times, i.e. for each $t > t_0$, by

$$d\mathbf{x} = \mathbf{a}(\mathbf{x})dt + \mathbf{b}(\mathbf{x})d\mathbf{B}, \quad (\text{II.2.2})$$

where $\mathbf{x} = \begin{bmatrix} q \\ p \end{bmatrix}$, $\mathbf{a} = \begin{bmatrix} p \\ -q \end{bmatrix}$, $\mathbf{b} = \begin{bmatrix} 0 & 0 \\ -q & 1 \end{bmatrix}$ and where $\mathbf{B} = \begin{bmatrix} B_u \\ B_w \end{bmatrix}$ is the vector of Brownian motions characterized by the power spectrum matrix

$$\mathbf{S} = \begin{bmatrix} S_u & S_{uw} \\ S_{uw} & S_w \end{bmatrix} = \varepsilon \boldsymbol{\nu} = \varepsilon \begin{bmatrix} \nu_u & \nu_{uw} \\ \nu_{uw} & \nu_w \end{bmatrix}, \quad (\text{II.2.3})$$

where $\varepsilon \ll 1$ and $\boldsymbol{\nu}$ is an order-one matrix. It is interesting to notice that (II.2.2) is a perturbation of a conservative system which evolves along closed trajectories of constant total internal energy H . The period of revolution of a complete orbit of the unperturbed system ($\varepsilon = 0$, so that $u = w = 0$),

$$T = 2 \int_{q_1}^{q_2} \frac{dq}{\dot{q}} = 2 \int_{-\sqrt{2H}}^{\sqrt{2H}} \frac{1}{\sqrt{2H - q^2}} dq = 2\pi, \quad (\text{II.2.4})$$

is independent of the considered energy level H .

Let \mathcal{D} be a closed domain in the phase plane and an initial condition $\mathbf{x}_0 \in \mathcal{D}$. Since vectors \mathbf{a} and \mathbf{b} are independent of time, the system is autonomous, i.e.

its evolution does not depend on the origin of time. In this case, the average first-passage time $\mu_f(\mathbf{x}_0) = \mathcal{E}\{t_f\}$ for the trajectories of the dynamical system to reach the boundary ∂D is given by the Pontryagin equation (I.6.25)

$$\mathcal{L}^* \{\mu_f(\mathbf{x}_0)\} = -1, \quad \text{for } \mathbf{x}_0 \in \mathcal{D} \quad (\text{II.2.5})$$

with the boundary conditions (I.6.26). For the sake of simplicity in the notations, the subscript "0" is omitted in the following developments. This convention prevails for both the initial position and velocity, q_0 and p_0 which are the components of \mathbf{x}_0 and, later, for the Hamiltonian H_0 . In (II.2.5), $\mathcal{L}^* \{\cdot\}$ is the Backward-Kolmogorov operator associated with the governing equation, see e.g. [13], given by (I.6.16) where the diffusion matrix is of order ε and is given by

$$\mathbf{J} = \varepsilon \mathbf{b}(\mathbf{x}, t) \boldsymbol{\nu} \mathbf{b}^T(\mathbf{x}, t) = \varepsilon \begin{bmatrix} 0 & 0 \\ 0 & q^2 \nu_u + \nu_w - 2q \nu_{uw} \end{bmatrix} \quad (\text{II.2.6})$$

The higher order derivative in $\mathcal{L}^* \{\cdot\}$ is therefore multiplied by a small coefficient, of order ε , which is responsible for a well-known boundary layer in perturbation methods [96]. With this in mind and following Khasminskii's approach [95], an asymptotic expansion method is developed in order to establish closed-form expressions for the solution of the Pontryagin equation. This not only avoids the numerical solution of (II.2.5) but also provides a much better understanding of the features of the problem, as explicit expressions for the mean first-passage time are obtained, under the sole hypothesis that $\varepsilon \ll 1$, i.e. that the dimensionless intensities of the external and parametric excitations are small. Following this approach, the operator is decomposed into two operators, each one acting at its own scale in ε , as

$$\mathcal{L}^* \{\cdot\} = \mathcal{L}_1 \{\cdot\} + \varepsilon \mathcal{L}_2 \{\cdot\}, \quad (\text{II.2.7})$$

where, after replacement of the derivatives in \mathbf{x} ,

$$\mathcal{L}_1 = p \frac{\partial}{\partial q} - q \frac{\partial}{\partial p} \quad ; \quad \mathcal{L}_2 = \frac{1}{2} (q^2 \nu_u + \nu_w - 2q \nu_{uw}) \frac{\partial^2}{\partial p^2}. \quad (\text{II.2.8})$$

Following the matched asymptotic expansion solution applied in [88, 94] to the capsizing of boats in random seas (with external forcing only, though), a composite solution to (II.2.5) is provided as the sum of the outer and inner solutions

$$\mu_f(p, q) = U_n(p, q) + G_n(p, q), \quad (\text{II.2.9})$$

where U_n is the outer solution obtained with the regular ansatz

$$U_n(p, q) = \frac{1}{\varepsilon} u_0(p, q) + u_1(p, q) + \dots + \varepsilon^{n-1} u_n(p, q) \quad (\text{II.2.10})$$

and G_n stands for the inner solution in the boundary layer, in the neighborhood of ∂D . The error of the approximate solution has the same order as the first neglected term, i.e. ε^n . In order not to include the overlap between the inner and outer solutions that anyway needs to be discarded in the composite solution [96], the outer and inner problems are respectively solved with the following right-hand sides, $\mathcal{L}^* \{U_n\} = -1$ and $\mathcal{L}^* \{G_n\} = 0$. While the efforts presented in this Chapter concentrate on the establishment of u_0 , the outer solution will be developed up to the second term u_1 in Section III.1. Collecting terms of likewise powers of ε in (II.2.5) yields:

$$\text{ord}(\varepsilon^{-1}) : \quad \mathcal{L}_1 u_0 = 0 \quad (\text{II.2.11})$$

$$\text{ord}(\varepsilon^0) : \quad \mathcal{L}_1 u_1 + \mathcal{L}_2 u_0 = -1 \quad (\text{II.2.12})$$

$$\text{ord}(\varepsilon^1) : \quad \mathcal{L}_1 u_2 + \mathcal{L}_2 u_1 = 0 \quad (\text{II.2.13})$$

The leading order solution U_0 is actually nothing but the result of the stochastic averaging method [97], which roughly assumes that the Hamiltonian is constant along one period of motion. The higher order terms provided by the asymptotic expansion extend the validity of the developments to moderate values of the small parameter, i.e. $\varepsilon \lesssim 1$. However, for problems slightly more complex than (II.2.1), the second and higher correction terms take awkward expressions which cuts down the advantages of Khasminskii's asymptotic expansion over the more usual stochastic averaging approach. This is discussed in Section III.1.

Operator \mathcal{L}_1 represents the derivative along the direction of the conservative system, i.e. along the orbits of constant Hamiltonian H . As a result, the leading order Equation (II.2.11) means that u_0 is constant along each orbit of constant energy. It is consequently a function of the Hamiltonian H only. Averaging (II.2.12) along a period T of the orbit, provides the information to determine $u_0(H)$. Indeed, as the orbits are closed, averaging $\mathcal{L}_1 u_1$ along each of these trajectories gives zero and Equation (II.2.12) becomes $\langle \mathcal{L}_2 u_0 \rangle = -1$, or

$$\frac{1}{2} \left[\langle q^2 \nu_u + \nu_w - 2q\nu_{uw} \rangle \frac{du_0}{dH} + \langle p^2 (q^2 \nu_u + \nu_w - 2q\nu_{uw}) \rangle \frac{d^2 u_0}{dH^2} \right] = -1, \quad (\text{II.2.14})$$

where the following relations have been used for the partial derivatives

$$\frac{\partial u_0}{\partial p} = p \frac{du_0}{dH} \quad ; \quad \frac{\partial^2 u_0}{\partial p^2} = \frac{du_0}{dH} + p^2 \frac{d^2 u_0}{dH^2} \quad (\text{II.2.15})$$

since $u_0 \equiv u_0(H)$ is a function of the initial Hamiltonian only and the operator $\langle \cdot \rangle$ represents the average over one period $T = 2\pi$ of the unperturbed motion,

$$\langle \cdot \rangle = \frac{1}{2\pi} \int_0^{2\pi} \cdot dt. \quad (\text{II.2.16})$$

The averaging of Equation (II.2.14) is derived, term by term, by changing the variables q and p into the energy-phase variables k and θ with

$$p = 2k \cos \theta \quad ; \quad q = 2k \sin \theta \quad (\text{II.2.17})$$

so that the Hamiltonian is now given by $H = 2k^2$.

Finally, at order ε^0 , the averaged Pontryagin equation reads

$$\frac{1}{\varepsilon} \left(m(H) \frac{du_0}{dH} + \frac{\sigma^2(H)}{2} \frac{d^2 u_0}{dH^2} \right) = -1 \quad (\text{II.2.18})$$

where u_0 , the leading order solution in the outer domain, is a function of the Hamiltonian H ($\equiv H_0$) in the initial configuration. The parameters $m(H)$ and $\sigma(H)$ are commonly known as drift and diffusion coefficients and are here given by

$$\begin{cases} m(H) = \varepsilon \left(\frac{H}{2} \nu_u + \frac{1}{2} \nu_w \right) = \frac{H}{2} S_u + \frac{1}{2} S_w \\ \sigma(H) = \sqrt{\varepsilon \left(\frac{H^2}{2} \nu_u + H \nu_w \right)} = \sqrt{\frac{H^2}{2} S_u + H S_w} \end{cases} \quad (\text{II.2.19})$$

The drift and diffusion coefficients obtained by stochastic averaging also characterize the evolution of the energy through the stochastic differential equation [13]

$$dH = m(H)dt + \sigma(H)dB(t), \quad (\text{II.2.20})$$

The governing equation and consequently its solution are independent of the cross spectral density S_{uw} . The general solution of (II.2.18) is of the form

$$u_0(H) = -\frac{8\nu_w + \nu_u C_1}{2\nu_u \nu_w} \ln(H\nu_u + 2\nu_w) + C_1 \frac{\ln H}{2\nu_w} + C_2, \quad (\text{II.2.21})$$

where constants of integration C_1 and C_2 need to be determined to satisfy the boundary conditions (I.6.26). Notice that the first boundary condition can also be satisfied in the outer solution which implies that there is no inner (boundary layer) solution at order ε^{-1} . Although the second condition straightforwardly yields $C_1 = 0$, the first boundary condition requires a little more attention. Indeed, the boundary condition is a priori written on the boundary of the domain of \mathcal{D} of any arbitrary shape in the state space (x, \dot{x}) . However, because $u_0(H)$ is a function of H only, there is no way to satisfy the boundary condition for any $\mathbf{x}_0 \in \partial\mathcal{D}$, otherwise than to have \mathcal{D} being a disk in the phase space. Because of this, we actually decide to restrict our study to the determination of the first-passage time through a domain shaped like a circle, i.e. through the contours of equation $H = H_c$. In other words, the considered problem can be expressed as the first-passage time through a state of a specifically chosen energy H_c , while starting from a smaller initial energy H_0 . If the domain \mathcal{D} was not shaped like a disk, an underestimation of the first-passage time might be obtained by

replacing the domain by the inscribing circle as the rotation is fast compared to the energy. Accounting for the boundary condition $\mu_f(H_c) = 0$, we finally obtain at first order

$$\mu_f(H_0) = \frac{u_0}{\varepsilon} = \frac{4}{S_u} \ln \left(\frac{H_c S_u + 2S_w}{H_0 S_u + 2S_w} \right) \quad (\text{II.2.22})$$

where the subscript “0” has been re-introduced to indicate this corresponds to trajectories starting with an initial energy equal to H_0 . As the Itô formulation (II.2.2) is only valid for positive times, this solution is only valid for a target energy higher than the initial energy.

II.3 Analysis and discussion

The average first passage time therefore takes a logarithmic form where the intensity of the parametric excitation is multiplied by the energy and appears in both the logarithm and the multiplying factor. Expression (II.2.22) presents two limit cases:

- when there is no parametric excitation, i.e. $S_u = 0$, the general solution degenerates into

$$\mu_f(H_0) = 2 \frac{\Delta H}{S_w}, \quad (\text{II.3.1})$$

which indicates that the first-passage time scales linearly with $\Delta H = H_c - H_0$, the difference between the target energy barrier and the initial energy in the system. With the terminology introduced below, this corresponds to an incubation regime, no matter the intensity of the forcing term;

- when there is no forcing term, i.e. $S_w = 0$, the general solution degenerates into

$$\mu_f(H_0) = \frac{4}{S_u} \ln \frac{H_c}{H_0} = \frac{4}{S_u} \ln \left(1 + \frac{\Delta H}{H_0} \right), \quad (\text{II.3.2})$$

corresponding to the solution developed in [49], see (II.1.5). In this case, the first-passage time scales with the ratio H_c/H_0 on a logarithmic scale. Furthermore, a non-zero initial energy is required for the oscillator to exit its initial configuration. Then, for any $H_0 > 0$, the oscillator can reach any energy barrier in a finite time, on average. With the terminology introduced below, this corresponds to a multiplicative regime, no matter the intensity of the parametric excitation.

These two limiting cases reflect that the parametric excitation $w(t)$ and the external forcing $u(t)$ show themselves differently in the problem. Notice that the linear and logarithmic scalings that are obtained here agree with the well-known responses of undamped linear oscillators under deterministic excitations. On one

hand, the envelope of the response under external forcing grows unbounded and linearly in case of harmonic excitation tuned to the natural frequency of the oscillator ($w = \sin t$). On the other hand, in the unstable configuration of the undamped Mathieu equation, the response envelope grows exponentially fast for a harmonic parametric excitation tuned to twice the natural frequency of the oscillator ($u = \sin 2t$).

The interplay between the two competing sources of excitation, i.e. does the first-passage time scale on a log or linear scale with H_c ?, depends on S_u , S_w , H_0 and H_c , as well as the relative smallness of some dimensionless groups made of these four parameters. To investigate this question, we rewrite (II.2.22) as

$$\mu_f(H_0) = \frac{4}{S_u} \ln \left(1 + \frac{\Delta H S_u}{H_0 S_u + 2S_w} \right) \quad (\text{II.3.3})$$

with $\Delta H = H_c - H_0$.

Incubation regime. This mathematical formulation naturally hints one particular regime, when the argument of the natural logarithm is close to one, i.e.

$$\frac{\Delta H S_u}{H_0 S_u + 2S_w} \ll 1 \quad \rightarrow \quad \Delta H \ll H_0 + \frac{2S_w}{S_u}. \quad (\text{II.3.4})$$

It is always possible to choose, for given H_0 , S_w and S_u , small enough values of the target energy level satisfying condition (II.3.4). Indeed, the system needs to pass first by these states of energy slightly larger than the initial one before reaching, eventually, states of much higher energy. These states belong to an *incubation regime* during which the general solution (II.3.3) may be linearized. Recalling that $\ln(1 + \epsilon) = \epsilon + \text{ord}(\epsilon^2)$ for $\epsilon \ll 1$, the mean first-passage time in this incubation regime reads,

$$\mu_f^{(I)} = \frac{4}{S_u} \left[\frac{\Delta H S_u}{H_0 S_u + 2S_w} + \text{ord} \left(\frac{\Delta H S_u}{H_0 S_u + 2S_w} \right)^2 \right] \simeq \frac{4\Delta H}{H_0 S_u + 2S_w} \quad (\text{II.3.5})$$

which indicates that the mean first-passage time is proportional to the increase in the Hamiltonian $\Delta H = H_c - H_0$. For very small values of ΔH , the first-passage time decreases and might reach the order of the period of the oscillator. In this case, the asymptotic method induces large errors on the result which is not reliable anymore.

This approximation ceases to be valid when (II.3.4) is not fulfilled anymore, i.e. for $\Delta H \simeq H_0 + \frac{2S_w}{S_u}$, which corresponds to an energy barrier $H_c = H_0 + \Delta H$ that is at least twice as large as the initial energy level. Although this is a priori prohibited because condition (II.3.4) is not satisfied, substituting $H_0 + \frac{2S_w}{S_u}$ for ΔH in (II.3.5) would yield $\mu_f \simeq \frac{4}{S_u}$. Because (II.3.5) is monotonic, the duration of the incubation regime, is therefore one order of magnitude smaller than $\frac{4}{S_u}$.

In order to give a simple definition, we could for instance and arbitrarily define an *incubation time* by

$$t_{\text{incub}} := \frac{1}{2S_u}, \quad (\text{II.3.6})$$

which corresponds to $\epsilon = \frac{1}{8}$, a number that is assumed to be small compared to 1. From a practical point of view, this means that the first-passage time might be estimated with (II.3.5) and that the resulting estimation is valid, provided it is shorter than t_{incub} . As a consequence of our arbitrary definition choice for t_{incub} , the error on the estimated first-passage time is, in the worst case, $1 - \ln(1 + \frac{1}{8})/(\frac{1}{8}) = 5.8\%$.

Now, Equation (II.3.3) can be rewritten

$$\mu_f(H_0) = \frac{4}{S_u} \ln \left(1 + \frac{\Delta H^*}{H_0^* + 1} \right) = 8t_{\text{incub}} \ln \left(1 + \frac{\Delta H^*}{H_0^* + 1} \right) \quad (\text{II.3.7})$$

where the dimensionless groups H_0^* and ΔH^* are defined by

$$H_0^* = \frac{H_0 S_u}{2S_w} \quad ; \quad \Delta H^* = \frac{\Delta H S_u}{2S_w}. \quad (\text{II.3.8})$$

Multiplicative regime. If $\Delta H^* \ll H_0^* + 1$, we recover condition (II.3.4), the logarithm may be linearized, the first-passage time is proportional to ΔH^* and is much smaller than the incubation time. Otherwise, if $\Delta H^* \gtrsim H_0^* + 1$, the logarithm cannot be linearized, and the expected first-passage time is of the order of the incubation time or more. Two other limiting cases are interesting.

Either $H_0^* \gg 1$ and the expected first-passage time required to go from a relatively large initial energy level to an even larger energy level tends to $4/S_u \ln(1 + \Delta H^*/H_0^*) = 4/S_u \ln(H_c/H_0)$. It therefore depends on by how much the initial energy is multiplied to obtain the target energy level. This regime is therefore called the *Multiplicative regime*. In this condition, the first-passage time is independent of the forcing excitation intensity S_w . In the overlap between the multiplicative and the incubation regimes the linearized solution reads

$$\mu_f^{(M)} = \frac{4}{S_u} \frac{\Delta H}{H_0}. \quad (\text{II.3.9})$$

Additive regime. Alternatively, $H_0^* \ll 1$ and the (large) first-passage tends to $4/S_u \ln(1 + \Delta H^*)$. In this latter case, no matter the smallness of the initial energy H_0 in the system, provided it is much smaller than $2S_w/S_u$, it does not influence the expected first-passage time. In this regime, the expected first-passage time only depends on the increase in energy ΔH^* . This regime is therefore called the *Additive regime*. In the overlap between the additive and the incubation regimes the linearized solution reads

$$\mu_f^{(A)} = \frac{2}{S_w} \Delta H, \quad (\text{II.3.10})$$

which recovers the limit case $S_u = 0$.

Figure II.2 presents the ratio $\frac{\mu_f S_u}{4} = \frac{\mu_f}{8t_{\text{incub}}}$ as a function of H^* and ΔH^* and identifies the three regimes (incubation, additive and multiplicative). For different values of H^* and ΔH^* , Figure II.3 shows four realizations of $H(t)$ as well as the expected first-passage time $H_c(\mu_f)$. Subplots *a*, *b*, *c* and *d* correspond to the four corners of Figure II.2, i.e. $H_0^* = 10^{-2}$ or 10^1 and $\Delta H^* = 10^{-1}$ or 10^1 . The parametric excitation is fixed at $S_u = 10^{-3}$, which corresponds to an incubation time $t_{\text{incub}} = 500$ and simply means that $H_c(\mu_f)$ increases more or less linearly for expected first-passage times shorter than 500. Whether or not the expected first-passage time versus the target energy level curve $\mu_f(H_c)$ exhibits a nonlinear profile depends on the target energy level. In case *a*, corresponding to the additive regime, the curve $\mu_f(H_c)$ is nonlinear as the first-passage time is longer than the incubation time and the expected first-passage time is governed by the energy increase ΔH^* . This is confirmed in the upper left corner of Figure II.2 which presents horizontal asymptotes in the additive regime. Similarly, case *b* representing the multiplicative regime presents a nonlinear $\mu_f(H_c)$ curve and, in this regime, the first-passage time is governed by the ratio H_c/H_0 . This is visible by the unit slope of the isocurves in Figure II.3. Finally, cases *c* and *d* corresponding to the incubation regime with a first-passage time much smaller than 500 present a linear increase of the expected first-passage time with the target energy.

The bottom left corner and the upper right corner in Figure II.2 represent the two limiting cases where the loading is either forcing or parametric, respectively. The additive regime therefore appears as a novelty of the combination of these two types of excitation.

Figure II.4 presents the first-passage time of a slightly perturbed system (ε is of order 10^{-3}) for different target energy barriers H_c and different excitations (forced excitation in (a) and parametric excitation in (b)). The logarithmic evolution when $S_w = 0$ and the linear evolution when $S_u = 0$ are respectively observable in bold in each Figure. The small circles represent Monte Carlo simulations. As expected, the first order solution μ_f provides accurate results for this small value of ε . The linearized solution (II.3.5) is represented in dotted line and fits well the exact solution for values of μ_f that are much smaller than the incubation time, i.e. on the upper Figure $\frac{S_u}{4}\mu_f \ll 1$. In both graphs, increasing the parametric or forced excitation decreases the first-passage time.

Monte Carlo data are obtained by simulation of Equation (II.2.1) departing from a given energy H_0 and until the energy reaches the higher expected target energy H_c . Time is recorded for each first passage of one of the expected values of H_c and this is repeated a large amount of times (2000 simulations in this case). This operation provides simulations of the first-passage time for one value of H_0 and various values of H_c and can be repeated independently for other values of H_0 .

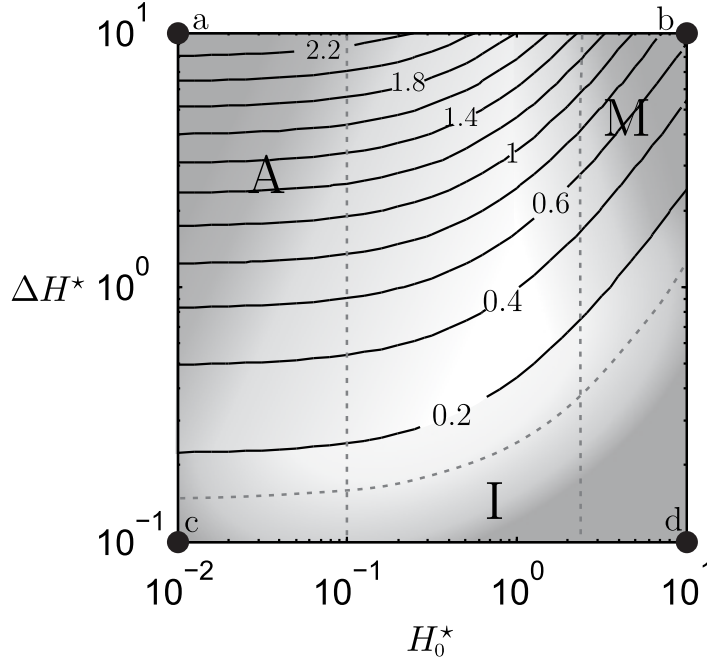


Figure II.2: Dimensionless first-passage time $\frac{\mu_f S_u}{4} = \frac{\mu_f}{8t_{incub}}$ as a function of H_0^* and ΔH^* and identification of the Incubation (I), Multiplicative (M) and Additive (A) regimes.

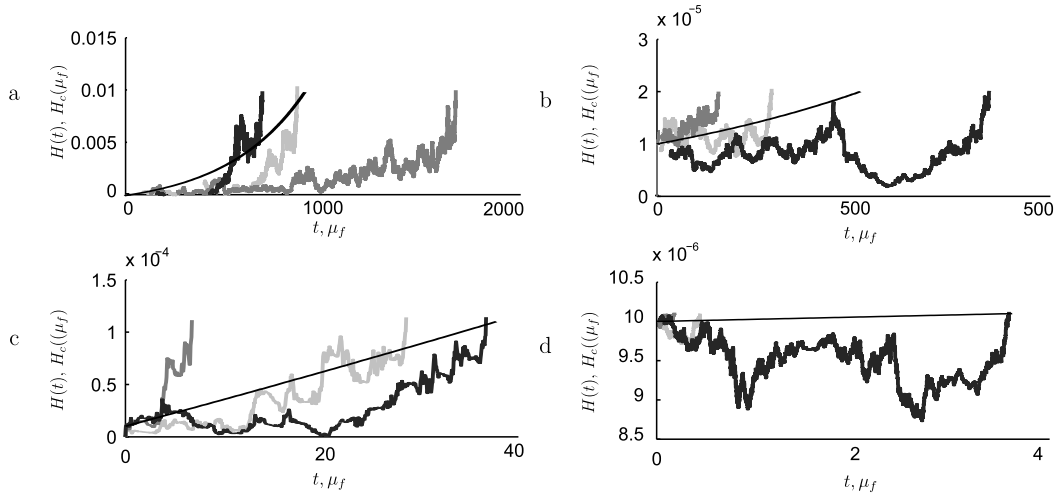


Figure II.3: Realizations of the Hamiltonian and average first-passage time with $S_u = 10^{-3}$ and $H_0 = 10^{-5}$ for the four corners of Figure II.2.

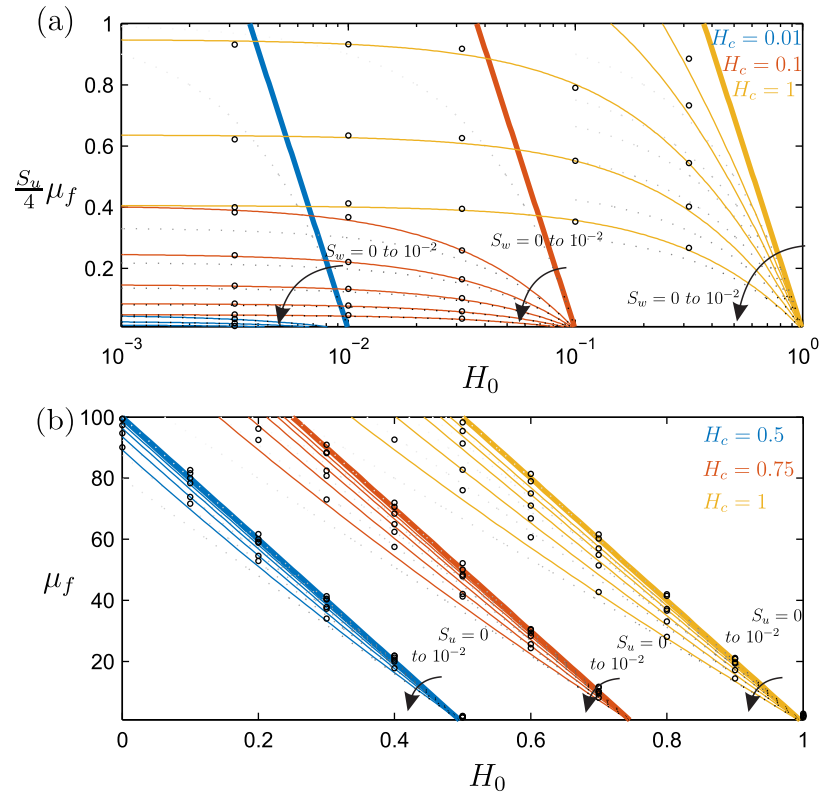


Figure II.4: Average first-passage times (a) for different values of S_w and $S_u = 10^{-2}$ and (b) for different values of S_u and $S_w = 10^{-2}$.

As a first variant, in Section III.1, the second order solution is developed in order to improve the accuracy of the solution for larger values of ε , i.e. for larger excitation intensities. As a second variant, Section III.2 will present the leading order solution of the damped oscillator.

II.4 Conclusion

Based on an asymptotic approach, this Chapter derives and discusses an analytical solution of the average first-passage time of a quasi-Hamiltonian oscillator simultaneously submitted to white noise parametric and forcing excitations of small intensities. It is observed that the asymptotic solution of the Pontryagin equation, at leading order, provides a good approximation of the solution when excitations are small. The derivation highlighted the dependence of the expected first-passage time on the Hamiltonian, globally, and not on the position and velocity separately. Three different regimes have been highlighted, namely the incubation regime (I), the multiplicative regime (M) and the additive regime (A). These three regimes exhibit different features and the behavioral responses of the system, mainly the linear or log scaling of the first-passage time with the target energy level, was thoroughly discussed and analyzed with the help of the two dimensionless groups H_0^* and ΔH^* .

At each step, analytical solutions were validated with Monte Carlo simulations in order to demonstrate the accuracy of the closed form solutions. The analysis performed here on the linear undamped oscillator under white noise excitations highlights a relevant framework for the first-passage time problem. The framework composed of the reduced energy and the three regimes will be used for the study of more complex systems in Chapter III.

Chapter III

Analytical determination of the first-passage time in more general conditions

This chapter successively releases the different assumptions of Chapter II. The influence of each simplification on the first-passage problem is described in details. In this context, one observes successively the *second order* term of the asymptotic expansion, the *damped* oscillator and the *variance* of the first-passage time; while all the other assumptions remain valid.

-
- III.1 Second order solution of the average first-passage time
 - III.2 Damped oscillator
 - III.3 Variance of the first-passage time
 - III.4 Conclusion
-

This Chapter is based on the following articles:

Vanvinckenroye, H., & Denoël, V. (2017). Average first-passage time of a quasi-Hamiltonian Mathieu oscillator with parametric and forcing excitations. *Journal of Sound and Vibration*, 406, pp. 328–345.

Vanvinckenroye, H. and Denoël, V. (2018). Second-order moment of the first passage time of a quasi-Hamiltonian oscillator with stochastic parametric and forcing excitations. *Journal of Sound and Vibration*, 427, pp. 178–187.

Chapter II	Chapter III			Chapter V
Reference case	III.1	III.2	III.3	
1st order	2nd order	1st order	1st order	N/A
undamped	undamped	damped	undamped	damped
average FPT	average FPT	average FPT	variance of the FPT	complete distribution
linear	linear	linear	linear	nonlinear
white noise excitations	white noise excitations	white noise excitations	white noise excitations	evolutionary excitation

Table III.1: Release of the assumptions of the reference case defining the different variants.

The previous Chapter fully focused on the first order solution for the average first-passage time of the undamped oscillator (II.2.1). In this Chapter, the different assumptions are released and discussed one by one. The different variants are presented in Table III.1 together with the organization of this Chapter. First, the *second order* solution of the asymptotic expansion as well as the boundary solution are developed and their importance in the domain is discussed. Then, the *damped* oscillator is considered and the influence of damping on the average first-passage time and the three identified regimes is studied. Finally, the *variance* of the first-passage time represents the spread of the distribution and is of high interest for risk assessment. Each of those assumptions is released while all others are kept unchanged in order to understand its influence on the problem. Each condition release brings complexity into the solution so that a more complex system (more than one condition simultaneously released) is too complex to be studied analytically. The purpose of this Chapter is not the development of an accurate solution for a complex system but a comprehension of each of the conditions and its influence on the first-passage time problem. Beside, a numerical approach is developed in Chapter V to provide an accurate estimation of the complete first-passage time distribution of a nonlinear damped system under evolutionary excitation, as well as its degenerate cases.

III.1 Second order and boundary layer solutions of the average first-passage time

This section establishes the second order (in the sense of perturbations) and boundary layer solutions of the average first-passage time as given in (II.2.9) and according to the asymptotic expansion developed in Chapter II following Khasminskii's approach [95]. This solution improves the accuracy of the solution and becomes significant for moderate values of ε . The importance of this term is

observed and the range of parameters where it becomes significant is described.

III.1.1 Pontryagin equation

First order developments have shown that averaging is more natural in the energy-phase space. In fact, the governing Equation (II.2.1) has been solved in the (q, p) space but the same solution could have been obtained using variables k and θ from the very beginning, i.e. solving

$$d\tilde{\mathbf{x}} = \tilde{\mathbf{a}}(\tilde{\mathbf{x}}, t)dt + \tilde{\mathbf{b}}(\tilde{\mathbf{x}}, t)d\mathbf{B}, \quad (\text{III.1.1})$$

where $\tilde{\mathbf{x}} = \begin{bmatrix} k \\ \theta \end{bmatrix}$, $\tilde{\mathbf{a}} = \begin{bmatrix} \gamma_1 \\ 1 + \gamma_2 \end{bmatrix}$ and $\tilde{\mathbf{b}} = \begin{bmatrix} -k \cos \theta \sin \theta & \frac{\cos \theta}{2} \\ \sin^2 \theta & -\frac{\sin \theta}{2k} \end{bmatrix}$ and where the Wong-Zakai correction terms are given, according to (I.6.7), by

$$\gamma = \varepsilon (\nu_w - 4k\nu_{uw} \sin \theta + 4k^2\nu_u \sin^2 \theta) \begin{bmatrix} \frac{\sin^2 \theta}{8k} \\ \frac{\cos \theta \sin \theta}{4k^2} \end{bmatrix}. \quad (\text{III.1.2})$$

The corresponding drift matrix $\tilde{\mathbf{J}} = \varepsilon \tilde{\mathbf{b}}(\tilde{\mathbf{x}}, t) \boldsymbol{\nu} \tilde{\mathbf{b}}^T(\tilde{\mathbf{x}}, t)$ is still of order ε . The invariant operators \mathcal{L}_1 and \mathcal{L}_2 become

$$\mathcal{L}_1 \{ \cdot \} = \frac{\partial \cdot}{\partial \theta} \quad ; \quad \varepsilon \mathcal{L}_2 \{ \cdot \} = \delta_1 \frac{\partial \cdot}{\partial k} + \delta_2 \frac{\partial \cdot}{\partial \theta} + \frac{1}{2} \tilde{J}_{11} \frac{\partial^2 \cdot}{\partial k^2} + \frac{1}{2} \tilde{J}_{22} \frac{\partial^2 \cdot}{\partial \theta^2} + \tilde{J}_{12} \frac{\partial^2 \cdot}{\partial k \partial \theta}. \quad (\text{III.1.3})$$

Again, from here, the subscript “0” is dropped. It will be reintroduced in (III.1.13). This formulation clearly indicates that the operator \mathcal{L}_1 represents the variation along the orbits of constant energy H or k , as announced and used in the previous Chapter.

Similarly to what was done to determine u_0 , the second order term u_1 is obtained by solving (II.2.12), with u_0 being pushed to the right-hand side since it is now known,

$$\mathcal{L}_1 \{ u_1 \} = \frac{\partial u_1}{\partial \theta} = -1 - \mathcal{L}_2 \{ u_0 \}. \quad (\text{III.1.4})$$

The solution of this equation takes the form

$$u_1(k, \theta) = u_{11}(k, \theta) + u_{12}(k), \quad (\text{III.1.5})$$

where

$$u_{11}(k, \theta) = \frac{k^2 S_u \sin 2\theta}{2(k^2 S_u + S_w)^2} \left[k^2 S_u (\cos 2\theta - 2) - 3S_w \right. \\ \left. + \frac{8 \sin^2 \frac{\theta}{2}}{3k \sin 2\theta} S_{uw} \left(2k^2 (2 \cos \theta + \cos 2\theta) - 6 \frac{S_w}{S_u} \right) \right]. \quad (\text{III.1.6})$$

is the general solution of the differential equation in θ while $u_{12}(k)$ plays the role of a constant of integration, independent of θ . The cross correlation S_{uw} influences the second order solution while it did not affect the first order one and, depending on the initial conditions, can be the governing term of u_{11} as the energy k appears in the denominator of S_{uw} . More details and complete derivation of expressions for u_{11} and u_{12} are given in Appendix B. The constant of integration is determined at the next order, with Equation (II.2.13) averaged over one period of the unperturbed oscillator

$$\langle \mathcal{L}_1 \{u_2\} \rangle + \langle \mathcal{L}_2 \{u_{11}\} \rangle + \langle \mathcal{L}_2 \{u_{12}\} \rangle = 0 \quad (\text{III.1.7})$$

whose solution reads, after some developments (see Appendix B),

$$u_{12}(k) = \frac{4k\nu_{uw}}{3} \frac{(k^2\nu_u + 3\nu_w)}{(k^2\nu_u + \nu_w)^2} + \frac{C_1}{\nu_w} \ln \left(\frac{k^2}{k^2\nu_u + \nu_w} \right) + C_2 \quad (\text{III.1.8})$$

and where constant C_1 is shown to vanish. The constant C_2 is determined by matching with the boundary layer solution in order to respect the first boundary condition.

Unlike for the general form (II.2.21) of u_0 , the boundary conditions (I.6.26) cannot be satisfied with the general form of solution for u_1 . A boundary layer solution therefore develops in the neighborhood of $\partial\mathcal{D}$, which is here restricted to a circle, in order to satisfy the second boundary condition. It is obtained by following the standard steps for the derivation of an asymptotic boundary solution [96, 98, 99, 100]. Therefore, the stretched coordinate $\zeta = \frac{H-H_c}{\sqrt{\varepsilon}}$ is introduced in order to focus on the small region in the neighborhood of $H = H_c$. Then, the equation to be solved $\mathcal{L}^* \{G_n\} = 0$ is considered at the different orders in $\sqrt{\varepsilon}$ and a regular ansatz in the stretched coordinate system

$$G_n(\zeta, \theta) = g_1(\zeta, \theta) + \sqrt{\varepsilon}g_2(\zeta, \theta) + \dots + \varepsilon^{\frac{n-1}{2}}g_n(\zeta, \theta) \quad (\text{III.1.9})$$

is substituted into the governing equation. The leading order equation reads

$$\frac{\partial g_1}{\partial \theta} + 4H_c \tilde{J}_{11}(H_c, \theta) \frac{\partial^2 g_1}{\partial \zeta^2} = 0 \quad (\text{III.1.10})$$

so that the leading order solution $g_1(\zeta, \theta)$ satisfying the boundary condition $g_1(0, \theta) = -u_1(H_c, \theta)$ and the matching condition $g_1(\zeta, \theta) \rightarrow 0$ when $\zeta \rightarrow -\infty$ is

$$g_1(\zeta, \theta) = \sum_{n=1}^{\infty} a_n e^{\sqrt{\frac{nc_1}{2}}\zeta} \sin \left(n\alpha(\theta) - \sqrt{\frac{nc_1}{2}}\zeta \right) \quad (\text{III.1.11})$$

with

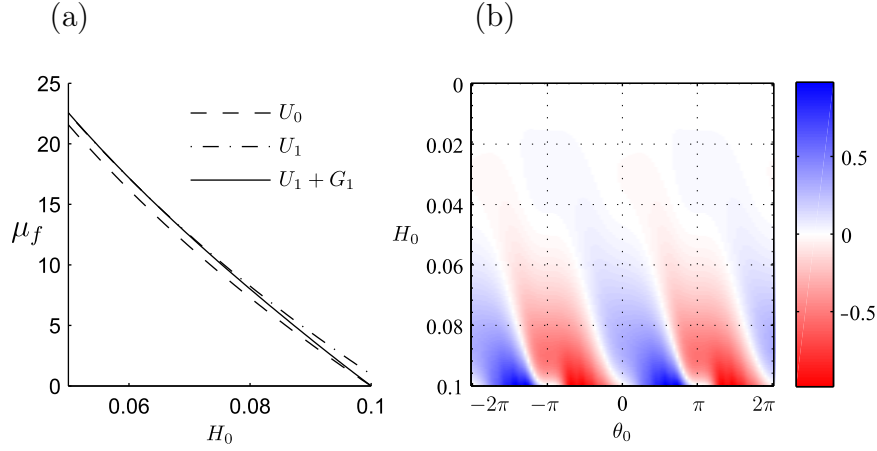


Figure III.1: (a) Comparison of the first order, second order and boundary layer terms with $\theta = 3\pi/4$ (b) Evolution of the boundary layer solution g_1 with $S_u = 0$, $S_w = 0.001$, $H_c = 0.1$.

$$c_1 = \frac{2\pi}{\int_0^T 4H_c \tilde{J}_{11}(H_c, s) ds}, \quad \alpha(\theta) = 2\pi \frac{\int_0^\theta 4H_c \tilde{J}_{11}(H_c, s) ds}{\int_0^T 4H_c \tilde{J}_{11}(H_c, s) ds},$$

and where coefficients a_n are shown to be given by

$$a_n = -\frac{1}{\pi} \int_0^{2\pi} u_1(H_c, \theta(\alpha)) \sin(n\alpha) d\alpha. \quad (\text{III.1.12})$$

Up to second order, the mean first-passage time is finally given by

$$\mu_f(p_0, q_0) = \frac{1}{\varepsilon} u_0[H(p_0, q_0)] + u_1[k(p_0, q_0), \theta(p_0, q_0)] + g_1 \left[\frac{H(p_0, q_0) - H_c}{\sqrt{\varepsilon}}, \theta(p_0, q_0) \right], \quad (\text{III.1.13})$$

with $u_0(H_0)$, $u_1(k, \theta)$ and $g_1(\zeta, \theta)$ given by relations (II.2.22), (III.1.6) and (III.1.11). Notice the subscript “0” has been re-introduced in the last results in order to stress out that the first-passage time depends on the initial energy level H_0 and the initial position q_0 and velocity p_0 .

III.1.2 Analysis and discussion

Figure III.1 (a) presents the first and second order solution U_0 and U_1 , together with the boundary layer solution g_1 . The boundary condition $\mu_f(H_c) = 0$ is respected for the leading order solution U_0 and when the second order and the

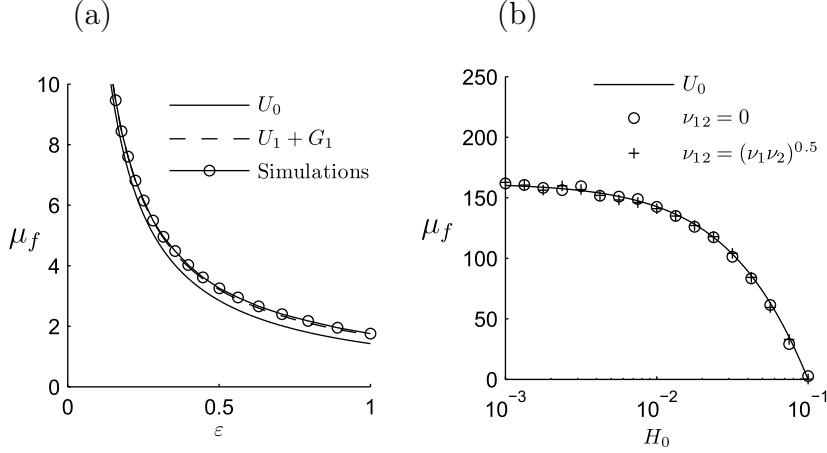


Figure III.2: (a) Comparison of the first and second order solution with simulations for different values of ε with $\nu_u = \nu_w = 1$, $H_0 = 0.01$, $H_c = 1$ and $\theta = 3\pi/4$ (b) Comparison of the solution for independent and fully correlated white noises with $S_u = 0.1$, $S_w = 0.01$ and $H_c = 0.1$.

boundary layer are both taken into account. While the first order solution depends on the Hamiltonian only, the two second order solutions depend on both the Hamiltonian H_0 and the phase θ_0 . Figure III.1 (b) presents the evolution of the boundary layer in the (H_0, θ_0) -plane. The highest values are observed for $H = H_c$, on the boundary and g_1 exponentially vanishes for decreasing initial energy levels.

Figure III.2 (a) presents the evolution of the first and second order solutions with the excitation intensities. The comparison with Monte Carlo simulations illustrates the accuracy of the asymptotic expansion as a function of the smallness of the parameter ε . As expected, the first order solution matches almost perfectly for small intensities until values of ε of about 0.1 while the second order solution is virtually perfect for values as large as $\varepsilon \simeq 1$. The precision of the method decreases with increasing values of ε but still provides very good results. Figure III.2 (b) compares the first order solution U_0 with simulations for fully correlated and independent white noises. As the excitation intensities are small ($\varepsilon = 0.1$), the first order solution is a good approximation and the first-passage time is therefore independent of the correlation between the forced and parametric excitations. This is confirmed by the superposition of the results of Monte Carlo simulations (dots and crosses).

III.2 Damped oscillator

As all physical systems are damped (at least slightly), it is natural to study the influence of the damping on the first-passage time. Moreover, the dynamics of

the oscillator –and thus the first-passage time– are expected to be influenced by the memory of the oscillator.

In order to limit the complexity of the following developments, only leading order terms of the first-passage time are determined. Following the observations of Section III.1, this means that the following results shall be used for small (and not moderate) values of ε . Also, in order to lighten the presentation, only main results are presented in the bulk of the text; details are presented in Appendix C.

The system observed here is

$$\ddot{x}(t) + 2\xi\dot{x}(t) + [1 + u(t)]x(t) = w(t), \quad (\text{III.2.1})$$

with ξ the small damping ratio, of order ε at most, so that rewriting $\xi = \varepsilon\nu_\xi$, the re-scaled damping ν_ξ is of order one at most.

III.2.1 Pontryagin equation

The first-passage time is the solution of Equations (II.2.11) and (II.2.12) with the new averaged Itô formulation of the system. This leads to the same formulation for \mathcal{L}_1 and an additional term in \mathcal{L}_2 , see (C.0.3). Performing the same developments as before in the undamped case (which are reproduced in Appendix C), the drift and diffusion coefficients $m(H)$ and $\sigma(H)$ are now given by

$$\begin{cases} m(H) = \frac{H}{2}S_u + \frac{1}{2}S_w - 2H\xi \\ \sigma(H) = \sqrt{\frac{H^2}{2}S_u + HS_w} \end{cases} \quad (\text{III.2.2})$$

and the expected first-passage time at first order finally reads

$$\begin{aligned} \mu_f(H_0) = & \frac{4}{S_u(1-a)} \left[\ln \left(1 + \frac{\Delta H^*}{H_0^*} \right) + \frac{(1 + H_0^* + \Delta H^*)^a - (1 + H_0^*)^a}{a} \right. \\ & \left. - \int_{H_0^*}^{H_0^* + \Delta H^*} \frac{(1+t)^a}{t} dt \right]. \end{aligned} \quad (\text{III.2.3})$$

with $a = \frac{8\nu_\xi}{\nu_u} = \frac{8\xi}{S_u}$.

III.2.2 Analysis and discussion

Damping enters in the average first-passage time (III.2.3) only through the parameter a , i.e. through its ratio with the dimensionless intensity of the parametric excitation. There are two interesting limiting cases:

- when there is no parametric excitation, i.e. $S_u = 0$, the general solution degenerates into

$$\mu_f = -\frac{1}{2\xi} \ln \left(1 + \frac{\Delta H^*}{H_0^*} \right) + \frac{\text{Ei}(aH_0^* + a\Delta H^*) - \text{Ei}(aH_0^*)}{2\xi} \quad (\text{III.2.4})$$

with $\text{Ei}(\cdot)$ the exponential integral defined by $\text{Ei}(x) = \int_{-\infty}^x \frac{e^t}{t} dt$. The limit solution for $\xi = 0$ is given by $\mu_f(H_0) = 2\frac{H_c - H_0}{S_w}$ which was already obtained in the undamped configuration. It is interesting though to notice that the linearity of the solution, i.e. the expected first-passage proportional to the increase in the Hamiltonian, regularly vanishes as damping is introduced into the problem.

- when there is no forcing term, i.e. $S_w = 0$, the solution degenerates into

$$\mu_f = \frac{4}{S_u(1-a)} \ln \left(1 + \frac{\Delta H^*}{H_0^*} \right) \quad (\text{III.2.5})$$

In this case, the damping does not modify the form of the first-passage time, which still increases like the logarithm of the ratio H_c/H_0 . This solution presents a positive first-passage time for $a < 1$, which means that the energy of the system can increase, on average, if the damping ratio has an intensity below a certain threshold, $\xi < S_u/8$. For $a \geq 1$, the dissipation mechanism drives the dynamical system to lower energy levels, on average. The evaluated expected first-passage time is negative. It has no meaning anymore since the Itô formulation on which the developments are based is no more valid. For a damping ratio equal to the critical threshold, the dissipated energy balances the injected energy and the first-passage time is not defined, as illustrated in Figure III.3 (a). Figure III.3 (b) presents time series of the system for different values of ξ so that the first-passage time is positive, not defined or invalid (negative, on average) for $\xi = -S_u$, $S_u/8$ or S_u .

Let us notice that the case where $S_u = 0$ and $S_w = 0$ is deterministic and provides in the undamped case a harmonic motion of constant energy and in the damped case an exponentially decreasing energy. The system is governed by $\ddot{x} + 2\xi\dot{x} + x = 0$, whose solution is

$$x(t) = e^{-\xi t} \left(x_0 \cos \omega_d t + \frac{\dot{x}_0 + \xi x_0}{\omega_d} \sin \omega_d t \right) \quad (\text{III.2.6})$$

with $\omega_d = \sqrt{1 - \xi^2}$. The initial position and velocity are given by x_0 and \dot{x}_0 . For small damping ratio, the Hamiltonian of the system evolves as $H(t) = H_0 e^{-2\xi t}$ and agrees with $\mu_f = \frac{-1}{2\xi} \ln \frac{H_c}{H_0}$, the limit solution of (III.2.3) for $\{S_u, S_w\} \rightarrow 0$.

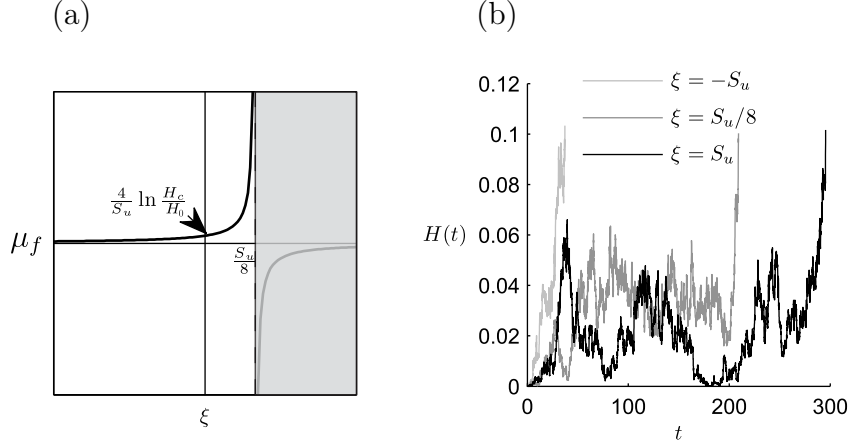


Figure III.3: (a) First-passage time μ_f as a function of the damping coefficient ξ for $S_w = 0$ (b) Realizations of the Hamiltonian for $H_0 = 10^{-5}$, $S_u = 10^{-2}$, $S_w = 10^{-3}$ and different values of ξ .

In this case the concept of expected first-passage time has no physical meaning if the damping is positive.

Three regimes were identified for the undamped oscillator in Section II.3. The asymptotic behaviors can be developed similarly for the damped system:

Incubation regime. By analogy with the undamped oscillator, the first-passage time in the incubation regime, i.e. for $\Delta H^* \ll H_0^* + 1$ is evaluated as the leading order term of the Mac-Laurin series expansion of (III.2.3) for small ΔH^* , which yields

$$\mu_f^{(I)} = \underbrace{\frac{4}{S_u} \frac{\Delta H^*}{H_0^* + 1}}_{\mu_f(H_0)|_{a=0}} \underbrace{\frac{H_0^* + 1 - (H_0^* + 1)^a}{(1-a)H_0^*}}_{f(a, H_0^*)}. \quad (\text{III.2.7})$$

Equation (III.2.7) shows that the first-passage time is still proportional to the dimensionless group $\Delta H^*/(H_0^* + 1)$ with an additional factor ($f(a, H_0^*) \geq 1$) modeling the increase of the first-passage time with the damping ratio. Notice that $f(a, H_0^*)$ is independent of the energy increase ΔH^* and is asymptotic to $1 + [1 - \ln(H_0^* + 1)] H_0^{*-1} a + \text{ord}(a^2)$ as $a \rightarrow 0$. Based on the expression of the average first-passage time when $S_w = 0$ given by (III.2.5), one defines an incubation time for the damped oscillator $t_{incub} = \frac{1}{2S_u(1-a)} = \frac{t_{incub}|_{a=0}}{1-a}$, corresponding to the domain where the logarithm can be linearized.

Additive regime. For $H_0^* \ll 1$, the average first-passage time becomes

$$\mu_f^{(A)} = \frac{4}{S_u(1-a)} \left[\ln \Delta H^* - \frac{(1 + \Delta H^*)^{1+a} F(1-a, -1/\Delta H^*)}{a\Delta H^*} \right. \\ \left. + \frac{(1 + \Delta H^*)^a}{a} + E\Gamma + \pi \cot(a\pi) + P\Gamma(a) \right] \quad (\text{III.2.8})$$

where the hypergeometric function ${}_2F_1$ is represented by $F(c, z) = {}_2F_1(1, 1, c, z)$, $E\Gamma$ is Euler's constant and $P\Gamma(x)$ represents the digamma function. Expression (III.2.8) is of little interest due to its high complexity. However, an important observation is the independence of the expression in the initial energy H_0^* , which is a typical feature of the additive regime, as illustrated for the undamped system in Section II.3.

Multiplicative regime. The multiplicative regime of the damped oscillator is defined by $a\frac{\Delta H^*}{H_0^*} \ll 1$ & $H_0^* \gg 1$, corresponding to the lower right triangle in the logarithmic plane of Figure III.4 (a). Increasing values of a restrict the multiplicative regime to larger values of H_0^* or smaller values of ΔH^* , i.e. to a smaller triangle. In this domain, the average first-passage time is given by

$$\mu_f^{(M)} = \frac{4}{S_u(1-a)} \left[\ln \left(1 + \frac{\Delta H^*}{H_0^*} \right) - \frac{\Delta H^*}{H_0^{*2-a}} \right]. \quad (\text{III.2.9})$$

When a is of an order smaller than one ($a \ll 1$), the first term dominates so that the average first-passage time mainly depends on the ratio $\frac{\Delta H^*}{H_0^*}$, corresponding to a unitary slope of the curves of same first-passage time in a logarithmic scale (see Figure III.4 (a)). When the order of magnitude of a is higher than 1, the second term dominates so that the average first-passage time mainly depends on the ratio $\frac{\Delta H^*}{H_0^{*2-a}}$, corresponding to a slope of the curves of same first-passage time equal to $2 - a$ in the graph of Figure III.4 (a). Consequently, the slope becomes negative for $a > 2$, and the average first-passage time increases with increasing values of H_0^* . For values of a of order 1, both terms have the same order and must be taken into account for the average first-passage time. The multiplicative regime is not anymore characterized by a unitary slope of the curves of first-passage time –the term *multiplicative* being related to the ratio $\frac{\Delta H^*}{H_0^*}$ – but rather by oblique asymptotes of equal slope corresponding to different powers of ΔH^* and H_0^* .

The particular case $a = 2$ is interesting since the average first-passage time is independent of the initial energy H_0^* in both the additive and multiplicative regimes. The limit of expression (III.2.3) as $a \rightarrow 2$ provides

$$\lim_{a \rightarrow 2} \mu_f = \frac{4\Delta H^*}{S_u} = \frac{2\Delta H}{S_w}. \quad (\text{III.2.10})$$

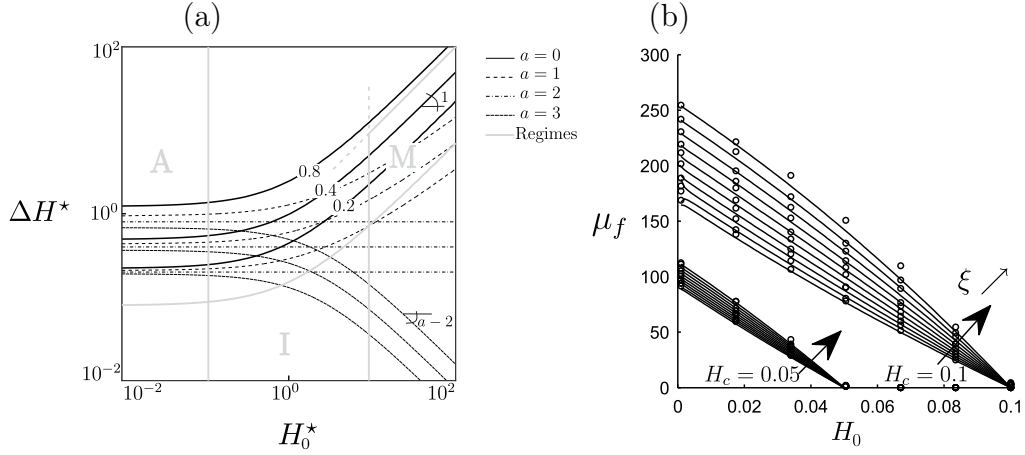


Figure III.4: (a) Representation of $\frac{\mu_f S_u}{4}$ as a function of H_0^* and ΔH^* for different damping ratios (b) Average first-passage time μ_f for different damping coefficients $\xi = 0$ to 0.005 with $H_c = 0.05$ and 0.1, $S_u = 0$, $S_w = 10^{-3}$.

First, Expression (III.2.10) shows that the solution for $a \rightarrow 2$ is unique in the additive and multiplicative regimes, and independent of H_0^* , which corresponds to horizontal straight lines of average first-passage time in Figure III.4 (a). Secondly, the average first-passage time for $a = 2$, $S_w \neq 0$ and $S_u \neq 0$ is identical to the average first-passage time of the undamped oscillator ($\xi = 0$) with $S_u = 0$ given in Section II.3 by Equation (II.3.1). This means that, from the first-passage time point of view and in presence of a forcing excitation ($S_w \neq 0$), the energy injected into the system by the parametric excitation u is perfectly balanced by the dissipation due to damping if $a = 2$, i.e. $\xi = \frac{S_u}{4}$.

Finally, the particular case $a = 1$ corresponding to a mathematical singularity of Expression (III.2.3) provides

$$\lim_{a \rightarrow 1} \mu_f = \frac{4}{S_u} \int_{H_0^*}^{H_0^* + \Delta H^*} \frac{\ln(1+t)}{t} dt. \quad (\text{III.2.11})$$

However, no singularity is observed in the first-passage time and the problem evolves regularly for values of a around 1.

Figure III.4 (a) shows the reduced expected first-passage time $\frac{\mu_f S_u}{4}$, exactly as in Figure (II.2) but for various damping ratios. It is seen that the damping ratio has little influence on the first-passage time in the incubation regime, while it increases the expected first-passage time in the additive regime where horizontal asymptotes are observed due to the independence of the average first-passage time in the initial energy H_0^* . In the multiplicative regime (right part of the map), the damping ratio changes the slope of the curves of equal first-passage times, that becomes negative for $a > 2$. In all regimes, increasing the damping ratio increases the first-passage time.

(III.2.3)	$S_u = 0$	$S_w = 0$	$\xi = 0$
$S_u = 0$	$-\frac{1}{2\xi} \ln \left(\frac{H_c}{H_0} \right) + \frac{\text{Ei}(4\xi H_c/S_w) - \text{Ei}(4\xi H_0/S_w)}{2\xi}$	Deterministic	$2 \frac{H_c - H_0}{S_w}$
$S_w = 0$	sym.	$\frac{4}{S_u - 8\xi} \ln \frac{H_c}{H_0}$ <i>if</i> $\xi < S_u/8$	$\frac{4}{S_u} \ln \frac{H_c}{H_0}$
$\xi = 0$	sym.	sym.	$\frac{4}{S_u} \ln \left(\frac{H_c S_u + 2S_w}{H_0 S_u + 2S_w} \right)$

Table III.2: Summary of the analytical results and limit cases at first order.

Figure III.4 (b) presents the first-passage time as a function of the initial energy H_0 for different values of ξ and H_c . The small circles represent results of Monte Carlo simulations while the full line is the analytical solution. As expected, the first-passage time increases with damping.

Table III.2 presents a summary of the analytical results and their limits.

III.3 Variance of the first-passage time

Because the considered system is stochastic, the time required to reach the total internal energy barrier $H_0 + \Delta H$, starting from energy H_0 is a random variable. Its mean value has already been investigated in Chapter II. The objective of this Section is to determine the second order statistical moment $\mathcal{E} \{t_f^2\}$, in order to provide some information about the spread of this statistical distribution.

III.3.1 Pontryagin equation

The generalized Pontryagin equation (I.6.23), when specified for $n = 2$, provides the following differential equation for the mean square first-passage time of an autonomous system

$$\mathcal{L} \{ \mathcal{E} \{t_f^2\} \} = -\mathcal{E} \{t_f\}, \quad \text{for } \mathbf{x}_0 \in \mathcal{D}. \quad (\text{III.3.1})$$

The boundary class is determined according to equations (I.6.27), see [86]. For $S_w \neq 0$, one finds $\alpha_l = 1$, $\beta_l = 0$ and $c_l = 1$ corresponding to an entrance class and for $S_w = 0$, $\alpha_l = 2$, $\beta_l = 1$ and $c_l = 2$ leading to a repulsively natural boundary class, as announced before, so that the initial condition is given by (I.6.26) while the boundary condition can be replaced by the quantitative condition (I.6.28).

The topology of the generalized Pontryagin equation (I.6.24) is the same for all orders so that one can expect strong similarities between the average and higher moments. Indeed, the homogeneous part of (I.6.24) is identical to that of (III.3.1) while the non-homogeneous part injects the previous order solution with its characteristics. This recurrence leads to very similar features for all statistical

moments. This is why the mean square and variance of the first-passage time are now studied in the light of the three previously identified regimes.

Accounting for the boundary conditions, it might be shown that the general solution of (III.3.1) for $n = 2$, with $\mathcal{E}\{t_f\} = \mu_f(\mathbf{x}_0)$ given by (II.2.22), is

$$\begin{aligned} \mathcal{E}\{t_f^2\} = & \frac{32}{S_u^2} \left[\mathcal{P}\left(\frac{H_0 S_u + 2S_w}{2S_w}\right) - \mathcal{P}\left(\frac{H_c S_u + 2S_w}{2S_w}\right) \right. \\ & + \ln\left(\frac{H_c S_u + 2S_w}{2S_w}\right) \ln\left(\frac{H_c S_u + 2S_w}{H_c S_u}\right) \\ & - \ln\left(\frac{H_0 S_u + 2S_w}{2S_w}\right) \ln\left(\frac{H_c S_u + 2S_w}{H_0 S_u}\right) \\ & \left. + \ln\left(\frac{H_c S_u + 2S_w}{H_0 S_u + 2S_w}\right) \right]. \end{aligned} \quad (\text{III.3.2})$$

The function \mathcal{P} stands for the real part of the polylogarithmic function and is defined as

$$\mathcal{P}(x) = \text{Re}[\text{Polylog}(2, x)] = \text{Re}\left[-\int \frac{\ln(1-x)}{x} dx\right] \quad \forall x > 1. \quad (\text{III.3.3})$$

This expression for the mean square first-passage time shows the relatively complex interactions between the forcing and parametric excitations. It is valid under the hypotheses that are required to separate the slow energy and the fast phase variables. These are equivalent to assuming a quasi-Hamiltonian system, or that the dimensionless intensities S_u and S_w are small compared to 1.

As a first validation, Figure III.5 compares this analytical solution to the mean square first-passage time $\mathcal{E}\{t_f^2\}$ obtained with Monte Carlo simulations (dots). Each curve corresponds to a different initial energy H_0 ($H_0 = 5, 10, \dots, 40$). The numerical simulations virtually fit and validate the analytical solution, especially in the range of large mean square first-passage time, i.e. where the average first-passage time is large too, which is a required assumption for the stochastic averaging. For target energy levels H_c which are slightly larger than the initial condition H_0 , the stochastic averaging is no longer accurate and a boundary layer solution using Khasminskii's approach needs to be developed, as in Section (III.1) where the boundary solution is developed for the average first-passage time.

As a second validation, we restrict to the case where there is no forcing excitation, i.e. $S_w = 0$, so that the second order moment is given by

$$\lim_{S_w \rightarrow 0} \mathcal{E}\{t_f^2\} = \frac{32}{S_u^2} \left(\ln\left(1 + \frac{\Delta H}{H_0}\right) + \frac{1}{2} \ln\left(1 + \frac{\Delta H}{H_0}\right)^2 \right). \quad (\text{III.3.4})$$

This expression corresponds to existing results in the literature [49].

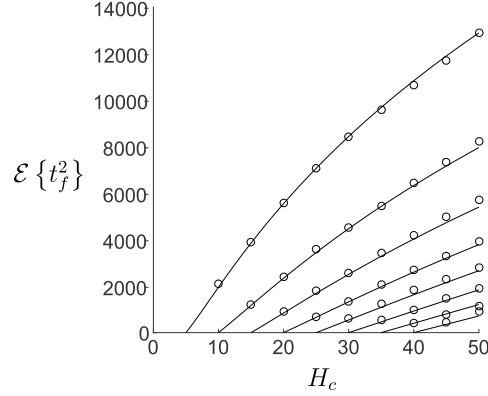


Figure III.5: Second order moment of the first-passage time as a function of the target energy H_c for different values of $H_0 = 5, 10, \dots, 40$, while $S_u = 0.1$ and $S_w = 0.05$; Monte Carlo simulations (dots) and analytical solution (full line).

III.3.2 Analysis and discussion

For further investigation, and similarly to the analysis of the first order moment μ_f that led to the identification of the three regimes (incubation, multiplicative, additive), the mean square first-passage time is rewritten in terms of the reduced initial energy and energy increase H_0^* and ΔH^* defined in (II.3.8). Equation (III.3.2) becomes:

$$\begin{aligned} \frac{S_u^2}{32} \mathcal{E} \{t_f^2\} = & [\mathcal{P}(1 + H_0^*) - \mathcal{P}(1 + H_0^* + \Delta H^*) \\ & + \ln(1 + H_0^* + \Delta H^*) \ln\left(\frac{1 + H_0^* + \Delta H^*}{H_0^* + \Delta H^*}\right) \\ & - \ln(1 + H_0^*) \ln\left(\frac{1 + H_0^* + \Delta H^*}{H_0^*}\right) \\ & + \ln\left(1 + \frac{\Delta H^*}{1 + H_0^*}\right)]. \end{aligned} \quad (\text{III.3.5})$$

This expression is plotted in Figure III.6 (b). This formulation shows that the second order moment of the first-passage time is expressed as the product of $\frac{32}{S_u^2}$ and an expression depending on H_0^* and ΔH^* only. This evidences the different influences of the parametric and forcing excitations S_u and S_w in the energetic behavior of the stochastic oscillator as those two intensities appear as a ratio in the reduced coordinates while S_u^2 also appears as a multiplicative factor, as expected from (II.2.22).

Three regimes were identified through the average first-passage time. The

asymptotic behaviors of the mean square first-passage time in each regime can be developed in a similar manner:

Incubation regime. For $\frac{\Delta H^*}{H_0^*+1} \ll 1$, the mean square is given by

$$\frac{S_u^2}{32} \mathcal{E} \{t_f^2\}^{(I)} = \frac{\Delta H^*}{H_0^*+1} \left(1 - \frac{\ln(1+H_0^*)}{H_0^*} \right) \quad (\text{III.3.6})$$

Additive regime. For $H_0^* \ll 1$ and $\Delta H^* \gg 1$, the second order moment becomes

$$\frac{S_u^2}{32} \mathcal{E} \{t_f^2\}^{(A)} = -\frac{\pi^2}{6} + \frac{\ln(\Delta H^*)}{2\Delta H^*} (4 + \Delta H^* \ln(\Delta H^*)) + \ln(1 + \Delta H^*). \quad (\text{III.3.7})$$

As expected, the limit depends on ΔH^* only, which corresponds to the horizontal asymptotes in the left part of Figure III.6 (b). This behavior was also observed in the average first-passage time. The qualification ‘‘additive’’ therefore remains. However the additive regime is now restricted to the upper left corner, while the entire left part was covered by the asymptotic solution for the average first-passage time. This means that there is no overlap between the incubation and additive regimes anymore.

Multiplicative regime. For $H_0^* \gg 1$, the asymptotic behavior of (III.3.5) is

$$\frac{S_u^2}{32} \mathcal{E} \{t_f^2\}^{(M)} = \ln \left(1 + \frac{\Delta H^*}{H_0^*} \right) + \frac{1}{2} \ln \left(1 + \frac{\Delta H^*}{H_0^*} \right)^2. \quad (\text{III.3.8})$$

This limit depends on the relative energy increase $\frac{\Delta H^*}{H_0^*}$ and confirms the unitary slopes observed in the right part of Figure III.6 (b).

The asymptotic behaviors in each regime are represented with dotted line in Figure III.6. The upper left Figure (a) is a copy of Figure II.2 and is repeated here to be seen in parallel with the other three Figures.

The spread in the distribution of the first-passage time is difficult to assess with the raw moment. Instead, one would naturally evaluate the spread of the distribution of the first-passage time with its variance $\sigma_f^2 = \mathcal{E} \{t_f^2\} - \mu_f^2$, which is represented in Figure III.6 (c) as a function of H_0^* and ΔH^* . The variance increases with ΔH^* . The low dependency on the initial energy H_0^* in the left part of the graph reveals a regular monotonic and slowly varying energy for low energy levels. Indeed, for low energy levels, the energy does not increase significantly for a given time (approximately the incubation time t_{incub}) and once a significant increase is observed, the increasing rate is higher. This can be observed on the simulations presented in Figure II.1.

The spread can even be better evaluated with the coefficient of variation defined as

$$cv_f = \frac{\sigma_f}{\mu_f}. \quad (\text{III.3.9})$$

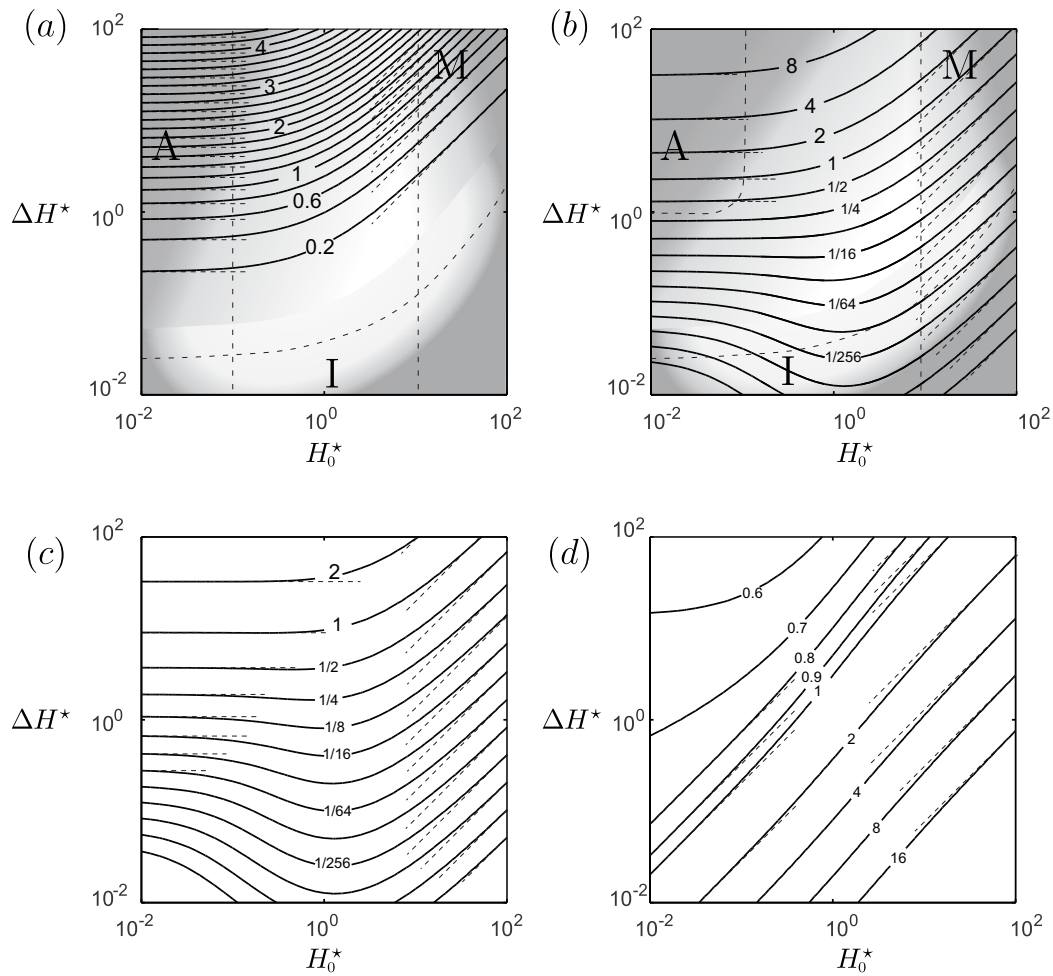


Figure III.6: Representation of (a) the average first-passage time $\frac{\mu_f S_u}{4}$, (b) the mean square $\frac{\mathcal{E}\{t_f^2\} S_u^2}{32}$ first-passage time, (c) the variance $\frac{\sigma_f^2 S_u^2}{32}$ and (d) the coefficient of variation cv_f . Dashed lines represent the asymptotic solutions in each regime.

It is represented in Figure III.6 (d).

Substitution of μ_f and σ_f into this equation provides a relatively cumbersome expression of the coefficient of variation. However simple solutions are obtained in the two following limit cases, when the loading is either of parametric type ($S_w = 0$), either of forcing type ($S_u = 0$).

First, when there is no parametric excitation, i.e. $S_u = 0$, the second order moment of the first-passage time is given by

$$\lim_{S_u \rightarrow 0} \mathcal{E} \{t_f^2\} = \frac{4\Delta H}{S_w^2} \left(H_0 + \frac{3}{2}\Delta H \right) \quad (\text{III.3.10})$$

and the mean square is a quadratic function of the energy increase ΔH . In this case, and based on the limit expression of the mean first-passage time for $S_u \rightarrow 0$ given in Chapter II, $\mu_f = \frac{2\Delta H}{S_w}$, the coefficient of variation is given by

$$\lim_{S_u \rightarrow 0} cv_f = \sqrt{\frac{1}{2} + \frac{H_0}{\Delta H}} \quad (\text{III.3.11})$$

and depends on the proportional energy increase $\frac{\Delta H}{H_0}$ only. This limit behavior is valid in the bottom left corner of Figure III.6 (d) and always provides a coefficient of variation that is larger than $\frac{\sqrt{2}}{2}$.

Second, when there is no forcing excitation, i.e. $S_w = 0$, the second order moment is given by

$$\lim_{S_w \rightarrow 0} \mathcal{E} \{t_f^2\} = \frac{32}{S_u^2} \left(\ln \left(1 + \frac{\Delta H}{H_0} \right) + \frac{1}{2} \ln \left(1 + \frac{\Delta H}{H_0} \right)^2 \right), \quad (\text{III.3.12})$$

which is well known from [49]. In this case, and considering $\mu_f = \frac{4}{S_u} \ln \left(1 + \frac{\Delta H}{H_0} \right)$, the coefficient of variation is given by

$$\lim_{S_w \rightarrow 0} cv_f = \sqrt{\frac{2}{\ln \left(1 + \frac{\Delta H}{H_0} \right)}}. \quad (\text{III.3.13})$$

This limit behavior is valid in the upper right corner of Figure III.6 (d). In this second limit case, the coefficient of variation also depends on the ratio $\Delta H/H_0$ only and is independent of the intensity of the parametric excitation.

The representation of the coefficient of variation cv_f and its asymptotes in Figure III.6 (d) leads to the following observations:

- The coefficient of variation decreases with the ratio $\frac{\Delta H^*}{H_0^*}$ which means that the variation of the first-passage time is low when going from a low initial energy to a much larger target energy. On the opposite, a relatively small energy increase presents a very large variation of the first-passage time.

This is first explained by the gentle evolution of the energy for low energy levels and secondly by the amplitude of the mean first-passage time that is much larger for high values of $\frac{\Delta H^*}{H_0^*}$ and therefore decreases the coefficient of variation.

- The two limit cases $S_u = 0$ and $S_w = 0$ corresponding to the bottom left and upper right corners have a simple dependence in the ratio $\frac{\Delta H}{H_0} = \frac{\Delta H^*}{H_0^*}$ and nicely match in-between. Although the exact expression obtained from (II.2.22) and (III.3.5) shows a dependency in both H_0^* and ΔH^* separately, one observes that the dependency in $\frac{\Delta H}{H_0}$ is almost valid everywhere as far as $cv_f > \frac{\sqrt{2}}{2}$, which is the limit of validity of the limit solution for $S_u = 0$.
- The additive regime, which is now restricted to the upper left corner, presents a different behavior than the limit case $S_u = 0$ in the bottom left corner. Indeed, the coefficient of variation in the additive regime obtained by combination of $\mu_f^{(A)}$ and $\sigma_f^{2(A)}$ according to expressions (II.3.10), (III.3.7) and (III.3.9) depends on ΔH^* only and thus presents horizontal asymptotes in the upper left corner. The limit between the additive regime characterized by horizontal asymptotes and the limit case $S_u = 0$ with unitary slopes can be considered to correspond to $cv_f = \frac{\sqrt{2}}{2}$.
- The characteristic value $cv_f = 1$ corresponds in the bottom left corner to the asymptote $\frac{\Delta H}{H_0} = 2$ and in the upper right corner to the asymptote $\frac{\Delta H}{H_0} = e^2 - 1 = 6.38$.
- The transition of a system from a low energy level to a much higher energy level, corresponding to the upper left corner of the parameter space, features the lowest coefficients of variation. From a practical standpoint, this means that small samples are sufficient to provide good estimations of the average first-passage time in the additive regime (upper left corner). In the rest of the parameter space, larger samples are required to provide estimations of the average first-passage time with small confidence intervals.

Figure III.7 presents two slices of Figure III.6 (d) for respectively $H_0^* = 10^{-2}$ (a) and $H_0^* = 10^2$ (b) so that the coefficient of variation is represented as a function of ΔH^* . Dotted lines represent the asymptotic solutions (additive and multiplicative) and limit solutions ($S_u = 0$ and $S_w = 0$). In Figure III.7 (a), the limit solution for $S_u = 0$ fits the general expression for small values of ΔH^* while the asymptotic solution for the additive regime, obtained from (II.3.10), (III.3.7) and (III.3.9), fits the general expression for values of ΔH^* that are much higher than one. In-between, for values of cv_f that approach $\frac{\sqrt{2}}{2}$, the general expression should be used. In Figure III.7 (b), the multiplicative regime

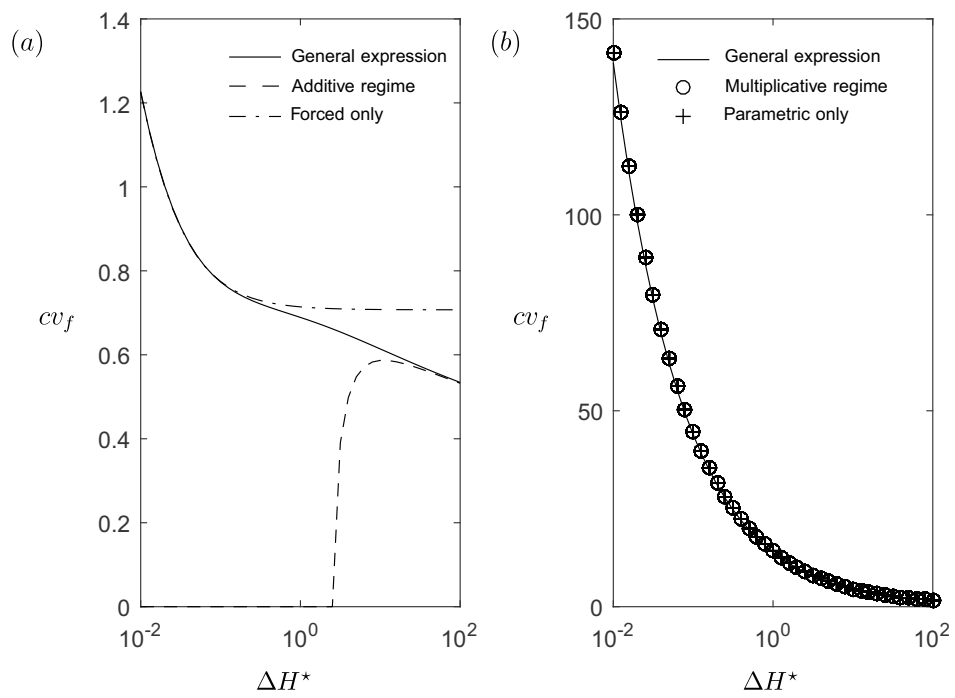


Figure III.7: Evolution of the coefficient of variation cv_f for (a) $H_0^* = 10^{-2}$ and (b) $H_0^* = 10^2$ and comparison with the asymptotic and limit solutions.

solution obtained from (II.3.9), (III.3.8) and (III.3.9) and the limit case solution for $S_w = 0$ (III.3.13) both perfectly fit the general expression. Indeed, the multiplicative regime fully covers the right part of the diagram and includes the limit case $S_w = 0$. For high values of H_0^* , the coefficient of variation can be directly approximated with expression (III.3.13).

III.4 Conclusion

As a first variant, the first order solution is improved by addition of the second order solution. In spite of the complexity of the analytical solutions, it is possible to derive a boundary layer solution that develops for target energy levels that are only slightly larger than the initial energy level. Unlike the first order solution, the second order one depends on both the initial kinetic and potential energies, i.e. position and velocity separately. It is also noted that the correlation between the forced and parametric excitations does not influence the leading order solution but appears in the second order solution. Although the smallness of the excitations is required for the asymptotic expansion, comparison with Monte Carlo simulations showed very good accuracy of the first order theoretical solutions for values of ε as large as 0.1. For the considered example, second order solutions virtually match Monte Carlo simulation results for values of ε as large as 0.5 (or more). As the first order solution of Chapter II is equivalent to the stochastic averaging method, the second order solution developed here is a beneficial contribution of the asymptotic expansion.

Secondly, the first-passage time is also developed for a damped oscillator. It was shown that the three regimes remain, with little influence of the damping in the incubation regime. Positive damping expectedly tends to increase the mean first-passage times, in all regimes, and eventually induces such a large dissipation that the first-passage time is not finite, on average.

Then, the variance of the first-passage time is derived. The form of the generalized Pontryagin equation being very similar for all statistical moments, the mean square first-passage time is studied with the same dimensionless groups H_0^* and ΔH^* , and in the same three regimes as the average first-passage time. Strong similarities are observed in the incubation and multiplicative regimes, while the additive regime is now restricted to large values of the dimensionless energy increase ΔH^* . As an estimator for the variability of the first-passage time, the coefficient of variation has been derived. It has been shown that a strong dependency in $\Delta H/H_0$, instead of H_0 and ΔH independently, is observed with decreasing influence, which means that small relative energy increases provide a significantly scattered first-passage time while large relative energy increases present a smaller variability and can be predicted with a higher confidence. For the sake of the analysis, simple analytical solutions have also been developed in the asymptotic and limit cases. They might be used for convenience in designing

experiments and understanding observed phenomena.

At each step, analytical solutions were validated with Monte Carlo simulations in order to demonstrate the accuracy of the closed form solutions. The dependence of the first-passage time with the initial and target energy is fully described by the general solution as well as in the three regimes.

Chapter IV

Some applications of the first-passage time

This chapter serves as a demonstration of the applicability of first-passage times to engineering problems. The oscillations of a pendulum as well as cable vibrations are presented as numerical examples. Then, the first-passage approach is experimentally applied to a tower crane oscillating in a turbulent wind flow and a pre-stressed steel strip.

IV.1 Introduction

IV.2 Application 1: The pendulum under horizontal and vertical excitations of its support

IV.3 Application 2: Cable vibrations under acceleration of one anchorage

IV.4 Algorithmic establishment of the first-passage time map from experimental data

IV.5 Application 3: A tower crane under gusty winds

IV.6 Application 4: A pre-stressed steel strip

IV.7 Conclusion

Part of this Chapter is based on the following articles:

Vanvinckenroye, H., Andrianne, T. and Denoël, V. (2018). First passage time as an analysis tool in experimental wind engineering. *Journal of Wind Engineering and Industrial Aerodynamics*, 177, pp. 366–375.

Delhez, E. (2018) Experimental and numerical study of first passage time. Master thesis. University of Liege. <https://orbi.uliege.be/handle/2268/224212>.

IV.1 Introduction

While first-passage times have been thoroughly studied in many aspects of numerical and theoretical modeling (Chapters II and III of this work among others), it is surprising that experimental investigations are very limited. In order to understand and characterize different crane instabilities in gusty wind conditions, Voisin performed experimental analyses and determined the susceptibility of a tower crane to autorotation when it is left free to rotate in a given environment [5, 6] (see Figure I.1 (a)). This approach allows to experimentally assess field configurations against undesired crane autorotation which could potentially lead to dramatic failures. Other experimental investigations can be found in the field of applied physics [101, 102], and usually aim at comparing experimental observations and approached analytical solutions. These applications in other fields of science suggest that it is a mistake to ignore the first-passage time representation of transient signals. Following this motivation, this chapter first presents numerical applications of the first-passage time to the motion of a pendulum and cable vibrations. The first-passage approach is then experimentally applied to a tower crane under gusty winds. Its rotative motion can be associated to a SDOF Mathieu oscillator. Wind tunnel data are processed within the framework of first-passage time and the results are compared with the simple theoretical model of Chapter III. A final example presents the experimental application of the first-passage approach to a pre-stressed steel strip, a MDOF system designed for academic purposes. This work is part of the master thesis of E. Delhez [103], and has been performed in the context of the PhD thesis of H. Vanvinckenroye, who had the opportunity to guide and follow E. Delhez within her research. As shown next, results are concluding and suggest the use of first-passage time maps as a complementary technique to usual analysis tools [104]. This is to our knowledge a first attempt at bringing first-passage times of stochastic systems into engineering.

IV.2 Application 1: The pendulum under horizontal and vertical excitations of its support

The most simple physical system related to a Mathieu oscillator is the pendulum. A mass M is suspended to a support by a rigid bar of zero mass and length L . This SDOF system is frequently considered as an academic study case, such as in [24, 41, 36, 29, 39] among many others. Vertical and horizontal motions of the support are respectively equivalent to parametric and external forces. Indeed, the governing equation of the system represented in Figure IV.1 is given by its rotative equilibrium

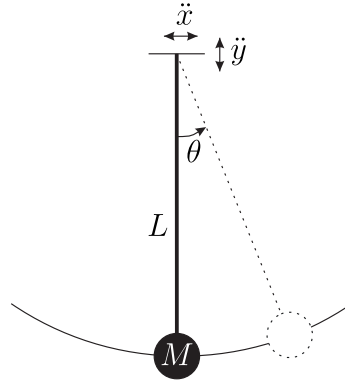


Figure IV.1: The forced and parametric pendulum. [1].

$$ML^2\ddot{\theta} + ML(g + \ddot{y}) \sin \theta = -ML\ddot{x} \cos \theta, \quad (\text{IV.2.1})$$

with θ the rotation of the pendulum. The gravitational acceleration is given by g while \ddot{x} and \ddot{y} respectively represent the horizontal and vertical accelerations of the support and are functions of time. The dot denotes the derivative with time t .

For small amplitudes, the equation can be linearized and becomes

$$ML^2\ddot{\theta} + ML(g + \ddot{y}) \theta = -ML\ddot{x}. \quad (\text{IV.2.2})$$

The free response, obtained by solution of (IV.2.1) with $\ddot{x} = \ddot{y} = 0 \text{ m/s}^2$ is the harmonic function $\theta(t) = \theta_0 \cos(\Omega^* t)$, with Ω^* the fundamental frequency of the pendulum given by $\Omega^* = \sqrt{g/L}$. Assuming the nondimensional time $\tau = \Omega^* t$, and the corresponding derivative given by the prime symbol, the nondimensional equation of motion can be rewritten as

$$\theta'' + \left(1 + \frac{y''}{g/\Omega^{*2}}\right) \theta = -\frac{x''}{g/\Omega^{*2}}. \quad (\text{IV.2.3})$$

Equation (IV.2.3) is comparable to the Mathieu equation (I.2.1) with $u = \frac{\ddot{y}}{g} = \frac{y''}{g/\Omega^{*2}}$ and $w = \frac{-\ddot{x}}{g} = \frac{-x''}{g/\Omega^{*2}}$, which confirms that the vertical excitation of the support acts as a parametric excitation and the horizontal excitation of the support acts as an external force. Moreover, an important observation is that the pendulum behavior is independent on the mass M , for given accelerations of the support.

The energy H of the pendulum is given by the Hamiltonian of equation (IV.2.1)

$$H = ML^2 \frac{\dot{\theta}^2}{2} + MgL \frac{\theta^2}{2} = MgL \left(\frac{\theta^2}{2} + \frac{\theta'^2}{2} \right) = Mgl\tilde{H}, \quad (\text{IV.2.4})$$

where \tilde{H} is the nondimensional energy, as defined for the analytical model in Equation (II.1.2). Assuming that the amplitude remains small, and that the excitations u and w (and consequently the accelerations \ddot{x} and \ddot{y}) are white noises of small intensity S_u and S_w , the average first-passage time for the pendulum to go from an initial energy H_0 to a target energy H_c is given by (II.2.22)

$$\mathcal{E} \{t_f\} = \frac{\mathcal{E} \{\tau_f\}}{\Omega^*} = \frac{4}{S_u \Omega^*} \ln \left(\frac{\tilde{H}_c S_u + 2S_w}{\tilde{H}_0 S_u + 2S_w} \right). \quad (\text{IV.2.5})$$

Knowing that

$$S_{\alpha x}(\kappa = \omega/\Omega^*) = \alpha^2 \Omega^* S_x(\omega), \quad (\text{IV.2.6})$$

one finds $S_u = \frac{\Omega^*}{g^2} S_{\ddot{y}}$ and $S_w = \frac{\Omega^*}{g^2} S_{\ddot{x}}$ and replacing the nondimensional variables in (IV.2.5) by their dimensional expressions, the average time taken by a pendulum departing from an initial energy H_0 to reach a higher energy H_c for the first time can be expressed as

$$\mathcal{E} \{t_f\} = \frac{4gL}{S_{\ddot{y}}} \ln \left(\frac{H_c S_{\ddot{y}} + 2S_{\ddot{x}} MgL}{H_0 S_{\ddot{y}} + 2S_{\ddot{x}} MgL} \right). \quad (\text{IV.2.7})$$

Similarly, the mean square first-passage time of the pendulum is given by the nondimensional expression (III.3.2) and can be rewritten in a dimensional form as

$$\begin{aligned} \mathcal{E} \{t_f^2\} = & \frac{32g^2 L^2}{S_{\ddot{y}}^2} \left[\mathcal{P} \left(\frac{H_0 S_{\ddot{y}} + 2S_{\ddot{x}} MgL}{2S_{\ddot{x}} MgL} \right) - \mathcal{P} \left(\frac{H_c S_{\ddot{y}} + 2S_{\ddot{x}} MgL}{2S_{\ddot{x}} MgL} \right) \right. \\ & + \ln \left(\frac{H_c S_{\ddot{y}} + 2S_{\ddot{x}} MgL}{2S_{\ddot{x}} MgL} \right) \ln \left(\frac{H_c S_{\ddot{y}} + 2S_{\ddot{x}} MgL}{H_c S_{\ddot{y}}} \right) \\ & - \ln \left(\frac{H_0 S_{\ddot{y}} + 2S_{\ddot{x}} MgL}{2S_{\ddot{x}} MgL} \right) \ln \left(\frac{H_c S_{\ddot{y}} + 2S_{\ddot{x}} MgL}{H_0 S_{\ddot{y}}} \right) \\ & \left. + \ln \left(\frac{H_c S_{\ddot{y}} + 2S_{\ddot{x}} MgL}{H_0 S_{\ddot{y}} + 2S_{\ddot{x}} MgL} \right) \right]. \quad (\text{IV.2.8}) \end{aligned}$$

The dimensions of the different parameters of the problem are given in Table IV.1. The smallness of the excitations intensities S_u and S_w can also be discussed as a function of the dimensional parameters

$$S_{u/w} = \frac{\Omega^*}{g^2} S_{\ddot{y}/\ddot{x}} \ll 1 \quad \rightarrow \quad \{S_{\ddot{y}}, S_{\ddot{x}}\} \ll \frac{g^2}{\Omega^*} = \sqrt{g^3 l}. \quad (\text{IV.2.9})$$

Parameters	dimensions
g, \ddot{x}, \ddot{y}	m/s^2
$S_{\ddot{x}}, S_{\ddot{y}}$	m^2/s^3
L	m
H	$kg \frac{m^2}{s^2}$
Ω^*	rad/s
t_f	s
$\tilde{H}, S_u, S_w, \tau_f$	—

Table IV.1: Dimensions of the different parameters of the pendulum problem.

Since the gravitational acceleration is a fixed constant $g = 9.81m/s^2$, the criteria is a function of the length of the pendulum only.

This example serves as a first application of the first-passage time to a physical problem with its dimensions.

IV.3 Application 2: Cable vibrations under acceleration of one anchorage

A taut cable is another structural element that is typically concerned by dynamic loadings. Since they are usually met in open structures like cable-stayed bridges, pylons, bracings, etc. evident dynamic excitations of cables are wind and rain, but the motion of the anchorages of the cable is also an important source of vibrations. In the case of a cable-stayed bridge, the motion of the deck under dynamic loading –typically traffic or wind excitation of the deck itself– provokes a dynamic loading of the cable. The component of the motion of the support that is perpendicular to the chord direction presents the typical feature of an external excitation while the parallel component induces parametric excitation. Let us consider a light cable of length L and inclination θ submitted to a vertical motion of its anchorage x , as illustrated in Figure IV.2. Considering a modal decomposition with sinusoidal modes and limiting the analysis to the first mode, the cable behaves as a SDOF system governed by [21, 105]

$$\ddot{q} + 2\xi\Omega^*\dot{q} + \Omega^{*2} \left(1 + \frac{x(t)}{X_0} \sin \theta \right) q + \frac{\pi^2}{4} \frac{\Omega^{*2}}{X_0 L} q^3 = \frac{2}{\pi} \ddot{x}(t) \cos \theta \quad (\text{IV.3.1})$$

where q is the modal coordinate, ξ is the damping coefficient, Ω^* is the fundamental frequency of the taut cable, $X_0 = \frac{NL}{EA}$ is the elastic elongation of the cable, with N the tension in the cable and EA its stiffness. In cable-stayed bridges, this governing equation can usually be linearized so that the cubic term in (IV.3.1) is neglected in the sequel. Defining the nondimensional time $\tau = \Omega^*t$,

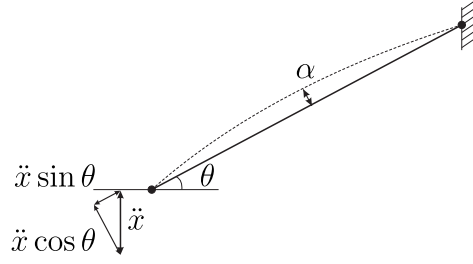


Figure IV.2: A inclined cable with vertical motion of one extremity. [1].

modal amplitude $\alpha = \frac{q}{X_0}$ and motion of the support $f = \frac{x}{X_0}$, Equation (IV.3.1) takes the nondimensional form

$$\alpha'' + 2\xi\alpha' + (1 + f(\tau) \sin \theta) \alpha = \frac{2}{\pi} f''(\tau) \cos \theta \quad (\text{IV.3.2})$$

that is directly comparable to the Mathieu oscillator of Equation (I.2.1) with $u(\tau) = f(\tau) \sin \theta$ and $w(\tau) = \frac{2}{\pi} f''(\tau) \cos \theta$.

The specific energy H –or energy by unit of mass– of the taut cable is given by the Hamiltonian of equation (IV.3.1)

$$H = \frac{\dot{q}^2}{2} + \Omega^{*2} \frac{q^2}{2} = X_0^2 \Omega^{*2} \left(\frac{\alpha^2}{2} + \frac{\alpha'^2}{2} \right) = X_0^2 \Omega^{*2} \tilde{H} \quad (\text{IV.3.3})$$

where \tilde{H} is the nondimensional energy as defined for the analytical model in Equation (II.1.2).

From the nondimensional formulation, and using relation (IV.2.6), the power spectral densities of the parametric and external excitations can be expressed as

$$\mathcal{S}_u(\kappa) = \left(\frac{\sin \theta}{X_0} \right)^2 \Omega^* \mathcal{S}_x(\omega) \quad \text{and} \quad \mathcal{S}_w(\kappa) = \left(\frac{2 \cos \theta}{\pi X_0} \right)^2 \frac{1}{\Omega^{*3}} \mathcal{S}_{\ddot{x}}(\omega) \quad (\text{IV.3.4})$$

with $\kappa = \omega/\Omega^*$ the nondimensional circular frequency corresponding to the nondimensional time τ .

The average first-passage time of the cable submitted to small white noise excitations u and w can be predicted with the analytical model of Chapter III. It is known from [106] that the power spectrum of a broadband parametric excitation mainly influences the first-passage time through its value at the double of the fundamental frequency of the system. Since the spectrum of the second derivative of x can be expressed as $\mathcal{S}_{\ddot{x}}(\omega) = \omega^4 \mathcal{S}_x(\omega)$, we decide to consider a white noise acceleration of the support with constant spectral density $\mathcal{S}_{\ddot{x}}(\omega) = S_{\ddot{x}}$ and its second integral for the position that can be expressed by

$$\mathcal{S}_x(\omega) = \frac{S_{\ddot{x}}}{\omega^4}, \quad (\text{IV.3.5})$$

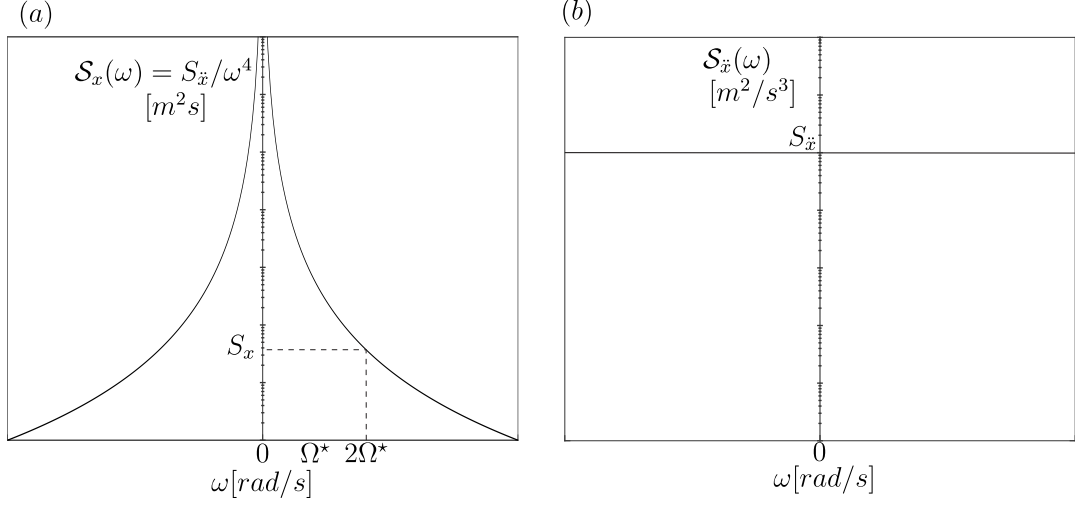


Figure IV.3: Power spectral densities of (a) the position and (b) the acceleration of the support.

as illustrated in Figure IV.3. In these conditions, the first-passage time of the cable can be computed by the analytical solution of Chapter III assuming an equivalent white noise position of the anchorage of constant spectral intensity $S_x = \frac{S_{\ddot{x}}}{(2\Omega^*)^4}$ so that the equivalent excitations intensities are given by

$$S_u = \left(\frac{\sin \theta}{X_0} \right)^2 \frac{1}{\Omega^{*3}} S_{\ddot{x}} \quad \text{and} \quad S_w = \left(\frac{2 \cos \theta}{\pi X_0} \right)^2 \frac{1}{\Omega^{*3}} S_{\ddot{x}}. \quad (\text{IV.3.6})$$

The average first-passage time of the cable can be predicted by

$$\begin{aligned} \mathcal{E} \{t_f\} &= \frac{4}{S_u \Omega^{*3} (1-a)} \left[\ln \left(1 + \frac{\Delta \tilde{H}}{\tilde{H}_0} \right) + \frac{(1 + (\tilde{H}_0 + \Delta \tilde{H}) \frac{S_u}{2S_w})^a - (1 + \tilde{H}_0 \frac{S_u}{2S_w})^a}{a} \right. \\ &\quad \left. - \int_{\tilde{H}_0}^{\tilde{H}_0 + \Delta \tilde{H}} \frac{(1+z \frac{S_u}{2S_w})^a}{z} dz \right] \\ &= \frac{4}{S_x^*} \left(\frac{X_0}{\sin \theta \Omega^*} \right)^2 \left[\ln \left(1 + \frac{\Delta H}{H_0} \right) + \frac{(1 + (H_0 + \Delta H) \frac{1}{2} \left(\frac{\pi \tan \theta}{8 X_0 \Omega^*} \right)^2)^a - (1 + H_0 \frac{1}{2} \left(\frac{\pi \tan \theta}{8 X_0 \Omega^*} \right)^2)^a}{a} \right. \\ &\quad \left. - \int_{H_0}^{H_0 + \Delta H} \frac{(1 + \frac{z}{2} \left(\frac{\pi \tan \theta}{8 X_0 \Omega^*} \right)^2)^a}{z} dz \right] \end{aligned} \quad (\text{IV.3.7})$$

with $a = \frac{8\xi}{S_u} = \frac{8\xi \Omega^{*3} X_0^2}{S_{\ddot{x}} \sin^2 \theta}$.

In a first step, and for comparison with analytical results (IV.3.7), Equation (IV.3.1) is simulated under white noise acceleration of the support. Then, for the sake of the illustration and in order to remain as close as possible to realistic

Ω^*	$7.8rad/s$
L	$110.505m$
EA	$1734.6 \cdot 10^6 N$
N	$4902.7 \cdot 10^3 N$
ξ	0.5%
θ	$\pi/4$

Table IV.2: Numerical values of the parameters of a cable of the Ben-Ahin bridge (Belgium) [21, 105].

conditions, a time correlated acceleration of the support is chosen as an Ornstein-Uhlenbeck process with correlation time T_c . The Ornstein-Uhlenbeck process is a process with exponentially decreasing correlation and the white noise acceleration developed first corresponds to the limit case of the Ornstein-Uhlenbeck with correlation time equal to zero.

The example treated here is a taut cable of the Ben-Ahin cable-stayed bridge (Belgium). Numerical values of the cable parameters are obtained from [21, 105] and are given in Table (IV.2). One considers a cable departing from an initial energy $H_0 = 0.001m^2/s^2$ –corresponding to an initial amplitude of oscillations of $5.7mm$ – and reaching the target energy $H_c = 0.041m^2/s^3$ –corresponding to a target amplitude of $3.7cm$. The spectral density of the acceleration of the deck is taken as $S_{\ddot{x}} = 0.1m^2/s^3$ and the correlation time of the acceleration is successively taken equal to 0 , $T/10$ and T with $T = 1/\Omega^*$.

Figure IV.4 (a) presents the complete distribution of the first-passage time $p_f(t_f)$ obtained with 2000 Monte Carlo simulations and for various values of the correlation time T_c . The first distribution for $T_c = 0s$ corresponds to a white noise acceleration of the support and its average value can be directly compared to the analytical expression (IV.3.7) $\mathcal{E}\{t_f\} = 4.29s$. Respective averages of the distributions are indicated with circles. A slight increase of the values of the first-passage time with the correlation time can be observed. The evolution of the average first-passage time obtained by MC simulations is represented in Figure IV.4 (b) as a function of the ratio T_c/T . While the average monotonically increases with T_c/T , the influence remains negligible as long as $T_c/T \lesssim 1$. A sudden increase is observed for $T_c/T > 1$, i.e. when the correlation time of the acceleration of the anchorage exceeds the fundamental period of the cable.

As a conclusion, the average first-passage time of the cable under acceleration of the support can be obtained by the analytical expression (IV.3.7) as long as the time-scale of the acceleration of the support remains smaller than the time-scale of the cable. The analytical model offers a good estimation of the first-passage time as a function of the cable parameters.

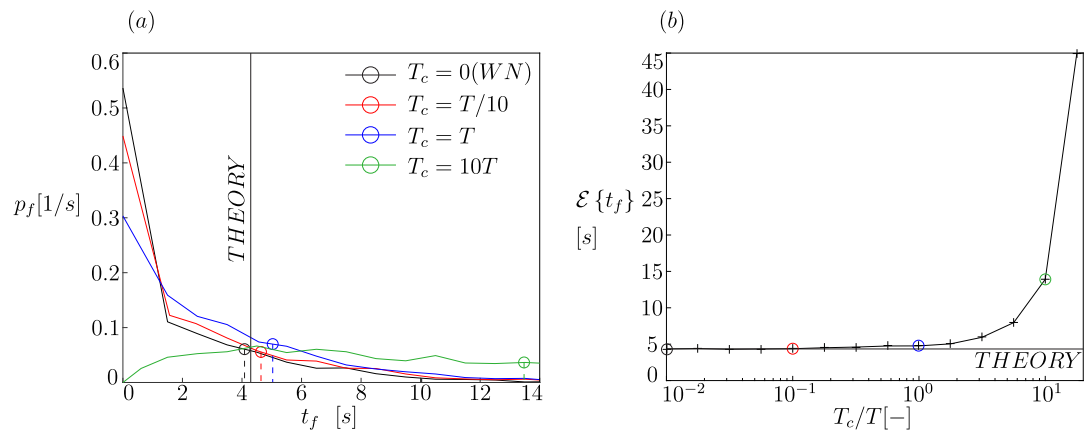


Figure IV.4: Monte Carlo simulations of a cable under Ornstein-Uhlenbeck excitation with various correlation times T_c . (a) Complete distribution (b) Evolution of the average with the correlation time.

IV.4 Algorithmic establishment of the first-passage time map from experimental data

IV.4.1 Introduction

Figure II.2 shows a map of the first-passage time of the system energy, as a function of the initial energy and of the energy increase. This is an appropriate way to represent the different regimes in which a system could evolve: Incubation, Multiplicative or Additive. In this section, an efficient algorithm is developed to determine this map from measured realizations of the stochastic response.

Based on the time series of the displacement and velocity –possibly obtained by differentiation of the position– of a system, the time series of the dimensional energy $H(t)$ and dimensionless energy $\tilde{H}(t)$ is established and the first-passage time map as a function of \tilde{H}_0 and $\Delta\tilde{H}$ can be constructed.

The algorithm is based on the construction of the envelope of the time series similarly to the rainflow algorithm [107], which is used in fatigue assessment to reduce a varying stress signal into a set of stress reversals and hereby count the number of half-cycles that can lead to fatigue. That algorithm consists in virtually rotating the time signal by 90° and considering a water drop flowing from one point. The path followed by the drop provides information about the minima and maxima, as well as an estimation of the number of significant cycles in the signal.

The Matlab code of the developed algorithm is freely available under GNU license on the ULiège repository [108].

IV.4.2 The algorithm

The extraction of first-passage times from a time series is composed of several sequential steps. They are explained after some general nomenclature is introduced.

The *main envelope* $\tilde{E}(t; t_0)$ is the monotonically increasing function corresponding to the highest energy level ever reached at time $t > t_0$. The main envelope is associated with the initial time $t_0 = 0$, where the initial energy is $\tilde{H}_0 = \tilde{H}(0)$, so that $\tilde{E}(t_0; t_0) = \tilde{H}_0$ and $\tilde{E}(t; t_0) \geq \tilde{E}(t_0; t_0)$, $\forall t > t_0$. The main envelope is represented in blue in Figure IV.5. This curve provides the target energy levels $\tilde{H}_c = \tilde{E}(t_f; t_0)$ as a function of the corresponding first-passage times t_f . The inverse function is not a single-valued function, but if we restrict it to the minimum time corresponding to each energy (i.e. discarding the plateau's in the main envelope), it provides the first-passage time as a function of the energy increase $\Delta\tilde{H}$,

$$t_f(\Delta\tilde{H}; \tilde{H}_0) = \tilde{E}^{-1}(\tilde{H}_0 + \Delta\tilde{H}). \quad (\text{IV.4.1})$$

This time is to be understood as a time elapsed from t_0 where the initial energy is \tilde{H}_0 . This provides a coarse estimation of the first-passage time. A refined estimator can be obtained by pretending that the recording has started a little later, at another time t' where the energy was also equal to \tilde{H}_0 . By restricting the time series to the window $t > t'$, another estimation of $t_f(\Delta\tilde{H}; \tilde{H}_0)$ is obtained and statistics of the first-passage time, starting from initial energy level \tilde{H}_0 can be obtained, even from a single realization of the process. The method can be generalized for other values of the initial energy, in such a way to provide a map of the average first-passage time, for various combinations of \tilde{H}_0 and $\Delta\tilde{H}$. Nevertheless, it would be computationally ineffective to determine this map in this way.

For the needs of the following algorithm, we also define the *partial envelope* $\tilde{E}(t; t')$ as the main envelope of the remaining part of the signal starting at time t' . The green and red plots in Figure IV.5 show two examples of local envelopes. As a corollary the partial envelope associated with time t_0 corresponds to the main envelope. Unless $\tilde{H}(t')$ is the largest energy level over all times before time t' , the local envelope starts below the main envelope and eventually reaches it after some time. The part of the partial envelope that is different from the main envelope is called the *local envelope*.

It is important to notice that the local envelope might coincide with the time series $\tilde{H}(t)$, depending on the sign of the local derivative at time t' . If the energy $\tilde{H}(t')$ is minimum or increases, then $\tilde{H}(t)$ coincides with the *local envelope* for $t \geq t'$ and until the next local maximum (see beginning of red curve in Figure IV.5). On the contrary if the energy presents a maximum or decreases at time t' , then the *local envelope* presents a jump until the next point where the energy is higher (see beginning of green curve in Figure IV.5).

In order to develop an efficient algorithm, the time series is first scanned through in order to determine, for each time step, whether the energy $\tilde{H}(t)$ is increasing or decreasing. This can be efficiently done with vector operations. For an increasing energy, the index of the next maximum is stored and for a decreasing energy, the index of the next higher energy is stored.

Secondly and using this information, the *main envelope* is constructed, starting from $t = 0$ until the end of the time series (see blue curve in Figure IV.5). The main envelope is straightforwardly elaborated as a succession of local envelopes, depending on the ascending or descending character of the signal. The main envelope is stored and will be used as support for the next steps.

Third, the energy axis is discretized in a finite number of intervals. These intervals are chosen with uniform sizes on a logarithmic scale, as this is the physical scaling suggested by the stochastic model. These intervals define bins in the $\tilde{H} - \Delta\tilde{H}$ plane.

Fourth, going point by point through the entire signal, each time step can be considered as the first point $t' \neq t_0$ of a shorter time series with initial energy

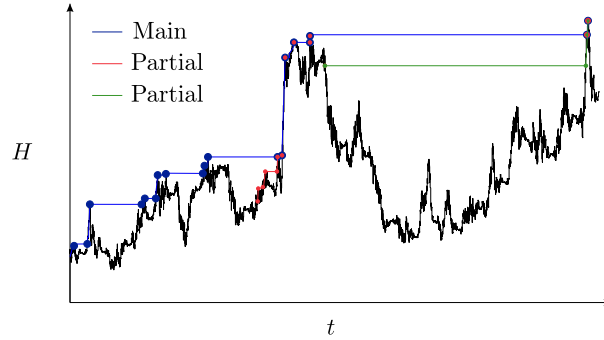


Figure IV.5: Main and partial envelopes reconstruction.

$\tilde{H}'_0 = \tilde{H}(t')$. The *partial envelope* $\tilde{E}(t; t')$ provides estimators of the first-passage times t_1 for that initial energy and various target energies (or different energy increases). A counting procedure allocates, in the appropriate bins, the first-passage times associated with the target energies, starting from \tilde{H}'_0 . To construct *partial envelopes*, the process is the same, except that the main envelope is now known. If the point $\tilde{H}(t_0)$ is part of the main envelope, then the partial envelope follows the main envelope from that point until the end of the signal. If $\tilde{H}(t_0)$ is not a point of the main envelope, then the envelope is reconstructed as a succession of local envelopes until the main envelope is reached. Once the main envelope is reached, the partial envelope follows the main envelope until the end of the signal.

Finally, since the same discretized energy level will have several occurrences in the original time series, several values of the first-passage time will be observed for each $\tilde{H}_0 - \Delta\tilde{H}$ combination (in each bin). Averaging of all these first-passage times provides the average first-passage time map.

A pseudo-code of this algorithm, where *main* and *partial* envelopes are established as a succession of *local* envelopes (nested function), is given in Appendix D and Matlab routines are also provided under GNU license, freely available from the ULiège repository [108].

IV.5 Application 3: A tower crane under gusty winds

IV.5.1 A mathematical model of a tower crane

The dynamics of a crane spinning in a turbulent velocity field can be modeled with a governing equation of the type:

$$I\ddot{\theta} + C\dot{\theta} = M_w(t) \quad (\text{IV.5.1})$$

where $\theta(t)$ is the angular position of the crane jib in a horizontal plane and $M_w(t)$ is the aerodynamic load resulting from the wind flow [1]. Considering that the rotation of the crane is associated with slower timescales than those of the wind flow along a characteristic length of the crane (say its diameter), the quasi-steady assumption [109] is considered. The aerodynamic torque is therefore expressed by

$$M_w = \frac{1}{2}\rho_{air}C_MHB^2\|\mathbf{v}_{rel}\|^2 \quad (\text{IV.5.2})$$

as a function of the air density ρ_{air} , the moment coefficient C_M , the circumscribed dimensions of the lattice cross section $H \times B$ (height \times span) and the relative wind velocity \mathbf{v}_{rel} .

There is no angle-proportional term (no stiffness) in the rotative equilibrium (IV.5.1), since the spinning crane is assumed to be ideally balanced. If the wind was uniform and steady, without turbulence, the crane would find an equilibrium position in the mean direction of the wind; in other words, the stiffness in the problem comes from the aerodynamic loading $M_w(t)$. In this paper, we are concerned with small amplitude rotations of the crane, which also partly justifies a linearized version of the inertial and internal forces in the governing equation, therefore simply modeled by the rotative inertia I and viscosity C .

In the horizontal plane of the crane, the wind velocity is characterized by its mean component U and its fluctuating components u and w respectively parallel and perpendicular to the wind direction (see Figure IV.6 (c)), which are stochastic processes characterized by their power spectral densities $\mathcal{S}_u(\omega)$ and $\mathcal{S}_w(\omega)$. For small incidences, the moment coefficient can be linearized too so that $C_M(\alpha) = \frac{\partial C_M}{\partial \alpha}\bigg|_{\alpha=0} \alpha$ with α the relative angle between the crane and the instantaneous wind velocity vector. The relative velocity entering in (IV.5.2) is given by:

$$\mathbf{v}_{rel} = (U + u, w) - (-r\dot{\theta} \sin \theta, r\dot{\theta} \cos \theta). \quad (\text{IV.5.3})$$

with r the abscissa of the aerodynamic focus along the jib, i.e. the point at which the moment coefficient does not vary with the lift coefficient [109]. In this model we subscribe to the common assumption that u and w are small compared to U , although they might affect higher order statistics [109]; also we assume that rotations are small around the equilibrium configuration, i.e. $\theta \ll 1$ and that the rotative velocity of the crane, of order $B\dot{\theta}$ is also small compared to U . The squared norm of the relative velocity and the apparent angle of attack are therefore expressed as

$$\|\mathbf{v}_{rel}\|^2 = U^2 + 2Uu \quad \text{and} \quad \alpha = \theta - \frac{w - r\dot{\theta}}{U} \quad (\text{IV.5.4})$$

which is identical to usual assumptions for wings [110] and bridge decks [111, 112].

Grouping together rigidity and damping terms, Equation (IV.5.1) is rewritten

$$I\ddot{\theta} + \left(C + M^* \frac{r}{U} \left(1 + 2 \frac{u}{U} \right) \right) \dot{\theta} + M^* \left(1 + 2 \frac{u}{U} \right) \theta = M^* \frac{w}{U} \quad (\text{IV.5.5})$$

where, as soon as $U \neq 0$, the reference torque M^* is defined as

$$M^* = -\frac{1}{2} \rho_{air} H B^2 U^2 \frac{\partial C_M}{\partial \alpha} > 0. \quad (\text{IV.5.6})$$

As introduced earlier, this quantity also plays the role of a stiffness, aligning the crane with the mean wind orientation $\theta = 0$ when there is no turbulence.

A dimensionless version of the governing equation is obtained by introducing the circular frequency of the oscillator $\Omega^* = \sqrt{M^*/I}$ as well as the structural and aerodynamic damping coefficients, $\xi_s = \frac{C\Omega^*}{2M^*}$ and $\xi_a = \frac{r}{2U}\Omega^*$. It reads

$$\theta'' + (2\xi_s + 2\xi_a(1 + \tilde{u}))\theta' + (1 + \tilde{u})\theta = -\tilde{w}, \quad (\text{IV.5.7})$$

where symbol $'$ represents a derivative with respect to the non-dimensional time $\tau = \Omega^* t$, and where $\tilde{u} = 2\frac{u}{U}$ and $\tilde{w} = \frac{w}{U}$ represent the dimensionless components of the wind fluctuations.

The Hamiltonian of the dimensional system (IV.5.5) is given by the conservative part of the equation and is defined as

$$H = I \frac{\dot{\theta}^2}{2} + M^* \frac{\theta^2}{2} = \frac{I}{2} \left(\dot{\theta}^2 + \Omega^{*2} \theta^2 \right) \quad (\text{IV.5.8})$$

while the dimensionless Hamiltonian is given by the conservative part of Equation (IV.5.7):

$$\tilde{H} = \frac{\theta'^2}{2} + \frac{\theta^2}{2} = \frac{H}{M^*}. \quad (\text{IV.5.9})$$

It is therefore observed that M^* also plays the role of a characteristic energy.

The dimensional tower crane Equation (IV.5.1) has been reduced to the nondimensional Equation (IV.5.7) after some simplifications. This last expression is equivalent to Equation (II.2.1) so that the analytical developments for the average first-passage time of the damped oscillator can be transposed to the tower crane problem.

Particularization of expression (III.2.3) to the non-dimensional tower crane governing equation (IV.5.7) provides the non-dimensional average first-passage time:

$$\mathcal{E} \{ \tau_f \} = \frac{4}{S_{\tilde{u}}(1-a)} \left[\ln \left(1 + \frac{\Delta \tilde{H}}{\tilde{H}_0} \right) + \frac{\left(1 + (\tilde{H}_0 + \Delta \tilde{H}) \frac{S_{\tilde{u}}}{2S_{\tilde{w}}} \right)^a - \left(1 + \tilde{H}_0 \frac{S_{\tilde{u}}}{2S_{\tilde{w}}} \right)^a}{a} - \int_{\tilde{H}_0}^{\tilde{H}_0 + \Delta \tilde{H}} \frac{\left(1 + t \frac{S_{\tilde{u}}}{2S_{\tilde{w}}} \right)^a}{t} dt \right] \quad (\text{IV.5.10})$$

Applying the property (IV.2.6), the average first-passage time of the governing equation (IV.5.5) is finally given by

$$\mathcal{E}\{t_f\} = \frac{1}{S_{u/U}(1-a)} \frac{1}{\Omega^{*2}} \left[\ln \left(1 + \frac{\Delta H}{H_0} \right) + \frac{\left(1 + \frac{H_0 + \Delta H}{M^*} \frac{2S_{u/U}}{S_{w/U}} \right)^a - \left(1 + \frac{H_0}{M^*} \frac{2S_{u/U}}{S_{w/U}} \right)^a}{a} - \int_{H_0}^{H_0 + \Delta H} \frac{\left(1 + \frac{t}{M^*} \frac{2S_{u/U}}{S_{w/U}} \right)^a}{t} dt \right] \quad (\text{IV.5.11})$$

where a can also be expressed as a function of the problem parameters as $a = \frac{C}{1S_{u/U}} \frac{1}{\Omega^{*2}} = \frac{2\xi_s}{S_{u/U}\Omega^*}$.

There are two discrepancies between this mathematical model and the simple tower crane model. First, the theoretical solutions are derived for delta-correlated noises $u(t)$ and $w(t)$. In the considered problem, the power spectral densities of the turbulence components are assumed to be broad enough in the frequency bands associated with the dynamics of the problem so that a replacement of the actual power spectral density by an equivalent white noise intensity might be operated. This is classical in buffeting analysis [113] and has also been discussed in the scope of first-passage times [103]. Second, the problem at hand features a parametric excitation in the velocity-dependent term, see (IV.5.7). In order to get rid of that term, the pivot of the crane model was chosen close to the aerodynamic center so that $r \ll B$.

IV.5.2 Experimental investigations

Experimental setup and identification of the mechanical properties of the model

The tests have been performed at the Wind Tunnel Laboratory of the University of Liège, in the low speed test section of dimensions $2.5m \times 1.8m \times 2m$. An homogeneous turbulent field is generated $12m$ upstream the tower model using a passive grid generator [114] (see Figure IV.7 (a)). The corresponding air flow has been characterized by 3-axis measurement of the wind velocity with a Cobra-probe with an acquisition frequency of $500Hz$. In a first step, long measurements have been performed where the tower crane is left free to rotate in a turbulent velocity field (see Figure IV.6 (a)). The rotation of the crane has been measured with a laser SICK OD2-P300W200I0 of range 100 to $500mm$ with an acquisition frequency of $1000Hz$.

The setup consists in a rectangular jib of section $H \times e = 0.042m \times 0.042m$ and length $B = 1m$ made of rigid machinable foam of density $\rho = 690kg/m^3$ (see Figure IV.6 (c)). The pivot is placed at $0.4m$ of one extremity so that the

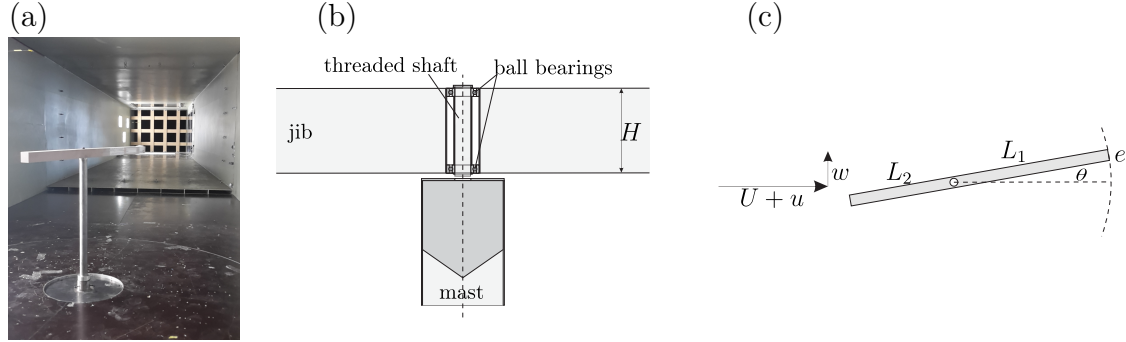


Figure IV.6: (a) Experimental setup in the wind tunnel (b) Vertical view and mechanical conception of the pivot (c) Plan view of the setup configuration.

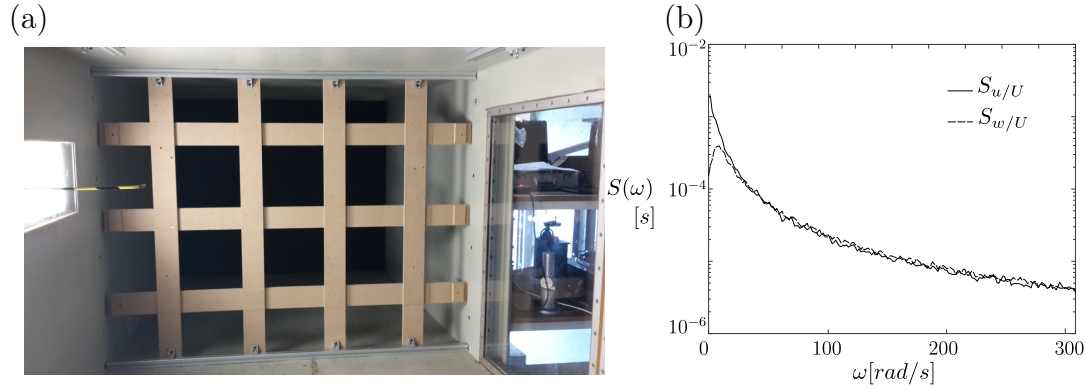


Figure IV.7: (a) Coarse grid used for the first-passage time measurements (b) Turbulence components parallel (u) and perpendicular (w) to the main wind direction with the coarse grid .

jib has a length $L_1 = 0.6m$ and the counter-jib a length $L_2 = 0.4m$ and the inertia is given by $I = \rho H e \frac{L_1^3 + L_2^3}{3} = 0.11kgm^2$. Friction between the mast and the pivot is minimized by means of two ball bearings vertically aligned in the pivot as illustrated in Figure IV.6 (b). The two ball bearings are adjusted in a circular drilling in the foam. A threaded shaft ensures the verticality and the rigidity of the fixation with the hollow vertical mast.

Finally, the mechanical properties of the physical model have been characterized through measurement of the free response of the crane when it is launched in wind-off conditions. The acceleration has been measured with a wireless accelerometer with acquisition frequency of $200Hz$. The crane has been manually launched in order to observe the free response decay. The corresponding theoretical governing equation is

$$I\ddot{\theta} + C\dot{\theta} = 0. \quad (IV.5.12)$$

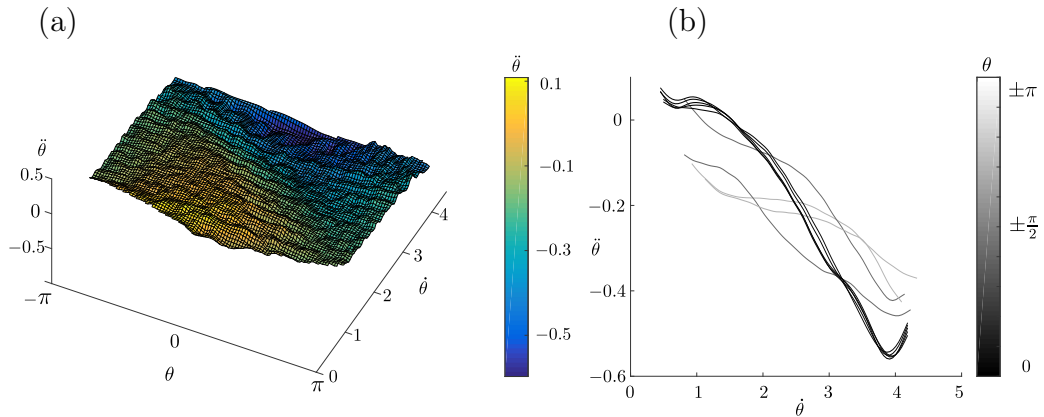


Figure IV.8: Representation of the restoring force function (a) as a function of position and velocity and (b) as a function of velocity for $\theta = 0, \pm\frac{\pi}{50}, \pm\frac{\pi}{25}, \pm\frac{\pi}{2}$ and $\pm\pi$.

Note that the aerodynamic damping associated with the rotation of the crane is again neglected because of the position of the pivot ($r = 0$). This equation governing the free response of the crane is a particular case of a very general model $\ddot{\theta} + G(\theta, \dot{\theta}) = 0$, where $G(\theta, \dot{\theta})$ is the (possibly nonlinear) restoring force function. In the assumed model, the restoring force function should be a plane independent on the angular position θ . However, slight imperfections in the setup have resulted in a slightly different result, as shown by the surface represented in Figure IV.8. This restoring force function has been obtained by measuring the free response of the crane with 3-D accelerometers, then integrating to obtain angular velocity and angular positions. Finally the restoring force function is obtained by plotting the acceleration against the position and velocity. Results shown in Figure IV.8 (a) represent an average response over 6 launches. Holes in the map are due to the interpolation algorithm. Figure IV.8 (b) represents slices of the map for different values of θ .

As expected, an overall decreasing behavior is observed with $\dot{\theta}$. However, this evolution is slightly nonlinear and dependent on θ . While the acceleration was expected to be always negative due to damping, a small geometrical imperfection influences the acceleration in the neighborhood of $\theta = 0$ and for small values of the rotational velocity. For a series of reasons such as small gaps in the ball bearings, small play between the supporting tube and the cylindrical support of the jib (see Figure IV.6 (a)), the slight deflection of the jib, and other imperfections, the jib does actually not revolve in a perfectly horizontal plane, creating therefore zones with lower potential energy. These zones are relatively wide and do not hinder the good adjustment of parameters of the linear model, as shown in Section IV.5.3.

Grid Turbulence

The turbulent field is characterized at a mean velocity $U = 3.6m/s$ and led to horizontal turbulence intensities $I_u = 6.2\%$ and $I_w = 4.8\%$ resp. parallel and perpendicular to the main direction. The power spectral densities of u/U and w/U are represented in Figure IV.7 (b) as a function of the pulsation ω .

The turbulence component u has a monotonically decreasing frequency content while the perpendicular component w presents a peak value for $\omega = 9.1rad/s$. Both contents are very similar for higher frequencies and for all frequencies we have $\mathcal{S}_w/U(\omega) \leq \mathcal{S}_u/U(\omega)$. The proportional turbulences u/U and w/U characterized here are supposed not to change significantly with the mean velocity U . The Mathieu oscillator is submitted to white noise excitations u and w so that in the next coming results constant values $S_{u/U}$ and $S_{w/U}$ are found to be equivalent to the narrow-band spectra $\mathcal{S}_{u/U}(\omega)$ and $\mathcal{S}_{w/U}(\omega)$.

IV.5.3 Results

The tower crane is left free to rotate under the turbulent flow for 6 hours. Its rotational displacement is measured and the velocity is obtained by differentiation. Figure IV.9 (a) shows the map of the average first-passage time reconstructed with the algorithm presented in Section IV.4 (in straight line). Dotted lines represent the average first-passage times obtained with the mathematical model presented in Section III.2. These lines are similar to those of Figure III.4, in the relatively high damped case ($a > 3$). This means that the damping ξ is large compared to the parametric excitation input S_u . It does not mean that damping is large.

While the dimensional problem depends on the four parameters Ω^* , $S_{u/U}(\omega)$, $S_{w/U}(\omega)$ and ξ_s , see Equation (IV.5.11), the first-passage time only depends on three combinations of those 4 parameters: $\frac{1}{S_{u/U}\Omega^{*2}}$, $\frac{2S_{u/U}}{S_{w/U}}$ and a , which means that an infinite number of different oscillators can present the same first-passage time map. In other words, two oscillators that would have two different natural circular frequencies Ω^* and subjected to turbulence intensities that are inversely proportional to Ω^{*2} , exhibit the same first-passage time map. The faster oscillator being excited with less energetic loadings than the slower oscillator, the energy of both oscillators will actually increase similarly, on average, and they will present the same first-passage time map.

However, the definition of $\tilde{H} = \frac{\theta^2}{2} + \frac{\dot{\theta}^2}{2\Omega^{*2}}$ requires the knowledge of Ω^* , defined as the fundamental pulsation of the time series $\theta(t)$. The characteristic frequency $\Omega^* = 1.95rad/s$ has been chosen and obtained as the maximum of the power spectral density of the angular position. This leaves us with the adjustment of 3 parameters.

The parameters of the model are obtained by a minimization of the mean-

square error between the experimental map and the corresponding theoretical one, defined as

$$\mathcal{R} = \frac{1}{n_1 n_2} \sum_i^{n_1} \sum_j^{n_2} \Delta_{i,j}^2 \frac{N_{i,j}}{N_{tot}} \quad (\text{IV.5.13})$$

where the summation is repeated over all $n_1 n_2$ bins and where $\Delta = \mathcal{E}\{\mathbf{t}_{f,exp}\} - \mathcal{E}\{\mathbf{t}_{f,th}\}$ is the difference between the experimental and theoretical $n_1 \times n_2$ matrices of first-passage times in the $(H_0, \Delta H)$ space. This error is weighted according to the number of observations $N_{i,j}$ of the first-passage time in each bin ($N_{tot} = \sum_i \sum_j N_{i,j}$). Implementation of a simple search algorithm provided the lowest residual. The corresponding values of the parameters are

$$S_{u/U} = 3.2 \times 10^{-5} s, \quad S_{w/U} = 6.4 \times 10^{-7} s \quad \text{and} \quad \xi_s = 0.11. \quad (\text{IV.5.14})$$

They correspond to the parameters of the equivalent Mathieu oscillator presented in Section IV.5.1. It is not the objective of this work to provide a physical meaning to those parameters. Indeed, they are just equivalent, in the sense of the minimization (IV.5.13), since the physical problem tested in the wind tunnel is not exactly governed by the same equation. Although the scope of this section is to highlight a possible field of application of first-passage times by exploiting the richness of the generic Mathieu oscillator, it is believed that the direct analysis, i.e. the direct determination of equivalent parameters given all actual properties of the physical problem, goes beyond the scope of this work. We just notice that $S_{u/U}$ and $S_{w/U}$ are short with respect to the timescale of the problem which justifies the slower evolution of energy. They have the same order of magnitudes as the turbulence intensities presented in Figure IV.7 (b). Also, we notice that $\xi_s = 0.11$ is a relatively small parameter, which is also a necessary condition for the stochastic averaging to apply. Being defined as a ratio between dissipative moments in the mechanical system and a stationary aerodynamic moment, see (IV.5.7), the damping coefficient ξ_s has not the classical meaning of a structural nor aerodynamic damping. It is therefore not abnormally large.

Despite the slight dissimilarities between the physical and numerical models, which are emphasized in the next section, the behavior in terms of first-passage times is very well captured, over several orders of magnitude.

IV.5.4 Discussion

The dimensional incubation time defined as $t_{incub} = \frac{1}{8\Omega^2 S_{u/U}(1-a)}$ is negative, which means that no incubation regime is observed due to the important structural damping (ξ compared to u/U). The other two regimes are clearly observable: the independence in \tilde{H}_0 in the additive regime is observed in the left part of Figure IV.9 (a) while the asymptotically constant (and negative) slope

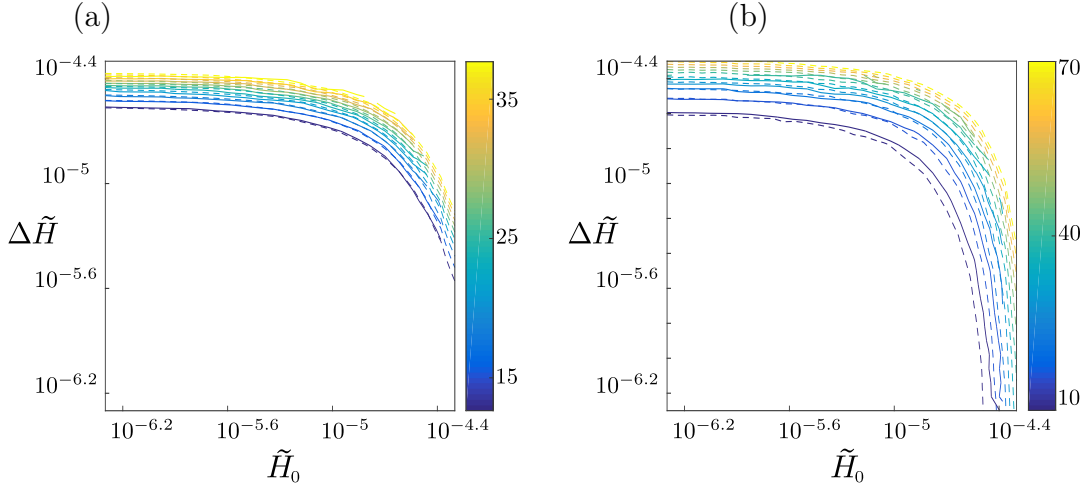


Figure IV.9: (a) Maps of the average first-passage time $\mathcal{E}\{t_f\}$ and (b) of the standard deviation of the first-passage time. Comparison between the experimental data (solid lines) and the theoretical model (dotted lines).

which is characteristic of the multiplicative regime is observed in the right part of the diagram. The notable change between both behaviors is observed around $\tilde{H}_0 = 10^{-5}$.

The tower crane model is a physical system presenting some differences with the idealized mathematical model of the stochastic Mathieu oscillator of Section III.2. First of all, all slight nonlinearities related to the angle of attack, the moment coefficient and the squared apparent velocity have been linearized in order to express the aerodynamic load as a linear function of the turbulence components u and w . Moreover, the quasi-steady model based on the sole consideration of the moment coefficient might be limited to represent the aerodynamic loading on the oscillating crane. Indeed, the aerodynamic moment results from the pressures distributed along the moving jib, which have to be multiplied by their respective lever arms and integrated. These pressures are random as a result of the turbulence, and should in principle be expressed as a slice cut of a spatial stochastic field including the space-coherence of the fluctuating wind. At last but not least, the turbulence components u and w present a broadband spectrum (see Figure IV.7 (b)) which is not exactly a δ -correlated noise as assumed in the Mathieu oscillator model. All these reasons conspire to make the actual physical model of the tower crane somehow different from an accurate aerodynamic model of the crane, but also different from the simple Mathieu oscillator model. While the tower crane is a physical problem presenting a significant complexity, to some extent, it is here demonstrated that its first-passage behavior can be captured and reproduced with a simple equivalent model.

This conclusion is very promising as to the utility of simple models to repre-

sent first-passage statistic in the buffeting analysis of slightly damped structures. Both the wind-tunnel results and the properties of the equivalent Mathieu oscillator can be exploited to infer some information on the reliability of the considered system. On one hand, very long measurements in the wind tunnel, and the appropriate post-processing in terms of first-passage times, as discussed in Section IV.4, can offer a fair picture of how the first-passage time scales with the problem parameters, in particular, in which regime a randomly excited structure evolves. On the other hand, the adjustment of an equivalent model, as suggested in this paper, can be used to smoothen the slight imperfections of too short measurements or even to extrapolate to situations that could not be observed in the wind-tunnel.

As an example of extrapolation of the information provided by the Mathieu oscillator model, we discuss the standard deviation of the first-passage time. This information is as much important as the average first-passage time, as soon as reliability is concerned [115]. The counting algorithm presented in Section IV.4 can provide additional statistical information about first-passage time, including higher statistical moments and the standard deviation. The solid lines in Figure IV.9 (b) represent the first-passage time map of the measured energy. This is now compared to the standard deviation of the first-passage time obtained with the Mathieu oscillator model. Unfortunately, the closed form solutions of the second statistical moment are available in the undamped case only [116]. However, comparison is possible by means of Monte Carlo simulations. Using the set of parameters obtained by adjusting the mean first-passage time, given in (IV.5.14), we have simulated 10,000 simulations ($dt = 0.01$, and duration as long as required to observe the first-passages) of the system, in order to determine the standard deviation of the first-passage time. This has resulted in the dotted lines in the map IV.9 (b). Although a bit less accurate (partly because of looser confidence intervals for higher statistics), there is a fair matching between the measured standard deviation of first-passage times and those predicted by the simple model.

As to other possible extrapolations of the model, it is manifestly also a flexible tool to upscale the first-passage times measured in the wind tunnel to longer runs. Once a regime (incubation, additive or multiplicative) in which oscillations are taking place is reached, characterized and its boundaries are determined, the analytical model indicates how the first-passage time scales with respect to higher energy levels. As long as one is interested in first-passage times in this regime, the model might provide fair extrapolations, with all usual limitations of usage on extrapolation.

As a particular example, the model is able to predict for how long measurements would need to be performed in order to reach some larger energy levels. This has two important implications. On one hand, in a preliminary design stage of a wind tunnel setup, the model is able to evaluate for how long the wind tunnel

length l	0.501m
width b	25mm
thickness t	0.4mm
mass m	1.816kg
Young's Modulus E	206GPa
density ρ	7767kg/m ³

Table IV.3: Geometric and mechanical properties of the experimental setup.

campaign should be foreseen. On the other hand, the model might prove to be a valuable decision tool for those investigators who are already dealing with stability evaluations [5] and who would like to know whether is it worth prolonging their measurement before larger amplitude might be observed.

IV.6 Application 4: A pre-stressed steel strip

This last example is based on the experimental and numerical investigation performed by E. Delhez [103] during her Master thesis. The research was performed at the University of Liège in the context of this PhD thesis. The experimental setup presented in Figure IV.10 is composed of a vertical metal strip of length l pre-stressed by a mass m . Mechanical and geometrical properties of the structure are given in Table IV.3. Vertical and horizontal displacements are hindered at the top extremity by a clamp while the lower extremity is free to move vertically only thanks to a lateral guide. The horizontal force F_w applied in the lower part of the strip presents the typical features of an external excitation while the force F_u applied by acceleration of the mass m modifies the tension in the strip, and hereby its rigidity, and can be associated to a parametric excitation. Both excitations are applied through electrodynamic shakers equipped with accelerometers. Additionally, the deformation of the strip is measured by a laser transducer.

In a first step, numerical and experimental analysis of the MDOF structure lead to the identification of the modal characteristics of the strip. Mode shapes, frequencies and corresponding damping coefficients are determined. Assuming that the excitation intensities, and consequently the displacements, remain small and that the system is excited in such a way that the structure responds in only one mode, the MDOF system can be reduced to a SDOF system defined by the corresponding modal amplitude q . For practical reasons, the mode observed in this experimental study is the second bending mode, represented in Figure IV.11 and corresponding to the frequency $f^* = 39.3Hz$.

The modal amplitude q is governed by the following linear Mathieu equation

$$m_{eq}\ddot{q}(t) + c_{eq}\dot{q}(t) + (k_{eq} + F_u(t)k_{p,eq})q(t) = \alpha F_w(t) \quad (\text{IV.6.1})$$

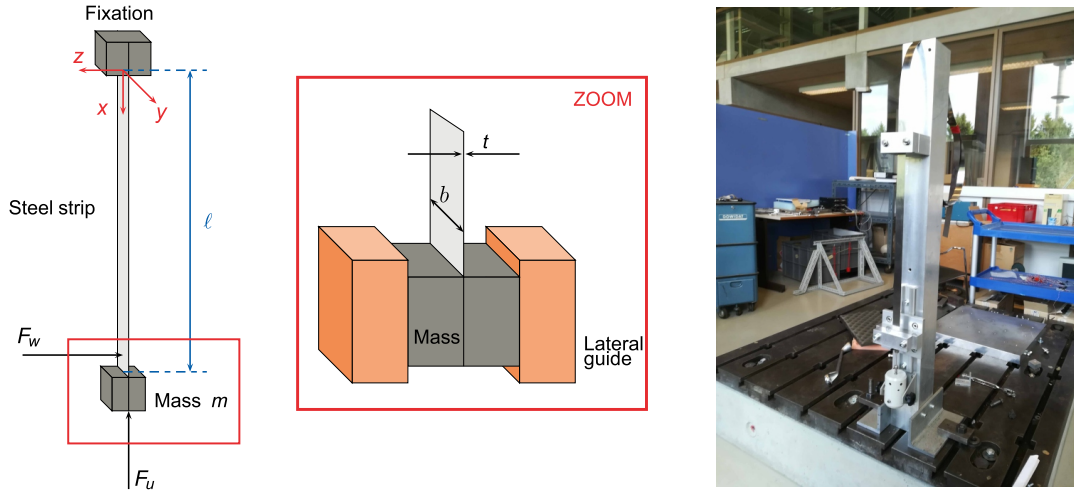


Figure IV.10: Illustrations of the pre-stressed steel strip [103].

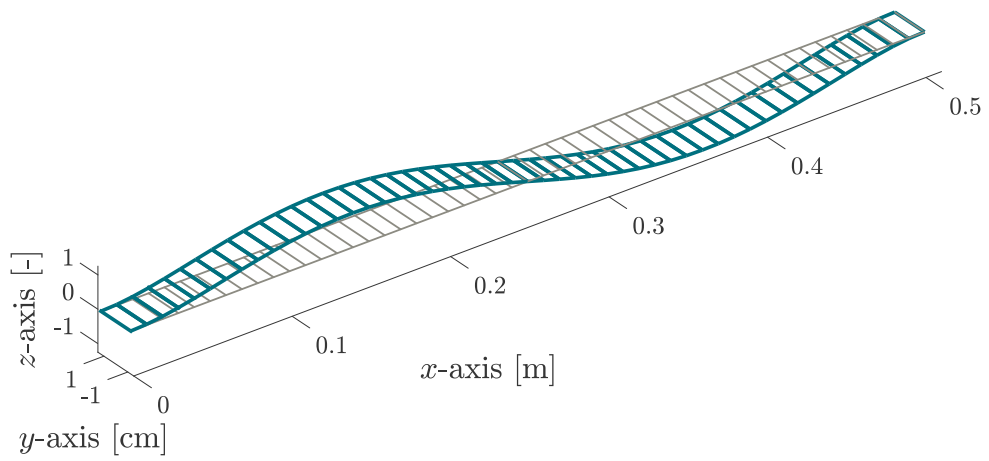


Figure IV.11: Second bending mode of the strip [103].

where m_{eq} , c_{eq} and k_{eq} are the equivalent mass, damping and stiffness of the SDOF system, obtained by projection of the mass, damping and stiffness of the strip onto the second bending mode. An additional stiffness component $k_{p,eq}F_u(t)$ is due to the pre-stress variation under the force $F_u(t)$ and the coefficient α stands for the projection of the force $F_w(t)$ on the mode and represents the value of the mode shape at the point of application of the force. The dot denotes a derivative with respect to time t . The values of the SDOF system parameters are the following ones

$$m_{eq} = 0.05kg, \quad c_{eq} = 0.08N.s.m^{-1}, \quad k_{eq} = 3273N.m^{-1} \quad \text{and} \quad k_{p,eq} = 39m^{-1}. \quad (\text{IV.6.2})$$

Defining the fundamental circular frequency of the mode $\Omega^* = 2\pi f^* = \sqrt{\frac{k_{eq}}{m_{eq}}}$ and the nondimensional time $\tau = \Omega^*t$, Equation (IV.6.1) can be rewritten in the nondimensional format

$$q''(\tau) + 2\xi q'(\tau) + (1 + u(\tau))q(\tau) = w(\tau) \quad (\text{IV.6.3})$$

with the primes denoting a derivative with the nondimensional time τ , the damping coefficient $\xi = \frac{c_{eq}\Omega^*}{2k_{eq}} = 0.3\%$ and the external and parametric forces given by

$$u(\tau = \Omega^*t) = F_u(t) \frac{k_{p,eq}}{k_{eq}} \quad \text{and} \quad w(\tau = \Omega^*t) = \frac{\alpha F_w(t)}{k_{eq}}. \quad (\text{IV.6.4})$$

A numerical analysis shows that a broadband excitation might be reduced to a narrow-band excitation, provided that the bandwidth of the parametric excitation includes the double of the fundamental frequency, and provided that the bandwidth of the external excitation includes the fundamental frequency. In this context, and in order to avoid excitation of other modes of the MDOF structure, the steel strip is submitted to narrow-band white noise excitations of intensities $S_{F_u} = S_{F_w} = 5 \times 10^{-3}N^2s$. The parametric force F_u covers the bandwidth $[0.77; 2.57]f_0$ while the external force covers the bandwidth $[0.87; 1.13]f_0$, as illustrated by the power spectra S_{F_u} and S_{F_w} in Figure IV.12. The excitation intensities of the reduced forces $u(\tau)$ and $w(\tau)$ are given, using the property (IV.2.6), by the expressions

$$S_u = S_{F_u} \Omega^{*2} \left(\frac{k_p}{k_{eq}} \right)^2 = 1.8 \times 10^{-4} \quad \text{and} \quad S_w = S_{F_w} \Omega^{*2} \left(\frac{\alpha}{k_{eq}} \right)^2 = 2.5 \times 10^{-10}. \quad (\text{IV.6.5})$$

The energy of the SDOF system is defined as the Hamiltonian of Equation (IV.6.3)

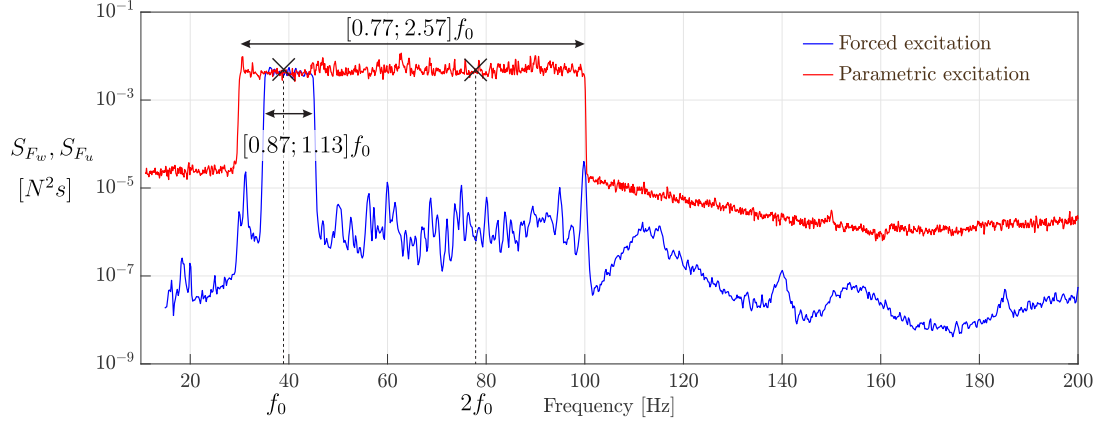


Figure IV.12: Power spectral densities of the narrow-band parametric and forced excitations applied to the strip.

$$H = \frac{q^2}{2} + \frac{q'^2}{2} = \frac{q^2}{2} + \frac{\dot{q}^2}{2\Omega^{*2}} \quad (\text{IV.6.6})$$

and corresponds to the definition of the energy (II.1.2) used in the analytical model.

Figure IV.13 presents the average first-passage time map obtained experimentally, analytically and numerically as a function of the reduced initial energy $H_0^* = \frac{H_0 S_u}{2S_w}$ and energy increase $\Delta H^* = \frac{\Delta H S_u}{2S_w}$. The experimental map is obtained by excitation of the steel strip and measurement of the system response. The first-passage map is reconstructed using the algorithm detailed in Section IV.4. Possible nonlinearities, multimodal response as well as modal interactions are included in the represented map (in straight line). Analytical results are obtained by Expression (III.2.3) for a SDOF linear Mathieu oscillator under broadband excitations. Finally, numerical results are obtained by Monte Carlo simulations of the linear MDOF system with adjusted parameters and also includes the possible response of the strip in several modes.

A good correspondence is observed between numerical and experimental results, as well as analytical results. It is important to highlight the fact that the analytical solution represented here is not fitted to the experimental results, but based on a mechanical model for the determination of the parameters S_u , S_w , a and Ω^* . Therefore, the small discrepancies can be explained by the narrow-band excitations, small nonlinearities into the system, the parameter adjustment method or the multimodal response of the strip.

The experimental curves also represent the three regimes. The incubation regime is observed since a linear spacing of the curves is visible in the lower part of the diagram. A horizontal tendency is observed in the left part of the diagram, corresponding to the additive regime. However, a slight tendency of

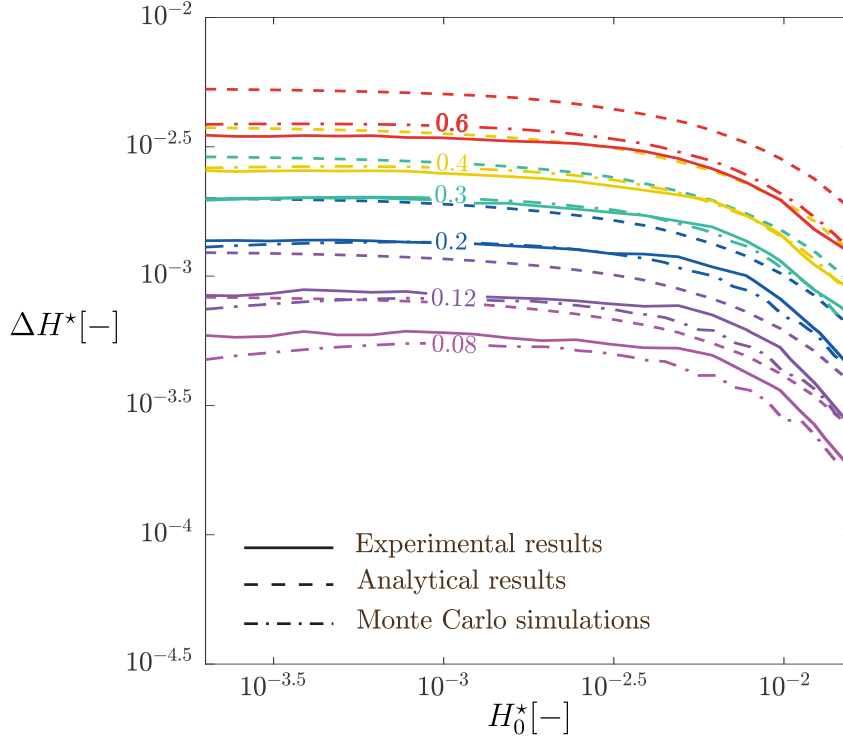


Figure IV.13: Average first-passage time map of the steel strip $\mathcal{E}\{\tau_f\} \frac{S_u}{4} = \mathcal{E}\{t_f\} \frac{S_u \Omega^*}{4}$. Comparison of analytical, experimental and numerical results.

the lower curves to go down when H_0^* decreases suggests that the additive regime might be restricted to higher values of ΔH^* in this case. In the right part of the diagram, the negative slope and parallel curves are observed, as a suggestion of the multiplicative regime. However, the observed levels of energy H_0^* are too small for the multiplicative regime to be completely developed.

The results of Figure IV.13 are very conclusive for several reasons. First, the three regimes are reproduced with their typical features. Then, the behavior of the MDOF steel strip can be approximated by and directly related to the behavior of a SDOF Mathieu oscillator. The characteristics of the Mathieu oscillator are predicted, which means that experimental measurements of the first-passage time are not necessary for the prediction the first-passage time of the strip under different conditions, or for other levels of energies, as long as some conditions are respected.

IV.7 Conclusion

The first-passage time is a tool that is applicable in many engineering problems, as soon as random excitations, such as wind turbulence, are concerned. Numerical examples are provided as a first step to direct applications of the first-passage approach. The closed-form solution of the average first-passage time under combined forced and parametric excitations highlighted the existence of various regimes. Among them, the additive and the multiplicative regimes have been observed in the stochastic dynamics of a tower crane in a turbulent flow. This system has been shown to be rather accurately modeled by a simple Mathieu oscillator, at least in terms of first-passage times since there exists an equivalent system presenting the same energy evolution from a first-passage time point of view. Indeed, average and second order first-passage time maps are very similar and the theoretical model may be used to understand and predict the tower crane behavior. Finally, the example of the pre-stressed steel strip is presented, where the corresponding Mathieu oscillator has been accurately identified and the three regimes observed. These experimental investigations provide a first link between an analytical but simplified result and a more complex reality and encourage the use of the first-passage as an analysis tool for the comprehension and the conceptual design in engineering applications.

Chapter V

A numerical approach for the first-passage time of a nonlinear system under evolutionary excitation:

The Galerkin scheme

This chapter develops a numerical method for the first-passage time distribution and the reliability function of nonlinear systems under external evolutionary excitation. Two distinct definitions of the energy are employed and their influence on the accuracy of the solution is detailed. A specific scheme is developed for the undamped oscillator. This research has been conducted during a visit of H. Vanvinckenroye at Columbia University.

- V.1 Introduction
 - V.2 Markovian modeling of the response energy
 - V.3 Amplitude-based energy envelope
 - V.4 Potential energy envelope
 - V.5 Conclusion
-

This Chapter is based on the following article:

Vanvinckenroye, H., Kougioumtzoglou I. A. & Denoël, V. (2018). Reliability function determination of nonlinear oscillators under evolutionary stochastic excitation via a Galerkin projection technique. *Nonlinear Dynamics*. Under review.
<http://hdl.handle.net/2268/223043>.

V.1 Introduction

The reliability function is defined as the probability of not reaching the design state in a given time interval and is governed by the Backward-Kolmogorov equation (I.6.16). The difficulty encountered in solving this equation analytically [117] has raised the need for approximate solution approaches. Although Monte Carlo simulation (MCS) schemes [118, 1, 119, 53] exhibit increased versatility, in many cases, they can be computationally daunting. Thus, alternative more computationally efficient approaches are required. Indicatively, these range from the more analytically oriented ones [120, 66, 76, 74, 121], such as relying on a Poisson distribution assumption [66], to the purely numerical schemes [122, 69, 120, 123, 71], such as discretized versions of the Chapman-Kolmogorov equation [70, 117] or probability density evolution schemes [124].

A rather standard technique for determining the first-passage time distribution and the reliability function of a system response relates to a stochastic averaging treatment of the governing equation of motion [125, 126, 127, 97, 128]. This is typically coupled with statistical linearization [129, 130, 131] and a Galerkin projection scheme for solving approximately the Backward-Kolmogorov partial differential equation [132], for determining the time-dependent reliability function and, finally, the first-passage time probability distribution. Although the aforementioned Galerkin scheme was extended recently to account for complex nonlinear/hysteretic systems, also endowed with fractional derivative elements [72, 133], the excitation has been mostly modeled as a standard Gaussian white noise process. The few papers that consider non-stationary excitations refer to linear systems [134]. In this regard, the Galerkin scheme developed in [71] is generalized herein to account for stochastic excitations with arbitrary evolutionary power spectrum forms, even of the non-separable kind [73, 72]. Further, a specific formulation is developed for the undamped oscillator (Section V.3.3). Finally, two distinct definitions for the response energy envelope are employed in the formulation (Sections V.3.2 and V.4). The accuracy of the technique is demonstrated by comparisons both with available analytical results, and with pertinent Monte Carlo simulations data. Because of the high complexity of the developments, the Galerkin scheme is developed for oscillators submitted to an external excitation only.

V.2 Markovian modeling of the response energy envelope

In this section, two alternative response energy envelope definitions are presented, whereas their benefits and limitations related to their use within a stochastic averaging solution treatment are discussed.

Consider a single-degree-of-freedom (SDOF) nonlinear oscillator governed by the nondimensional equation of motion

$$\ddot{x} + 2\xi\dot{x} + x + \varepsilon z(x, \dot{x}) = w \quad (\text{V.2.1})$$

where $w(t)$ is a broadband non-stationary stochastic excitation process with a non-separable, in general, evolutionary power spectrum $S_w(\omega, t)$ ¹. The linear damping coefficient is given by $\beta = 2\xi$, while $z(x, \dot{x})$ denotes an arbitrary nonlinear function, and the parameter ε controls the nonlinearity magnitude. Also, as in (II.2.1) and (III.2.1), the natural frequency of the corresponding linear oscillator is equal to one due to the normalization.

Further, relying on the standard assumptions of stochastic averaging [97], and considering a lightly damped oscillator, a linearized version of Equation (V.2.1) is defined as

$$\ddot{x} + \beta_e(H)\dot{x} + \omega_e^2(H)x = w \quad (\text{V.2.2})$$

where the equivalent damping β_e and stiffness ω_e^2 coefficients are given as functions of the amplitude-based energy envelope H . Specifically, due to the assumed pseudo-harmonic behavior of the oscillator response process, the displacement x and velocity \dot{x} can be expressed as [13, 71]

$$\begin{cases} x(t) = x(A(t), \theta(t)) &= A(t) \cos(\omega_e(H(t))t + \theta(t)) \\ \dot{x}(t) = \dot{x}(A(t), \theta(t)) &= -\omega_e(H(t))A(t) \sin(\omega_e(H(t))t + \theta(t)) \end{cases} \quad (\text{V.2.3})$$

and thus, manipulating Equation (V.2.3) leads to the *amplitude-based energy envelope*

$$H = \frac{A^2}{2} = \frac{x^2}{2} + \frac{\dot{x}^2}{2\omega_e^2(H)}. \quad (\text{V.2.4})$$

In Equation (V.2.3), A and θ denote the response amplitude and phase, respectively, assumed to be slowly varying functions of time. In this regard, the equivalent linear elements β_e and ω_e^2 are typically evaluated based on an average over one cycle approach as [131, 125]

$$\beta_e(H) = \beta + \varepsilon \frac{B(H)}{\sqrt{2H}\omega_e(H)} \quad \text{and} \quad \omega_e^2(H) = 1 + \varepsilon \frac{C(H)}{\sqrt{2H}} \quad (\text{V.2.5})$$

with

$$C(H) = \frac{1}{\pi} \int_0^{2\pi} \cos \theta z(\sqrt{2H} \cos \theta, -\sqrt{2H} \sin \theta) d\theta \quad (\text{V.2.6})$$

¹Please remind that, in this entire work, the power spectrum of the process $w(t)$ is defined so that its variance is given by $\sigma_w^2(t) = \frac{1}{2\pi} \int_{-\infty}^{\infty} S_w(\omega, t) d\omega = \int_{-\infty}^{\infty} S_w(\omega = 2\pi f, t) df$

and

$$B(H) = \frac{-1}{\pi} \int_0^{2\pi} \sin \theta z(\sqrt{2H} \cos \theta, -\sqrt{2H} \sin \theta) d\theta. \quad (\text{V.2.7})$$

It can be readily seen that the initial approximation step of defining the linearized Equation (V.2.2) has a negative effect on the accuracy of the ensuing stochastic averaging treatment by increasing the overall approximation degree of the technique; see also [127, 135] for a discussion. In this regard, to bypass this limitation, in particular for oscillators with nonlinear stiffness elements $z(x, \dot{x}) = z(x)$ submitted to a time-modulated white noise excitation $S_w(\omega, t) = S_0 F(t)$, an alternative to Equation (V.2.4) potential energy envelope definition can be utilized [127]. Specifically, defining the potential

$$u(x) = \int_0^y (y + \varepsilon z(y)) dy. \quad (\text{V.2.8})$$

and considering the transformation

$$\begin{cases} u(x) &= H \cos^2 \theta \\ \dot{x} &= -\sqrt{2H} \sin \theta \end{cases}, \quad (\text{V.2.9})$$

yields the *potential energy envelope* definition

$$H = u(x) + \frac{\dot{x}^2}{2}. \quad (\text{V.2.10})$$

Note that, in contrast to the commonly used definition of Equation (V.2.4), the potential energy envelope of Equation (V.2.10) involves no approximations for its definition. Thus, it is anticipated that an overall higher accuracy degree is exhibited when coupled with a stochastic averaging technique [97]. On the other hand, Equation (V.2.4) appears to be more versatile than Equation (V.2.10) in handling a wider range of nonlinearity types [127]. It is worth noting that for the linear case ($\varepsilon = 0$) Equation (V.2.10) degenerates into the amplitude-based energy envelope definition of Equation (V.2.4). In passing, the reader is referred to [136] as well, where the aforementioned limitation is addressed by an alternative amplitude definition based on the Hilbert transform. In the following sections, the technique developed in [71] is generalized to account for evolutionary stochastic excitations, while the performances of the two definitions in Equations (V.2.4) and (V.2.10) are assessed with respect to determining first-passage time statistics.

V.3 Stochastic averaging: Amplitude-based energy envelope definition

V.3.1 Backward-Kolmogorov equation

Adopting the amplitude-based energy envelope definition of Equation (V.2.4), and employing a standard stochastic averaging procedure [13, 62, 116], leads to decoupling of the energy H with the phase θ , and to a first order stochastic differential equation governing the dynamics of H . This procedure always provides the same solution as the first order asymptotic expansion used in Chapter II so that the average Itô equation takes the form

$$\dot{H} = m(H) + \sigma(H)\eta(t) \quad (\text{V.3.1})$$

where $\eta(t)$ is a δ -correlated white noise process of intensity one, $m(H)$ and $\sigma(H)$ are the drift and diffusion coefficients, respectively given by

$$\begin{cases} m(H) = \frac{S_w(\omega_e(H),t)}{2\omega_e^2(H)} - \beta_e(H)H \\ \sigma(H) = \sqrt{\frac{S_w(\omega_e(H),t)H}{\omega_e^2(H)}} \end{cases} \quad (\text{V.3.2})$$

The reliability function $P(t; H_0)$ related to the energy process (V.3.1) is given by the Backward-Kolmogorov equation (I.6.15). Using (I.6.32), this takes the form [134, 13]

$$\frac{\partial P}{\partial t} = \left(\frac{S_w(\omega_e(H_0),t)}{2\omega_e^2(H_0)} - \beta_e(H_0)H_0 \right) \frac{\partial P}{\partial H_0} + \frac{S_w(\omega_e(H_0),t)H_0}{2\omega_e^2(H_0)} \frac{\partial^2 P}{\partial H_0^2} \quad (\text{V.3.3})$$

with initial condition (I.6.20) and boundary condition (I.6.21). For the sake of simplicity in the notations, the subscript "0" is once more omitted in the following developments.

Defining $\tau = \beta t$; $s^2(H, \tau) = \frac{S_w(\omega_e(H), \tau)}{2\beta\omega_e^2(H)}$ and $\kappa(H) = \frac{\beta_e(H)}{\beta}$, Equation (V.3.3) becomes

$$\frac{\partial P}{\partial \tau} = (s^2(H, \tau) - \kappa(H)H) \frac{\partial P}{\partial H} + s^2(H, \tau)H \frac{\partial^2 P}{\partial H^2} \quad (\text{V.3.4})$$

Note that the quantity $s^2(H, \tau)$ for $\varepsilon = 0$ and $S_w(\omega, t) = S_0$ corresponds to the stationary response variance of a linear oscillator under Gaussian white noise excitation [131]. It is important to notice that the scaling used to derive (V.3.3) is formally invalid in the undamped case, i.e. if $\beta = 0$. However, since the linear damping coefficient β appears in (II.2.5) (through $\beta_e(H_0)$) as a regular perturbation of the problem, the solution of (V.3.3) actually regularly converges toward the solution of the undamped problem. This is shown in Section V.3.3.

V.3.2 Galerkin projection scheme

Linear oscillator

For $\varepsilon = 0$, Equation (V.3.4) degenerates into

$$\frac{\partial P}{\partial \tau} = (s_{\text{lin}}^2(\tau) - H) \frac{\partial P}{\partial H} + s_{\text{lin}}^2(\tau) H \frac{\partial^2 P}{\partial H^2} \quad (\text{V.3.5})$$

where $s_{\text{lin}}^2(\tau) = s^2(H, \tau)|_{\varepsilon=0} = \frac{S_w(1, \tau)}{2\beta}$. As the system is linear, the natural frequency ω_e is constant and equal to 1 so that the function $s(H, \tau)$ is a function of time only.

Next, following a separation of variables solution approach as in [132] (see also [134] for related work), the reliability function is expressed as an expansion in terms of eigenfunctions $\Phi_i(H)$ with time-variant coefficients $T_i(t)$ in the form

$$P(\tau; H) = \sum_{i=1}^{\infty} T_i(\tau) \Phi_i(H) \quad (\text{V.3.6})$$

In the following, as suggested by the solution of Equation (V.3.5) for the special case of white noise excitation [132], the eigenfunctions $\Phi_i(H)$ are chosen as the confluent hypergeometric functions $\Phi_i(H) = M(-\lambda_i, 1, H)$. These are defined as the solution of

$$H \frac{d^2 \Phi}{dH^2} + (1 - H) \frac{d\Phi}{dH} + \lambda \Phi = 0 \quad (\text{V.3.7})$$

and exhibit the orthogonality conditions

$$\int_0^{H_c} \Phi_i(H) \Phi_j(H) f(H) dH = 0 \quad \text{if } i \neq j \quad (\text{V.3.8})$$

with the weighting function $f(H) = e^{-H}$, while the corresponding eigenvalues λ_i relate to the boundary condition and are given by solving

$$M(-\lambda, 1, H_c) = 0. \quad (\text{V.3.9})$$

Next, substituting (V.3.6) into Equation (V.3.5) and employing Equation (V.3.8), yields a system of coupled differential equations for the time coefficients $T_i(\tau)$ of the form

$$\dot{T}_i(\tau) = -s^2(\tau) \lambda_i T_i(\tau) - (1 - s^2(\tau)) \sum_j T_j(\tau) \nu_{ij}; \quad (\text{V.3.10})$$

with initial condition $T_i(0) = F_{1,i}/F_{2,i}$ and defining

$$\begin{aligned} F_{1,i} &= \int_0^{H_c} \Phi_i(H) f(H) dH, \\ F_{2,i} &= \int_0^{H_c} \Phi_i^2(H) f(H) dH \text{ and} \\ \nu_{ij} &= \frac{\int_0^{H_c} H \Phi_i(H) \frac{d\Phi_j(H)}{dH} f(H) dH}{F_{2,i}}. \end{aligned} \quad (\text{V.3.11})$$

Clearly, for practical purposes, the series expansion of Equation (V.3.6) is truncated to a finite number of terms N and the coefficients $T_i(\tau)$ are obtained by solving the set of N coupled differential Equations (V.3.10) for $i = 1, \dots, N$, which can be expressed in the concise form

$$\dot{\mathbf{T}}(\tau) = -s^2(\tau)\boldsymbol{\lambda}\mathbf{T}(\tau) - (1 - s^2(\tau))\boldsymbol{\nu}\mathbf{T}(\tau) \quad (\text{V.3.12})$$

In Equation (V.3.12), the components of the vector $\mathbf{T}(\tau)$ are the $T_i(\tau)$ functions, $\boldsymbol{\lambda}$ is the diagonal matrix of the eigenvalues λ_i and the components of matrix $\boldsymbol{\nu}$ are the coefficients ν_{ij} . Additional details regarding the numerical evaluation of the eigenvalues and eigenfunctions, as well as the properties of the confluent hypergeometric functions can be found in [132] where numerical values of $\lambda_i(H_c)$, $F_{1,i}$, $F_{2,i}$ and ν_{ij} are given for $i, j = 1, \dots, 10$ and various values of H_c .

Nonlinear oscillator

For the general nonlinear case, i.e, $\varepsilon \neq 0$, Equation (V.3.4) can be separated into a linear and a nonlinear operator as [71]

$$\frac{\partial P}{\partial \tau} = \mathcal{L}_{\text{lin}} \{P\} + \mathcal{L}_{\text{nonlin}} \{P\} \quad (\text{V.3.13})$$

where the linear operator $\mathcal{L}_{\text{lin}} \{ \}$ is defined so that $\frac{\partial P}{\partial \tau} = \mathcal{L}_{\text{lin}} \{P\}$ when $\varepsilon = 0$ as in Equation (V.3.5). Specifically,

$$\begin{cases} \mathcal{L}_{\text{lin}} \{ \} &= (s_{\text{lin}}^2(\tau) - H) \frac{\partial}{\partial H} + s_{\text{lin}}^2(\tau) H \frac{\partial^2}{\partial H^2} \\ \mathcal{L}_{\text{nonlin}} \{ \} &= (s^2(H, \tau) - s_{\text{lin}}^2(\tau) - (\kappa(H) - 1) H) \frac{\partial}{\partial H} + (s^2(H, \tau) - s_{\text{lin}}^2(\tau)) H \frac{\partial^2}{\partial H^2} \end{cases} \quad (\text{V.3.14})$$

Further, without any loss of generality, the reliability function of the nonlinear oscillator is sought as a perturbation of the linear problem, yielding

$$P(\tau; H) = P_{\text{lin}}(\tau; H) + P_{\text{nonlin}}(\tau; H) \quad (\text{V.3.15})$$

where

$$P_{\text{nonlin}}(\tau; H) = \sum_{i=1}^{\infty} c_i(\tau) \Phi_i(H) \quad (\text{V.3.16})$$

i.e. a linear combination of the confluent hypergeometric functions in the same basis as that used also for the linear case in Equation (V.3.6); see also [71]. Substituting Equations (V.3.15)-(V.3.16) into (V.3.13) and taking into account that $\frac{\partial P_{\text{lin}}}{\partial \tau} = \mathcal{L}_{\text{lin}} \{P_{\text{lin}}\}$ provides the following residue:

$$\begin{aligned}
R(H, \tau) &= \frac{\partial P_{\text{lin}}(\tau; H)}{\partial \tau} + \frac{\partial P_{\text{nl}}(\tau; H)}{\partial \tau} - \mathcal{L}_{\text{lin}} \{P_{\text{lin}}(\tau; H) + P_{\text{nl}}(\tau; H)\} - \mathcal{L}_{\text{nl}} \{P_{\text{lin}}(\tau; H) + P_{\text{nl}}(\tau; H)\} \\
&= \frac{\partial P_{\text{nl}}(\tau; H)}{\partial \tau} - \mathcal{L}_{\text{lin}} \{P_{\text{nl}}(\tau; H)\} - \mathcal{L}_{\text{nl}} \{P_{\text{lin}}(\tau; H)\} - \mathcal{L}_{\text{nl}} \{P_{\text{nl}}(\tau; H)\} \\
&= \sum_{r=1}^{\infty} [\dot{c}_r(\tau) \Phi_r(H) - c_r(\tau) \mathcal{L}_{\text{lin}} \{\Phi_r(H)\} - c_r(\tau) \mathcal{L}_{\text{nl}} \{\Phi_r(H)\} - T_r(\tau) \mathcal{L}_{\text{nl}} \{\Phi_r(H)\}].
\end{aligned} \tag{V.3.17}$$

In practice, the summation operator in Equation (V.3.17) is truncated to a finite number N of terms so that the N coefficients $c_i(\tau)$ ($i = 1, \dots, N$) are obtained by solving a set of N coupled differential equations, derived by projection of the weighted residue onto each of the N basis functions $\Phi_i(H)$ [132]. The set of equations is given by

$$\int_0^{H_c} R(H, \tau) \Phi_i(H) f(H) dH = 0 \quad \text{with } i = 1, \dots, N \tag{V.3.18}$$

and, taking (V.3.8) into account, Equation (V.3.18) becomes

$$\begin{aligned}
\dot{c}_i(\tau) \int_0^{H_c} \Phi_i^2(H) f(H) dH &= \sum_{r=1}^N \left[c_r(\tau) \int_0^{H_c} \mathcal{L} \{\Phi_r(H)\} \Phi_i(H) f(H) dH \right. \\
&\quad \left. + T_r(\tau) \int_0^{H_c} \mathcal{L}_{\text{nl}} \{\Phi_r(H)\} \Phi_i(H) f(H) dH \right],
\end{aligned} \tag{V.3.19}$$

Alternatively, Equation (V.3.19) is cast in the form

$$\dot{\mathbf{c}}(\tau) = \mathbf{D}(\tau) \mathbf{c}(\tau) + \mathbf{e}(\tau) \tag{V.3.20}$$

where the components of the vector $\mathbf{c}(\tau)$ are the $c_i(\tau)$ functions, the matrix $\mathbf{D}(\tau)$ is given by

$$\mathbf{D}(\tau) = \begin{bmatrix} \frac{\int_0^{H_c} \mathcal{L} \{\Phi_1(H)\} \Phi_1(H) f(H) dH}{F_{2,1}} & \dots & \frac{\int_0^{H_c} \mathcal{L} \{\Phi_N(H)\} \Phi_1(H) f(H) dH}{F_{2,1}} \\ \vdots & \ddots & \vdots \\ \frac{\int_0^{H_c} \mathcal{L} \{\Phi_1(H)\} \Phi_N(H) f(H) dH}{F_{2,N}} & \dots & \frac{\int_0^{H_c} \mathcal{L} \{\Phi_N(H)\} \Phi_N(H) f(H) dH}{F_{2,N}} \end{bmatrix} \tag{V.3.21}$$

and the vector $\mathbf{e}(\tau)$ has the form

$$\mathbf{e}(\tau) = \begin{bmatrix} \frac{\sum_{r=1}^N T_r(\tau) \int_0^{H_c} \mathcal{L}_{\text{nl}} \{\Phi_r(H)\} \Phi_1(H) f(H) dH}{F_{2,1}} \\ \vdots \\ \frac{\sum_{r=1}^N T_r(\tau) \int_0^{H_c} \mathcal{L}_{\text{nl}} \{\Phi_r(H)\} \Phi_N(H) f(H) dH}{F_{2,N}} \end{bmatrix} \tag{V.3.22}$$

Note that as the initial condition $P(H, 0) = 1$ is satisfied by the linear solution $P_{\text{lin}}(H, 0) = 1$, considering Equation (V.3.15) yields $P_{\text{nl}}(H, 0) = 0$, or equivalently, $c_i(0) = 0$, $i = 1, \dots, N$.

V.3.3 Special case: Undamped oscillator

In the following, the system governed by

$$\ddot{x} + x + \varepsilon z(x, \dot{x}) = w(t) \quad (\text{V.3.23})$$

is considered, which is a special case of the general oscillator of Equation (V.2.1). Note that for $\varepsilon = 0$, Equation (V.3.23) yields an undamped linear oscillator. Although physically realistic systems always have some degree of damping, it can be argued that studying the undamped case still has some mathematical and practical merits. In fact, the limiting case of an undamped system leads to simplifications in the developments and to a deeper understanding of the physical phenomena [116, 49, 86]. Further, relatively straightforward extensions of results referring to the undamped case may be possible to account for slightly damped systems as well. For instance, the mathematical framework used for deriving the mean first-passage time of undamped oscillators in Chapter II was extended in Section III.2 for damped oscillators.

Formally, the Galerkin scheme developed in Sections V.3.2 and V.3.2 is only valid in the damped case, i.e. if $\beta \neq 0$. This results from the rescaling that was used to derive (V.3.3). In particular, the eigenvalues as well as the nondimensional excitation $s(\tau)$ are going to infinity if β vanishes. However, it is observed that the general solution given by (V.3.6) and (V.3.16) regularly converges, which is explained by the fact that damping enters in (II.2.5) as a regular perturbation of the undamped case. For completeness, the formulation of the Galerkin scheme for $\beta = 0$ is specifically developed in this section. It is then shown to be equivalent to the general solution developed in V.3.2 in the limit case $\beta \rightarrow 0$.

Specifically, the first order stochastic differential equation (V.3.1) remains unchanged, accounting for $\beta = 0$ in the definition of $\beta_e(H)$ (V.2.5) and the corresponding Backward-Kolmogorov equation becomes

$$\frac{\partial P}{\partial t} = (s^2(H, t) - \beta_e(H)H) \frac{\partial P}{\partial H} + s^2(H, t)H \frac{\partial^2 P}{\partial H^2} \quad (\text{V.3.24})$$

where the quantity $s^2(H, t)$ is now defined as $s^2(H, t) = \frac{S_w(\omega_e(H), t)}{2\omega_e^2(H)}$. Note that the term $\beta_e(H)$ for the system of Equation (V.3.23) is non-zero, in general, due to the dependence of the nonlinear function $z(x, \dot{x})$ on the response velocity \dot{x} . However, for the case $\varepsilon = 0$, Equation (V.3.23) yields a linear undamped oscillator, and the term $\beta_e(H)$ becomes zero. In a similar manner as in Section V.3.2, the reliability function is expressed as in Equation (V.3.6), whereas the eigenfunctions $\Phi_i(H)$ are now given by the Bessel functions of the first kind $\text{BesselJ}(0, \sqrt{4\lambda_i H})$, which are the solution of

$$H \frac{d^2 \Phi}{dH^2} + \frac{d\Phi}{dH} + \lambda \Phi = 0. \quad (\text{V.3.25})$$

It can be demonstrated that the confluent hypergeometric function (defined

as the solution of (V.3.7)) reduces to the Bessel function (defined as the solution of (V.3.25)) for $\beta \rightarrow 0$, i.e.

$$\text{BesselJ}(0, \sqrt{4\lambda_i H}) = \lim_{\beta \rightarrow 0} M(-\lambda_i, 1, H) \quad (\text{V.3.26})$$

Specifically, defining $\tilde{\lambda} = \beta\lambda$ and $\tilde{H} = \frac{H}{\beta}$, so that $\tilde{\lambda}$ and \tilde{H} are finite as β vanishes, and substituting into (V.3.7) yields

$$\tilde{H} \frac{d^2\Phi}{d\tilde{H}^2} + \frac{d\Phi}{d\tilde{H}} + \tilde{\lambda}\Phi = 0 \quad (\text{V.3.27})$$

which has the same form as Equation (V.3.25).

Further, the orthogonality conditions of Equation (V.3.8) hold true with the corresponding weighting function being equal to $f(H) = 1$. Next, substituting expression (V.3.6) into the Backward-Kolmogorov Equation (V.3.24) and projecting onto the basis of eigenfunctions, the time coefficients $T_i(\tau)$ are given by the solution of the set of differential equations

$$\dot{T}_j(t) = -s^2(t)\lambda_j T_j(t) \quad (\text{V.3.28})$$

with initial condition $T_j(0) = F_{1,j}/F_{2,j}$, and following (V.3.11) with $f(H) = 1$.

Similarly as in Section V.3.2, the solution of the nonlinear oscillator is expressed in the form of Equation (V.3.15), while Equations (V.3.13) degenerate into

$$\begin{cases} \mathcal{L}_{\text{lin}} \{ \} &= s_{\text{lin}}^2(t) \frac{\partial}{\partial H} + s_{\text{lin}}^2(t) H \frac{\partial^2}{\partial H^2} \\ \mathcal{L}_{\text{nl}} \{ \} &= (s^2(H, t) - s_{\text{lin}}^2(t) - \beta_e(H)H) \frac{\partial}{\partial H} + (s^2(H, t) - s_{\text{lin}}^2(t)) H \frac{\partial^2}{\partial H^2} \end{cases} \quad (\text{V.3.29})$$

with $s_{\text{lin}}^2(t) = \frac{S_w(1,t)}{2}$.

The basis of eigenfunctions developed in the undamped case is of high interest since the Bessel functions are computationally easier to obtain than the hypergeometric confluent functions; they are for instance implemented in most standard programming softwares. The degree of complexity and the computational burden encountered in the damped case when dealing with the hypergeometric functions might be significantly decreased by use of the Bessel functions basis. In particular, as soon as the damped system is nonlinear, the optimality of the basis of hypergeometric confluent functions to approximate the nonlinear part of the response can be hardly justified. In this respect, the basis of eigenfunctions developed in the undamped case, i.e. the Bessel functions, could potentially provide accurate solutions for lightly damped oscillators as well. This opportunity warrants further attention, and is identified as future work.

V.3.4 The first-passage time distribution and its statistical moments

The probability density function of the first-passage time can be determined by substituting (V.3.6) and (V.3.16) into (I.6.3) yielding

$$p_f(t; H) = - \sum_i \left(\dot{T}_i(t) + \dot{c}_i(t) \right) \Phi_i(H) \quad (\text{V.3.30})$$

with the time-dependent coefficients $\dot{T}_i(t)$ and $\dot{c}_i(t)$ given by (V.3.10) and (V.3.20), respectively. The first and second statistical moments of the first-passage time are given by

$$\begin{cases} \mathcal{E} \{t_f\} = \sum_i A_i \Phi_i(H) & \text{with } A_i = - \int_0^\infty \left(\dot{T}_i(t) + \dot{c}_i(t) \right) t \, dt \\ \mathcal{E} \{t_f^2\} = \sum_i B_i \Phi_i(H) & \text{with } B_i = - \int_0^\infty \left(\dot{T}_i(t) + \dot{c}_i(t) \right) t^2 \, dt \end{cases} \quad (\text{V.3.31})$$

where $\mathcal{E} \{ \}$ represents the statistical expectation. It is reminded here that the variable H of the eigenfunctions represents the initial energy H_0 where the index "0" has been omitted for the sake of simplicity.

Considering a linear undamped oscillator under white noise excitation ($S_w(\omega, t) = S_0$), since $\dot{T}_i(t) = -\frac{\lambda_i S_0}{2} T_i(t)$ and $\dot{c}_i(t) = 0$, Equation (V.3.31) becomes

$$\begin{cases} \mathcal{E} \{t_f\} = \sum_i A_i \Phi_i(H) & \text{with } A_i = \frac{2}{\lambda_i S_0} \frac{F_{1,i}}{F_{2,i}} \\ \mathcal{E} \{t_f^2\} = \sum_i B_i \Phi_i(H) & \text{with } B_i = \frac{8}{\lambda_i^2 S_0^2} \frac{F_{1,i}}{F_{2,i}} \end{cases} \quad (\text{V.3.32})$$

Analytical results are derived for this particular case in Section II.3 and III.1 for the mean and mean square first-passage times $\mathcal{E} \{t_f\}$ and $\mathcal{E} \{t_f^2\}$ based on a stochastic averaging treatment and are given by

$$\begin{cases} \mathcal{E} \{t_f\} = \frac{2}{S_0} \Delta H \\ \mathcal{E} \{t_f^2\} = \frac{4}{S_0^2} \Delta H \left(H + \frac{3}{2} \Delta H \right) \end{cases} \quad (\text{V.3.33})$$

where $\Delta H = H_c - H$ is the energy increase. Equality between (V.3.32) and (V.3.33) is demonstrated by projection of the two sides of the equations on the basis of eigenfunctions $\Phi_j(H)$, and showing that these projections are identical for all $\Phi_j(H)$. This is demonstrated in Appendix E and provides a theoretical validation of the Galerkin scheme in the case of an undamped and linear oscillator.

V.3.5 Numerical examples

Linear undamped oscillator under stationary white noise excitation

A linear undamped oscillator under Gaussian white noise excitation is considered next with parameters values $\varepsilon = 0$ and $S_w(\omega, t) = S_0$. Figures V.1 show the reliability function and the first-passage time distribution for $H_c = 2$, $S_0 = 0.1$, $N = 9$ and a range of values for H_0 . In Figure V.2, the reliability functions and respective first-passage distributions are plotted for $H_0 = 0$ and for various values of the truncation order N . The dashed lines correspond to the modified Galerkin scheme as developed in Section V.3.3 for undamped oscillators, whereas the solid lines correspond to the general Galerkin scheme of Section V.3.2 for the limiting case $\beta \rightarrow 0$. In fact, it is seen that even a direct implementation of the technique of Section V.3.2 (solid lines) with a very low value of β (i.e., $\beta \sim 10^{-9}$) still yields results of satisfactory accuracy, which are practically indistinguishable (especially for the $N = 9$ case) from results obtained by the more rigorous (for the undamped case) treatment of Section V.3.3 (dashed lines). This behavior can be construed as an indication of increased robustness of the technique. The circles and crosses correspond to Monte Carlo simulations data obtained by numerically integrating the governing equation of the original system (V.2.1) and its averaged formulation (V.3.1), respectively. This is done via a standard Runge-Kutta scheme (10000 realizations).

The significant discrepancy between Galerkin-based and MCS-based results observed at very early time instants is attributed to the fact that an infinite number of terms is required for the summation of Equation (V.3.6) to equal 1 at $\tau = 0$ [134]. As anticipated due to the differentiation of Equation (V.3.36), the degree of the discrepancy increases when computing first-passage distributions in Figure V.2 (right). Nevertheless, this is not deemed as a significant drawback of the technique, as the primary interest is directed to situations where the probability of first-passage time is higher than zero. Further, it is seen that quite satisfactory accuracy is achieved for a relatively small number of expansion terms. In fact, little improvement is obtained by increasing the terms from 5 to 9. The satisfactory degree of accuracy is also corroborated by the results in Table V.1 where the mean and mean square first-passage times obtained by the Galerkin scheme are compared with the analytical solution (V.3.33) as well as with Monte Carlo simulations. The relative error is calculated with respect to the Monte Carlo simulations.

Nonlinear Duffing oscillator under evolutionary stochastic excitation

As a second example, a Duffing oscillator of the form of Equation V.2.1 is considered whose restoring force is given by $z(x, \dot{x}) = x^3$. For this kind of nonlinearity, Equations (V.2.5) yield [71]:

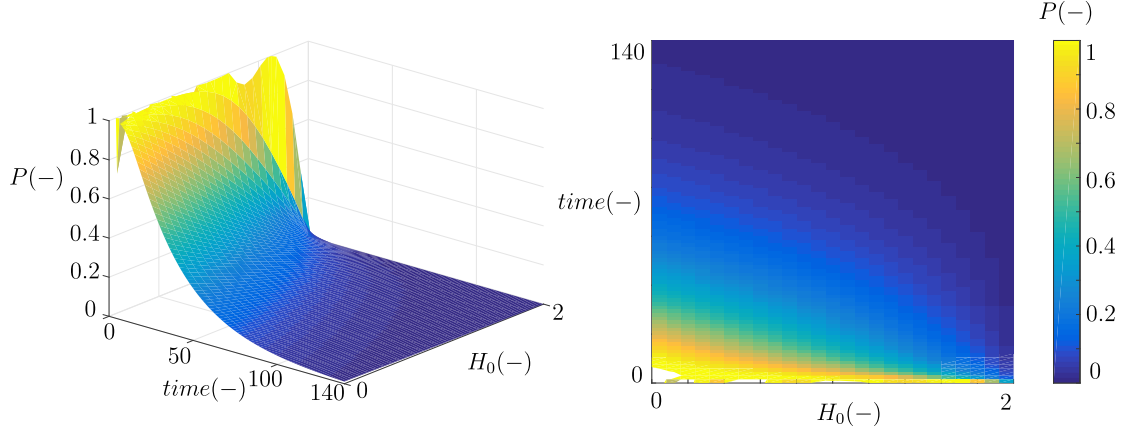


Figure V.1: Galerkin scheme based reliability function of a linear undamped oscillator under white noise excitation for $N = 9$ and a range of values for H_0 from 0 to $H_c = 2$.

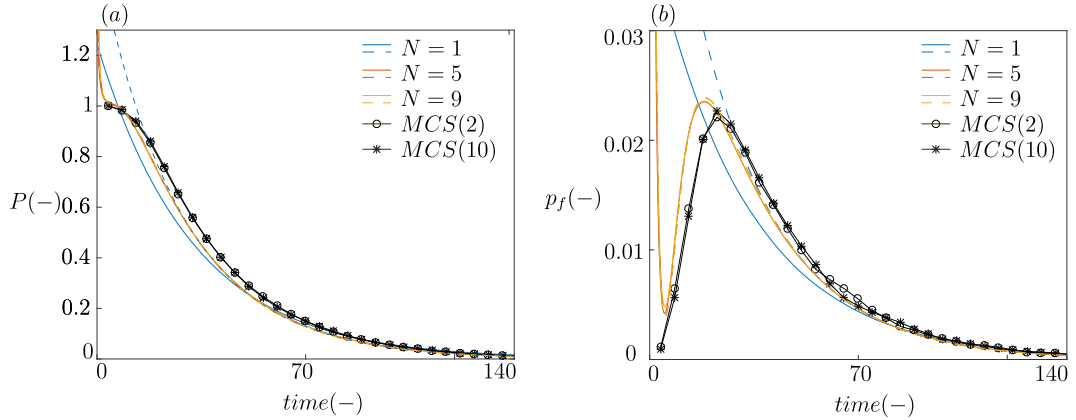


Figure V.2: (a) Reliability function and (b) probability density function of the first-passage time. Linear undamped oscillator under white noise constant excitation for $H_0 = 0$ and $N = 1, 5, 9$; comparisons with MCS data (10000 realizations).

	$\mathcal{E}\{t_f\}$		$\mathcal{E}\{t_f^2\}$	
	Value	Error	Value	Error
Galerkin scheme	40.93	0.58%	2443.1	0.91%
Analytical solution (V.3.33)	40.00	2.84%	2400	0.86%
Monte Carlo simulations	41.17	—	2421	—

Table V.1: Average and mean square first-passage times obtained by the Galerkin scheme, the analytical solution and Monte Carlo simulations for a linear undamped oscillator under white noise excitation with $H_0 = 0$ and $N = 9$.

$$\begin{cases} \beta_e & = \beta \\ \omega_e^2(H) & = 1 + \frac{3}{2}\varepsilon H \end{cases} \quad (\text{V.3.34})$$

Now, the oscillator is subjected to a non-stationary stochastic seismic excitation described by the non-separable evolutionary power spectrum [134]

$$S_w(\omega, t) = S_0 \frac{e^{-(c+\alpha(\omega))t}}{C} \quad (\text{V.3.35})$$

with $\alpha(\omega) = (\omega/5\pi)^2$ and c is a parameter controlling essentially the effective time duration of the excitation. The constant C is evaluated so that the maximum in time value of the spectrum is equal to S_0 for $\omega = \omega_0 = 1$. This yields $C = 4e^{-2} (c + (1/5\pi)^2)^2$. The spectrum is plotted in Figure V.3 for $c = 0.01$ (left) and for various values of c (right). Figure V.4 presents the reliability function (left) and the first-passage time distribution (right) for $c = 0.01$, $H_0 = 0$, $H_c = 0.18$, $\beta_0 = 0.02$, $S_0 = 0.01$, and $\varepsilon = 0.1$ by using the Galerkin scheme of Section V.3.2. Comparisons with Monte Carlo simulations data (10000 realizations) by numerically integrating Equation (V.2.1), in conjunction with a spectral representation scheme [137] for producing excitation samples compatible with the spectrum of Equation (V.3.35), are included as well demonstrating a satisfactory degree of accuracy. Similarly as in example V.3.5, the spurious results around $t = 0$ refer to approximately zero first-passage probability, and thus, are of little practical interest. Figure V.3 (right) shows the influence of the parameter c on the time duration of the excitation by plotting the time-dependent function $S_w(\omega, t)/S_0$ for $\omega = \omega_0 = 1$ and various values of c . Specifically, for $c = 0.01, 0.03, 0.05, 0.07$ and 0.09 , the duration of the excitation is respectively equal to $T_w = 476.8, 196.8, 123.9, 90.5$ and 71.2 . Obviously, for a shorter time duration, there is a smaller probability that the oscillator will ever cross the barrier before the excitation vanishes. Thus, it is expected that for adequately short excitation durations the corresponding time-dependent reliability function will converge to a non-zero value P_∞ , depicting the probability of never crossing the barrier over the specified time interval. Indeed, this is shown in Figure V.5 (left), where the reliability functions obtained via the Galerkin scheme for the various c values are plotted. This proportion increases as the excitation event shortens and is represented in Figure V.6. In this regard, the first-passage time pdf is given via Equation (V.3.36) as

$$p_f(t; H_0) = -\frac{\partial P(t; H_0)}{\partial t} + P_\infty \delta(t - \infty) \quad (\text{V.3.36})$$

where the term $-\partial P/\partial t$ is plotted in Figure V.5 (right), and the values P_∞ are shown in Figure V.6. This results in an area under the distribution (see Figure V.5 right) that is smaller than the unit over the range $[0, \infty[$.

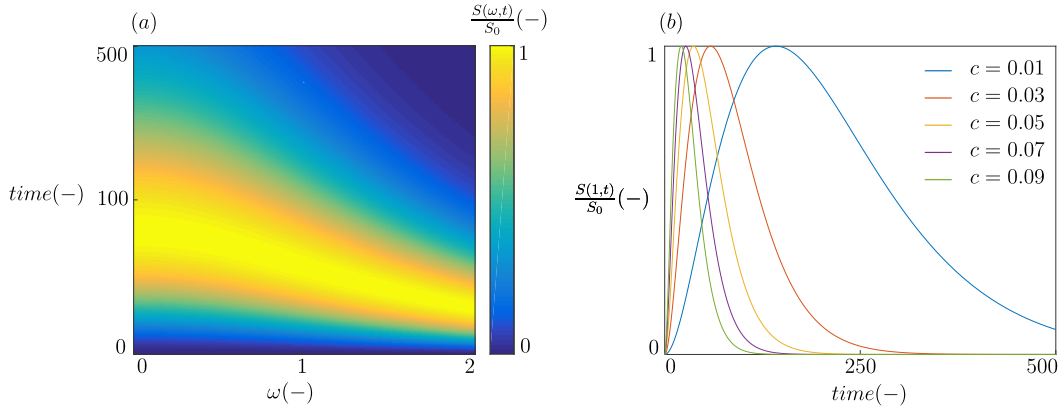


Figure V.3: Non-stationary stochastic seismic excitation with a non-separable evolutionary power spectrum. (a) Time and frequency evolution of $S(\omega, t)/S_0$ for $c = 0.01$ and (b) time evolution of $S(1, t)/S_0$ and influence of the parameter c on the excitation duration.

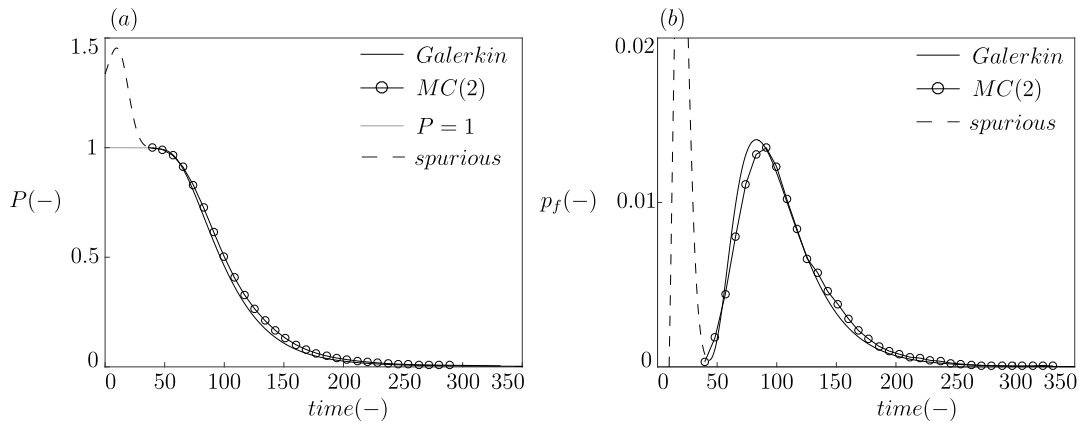


Figure V.4: (a) Reliability function and (b) first-passage time distribution of a Duffing oscillator under evolutionary excitation for $N = 5$ and $c = 0.01$ via the Galerkin scheme; comparisons with MCS data (10000 realizations).

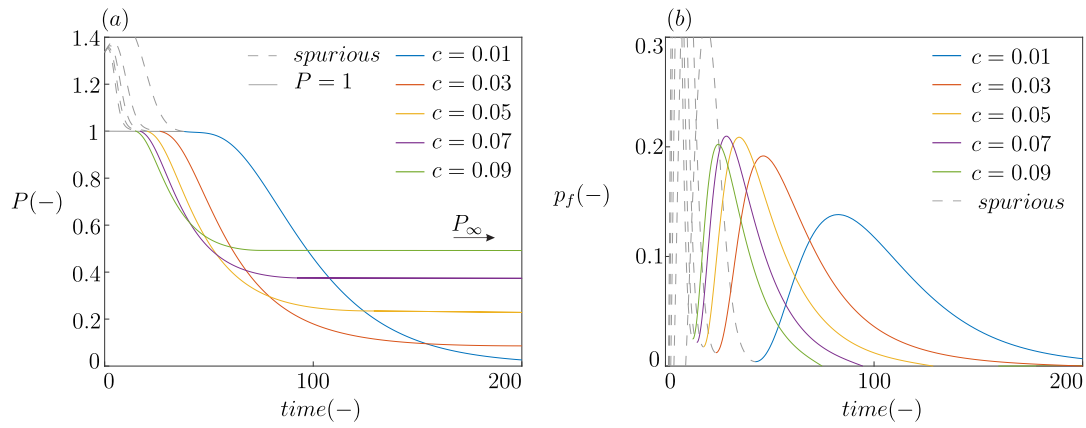


Figure V.5: (a) Reliability function and (b) first-passage time distribution of a Duffing oscillator under evolutionary excitation for $N = 5$ and various values of c .

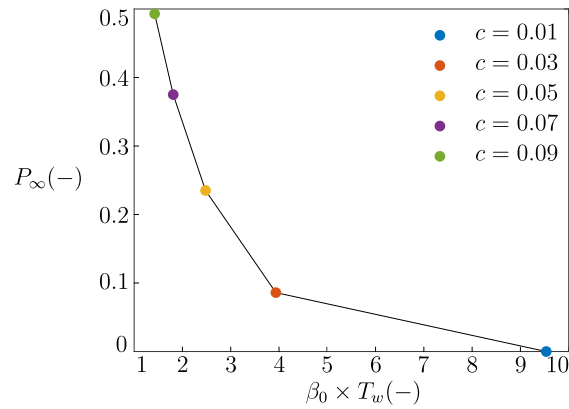


Figure V.6: Converged value of reliability function as a function of the effective time duration of the excitation T_w .

V.4 Stochastic averaging: Potential energy envelope definition

V.4.1 Backward-Kolmogorov equation and Galerkin scheme for a Duffing nonlinear oscillator

The potential energy envelope definition of Equation (V.2.10) is considered in this section for addressing the first-passage problem of nonlinear oscillators under evolutionary stochastic excitation. As noted in Section (V.2), although Equation (V.2.10) (in contrast to Equation (V.2.4)) involves no approximations for its definition, apparent difficulties arise in treating analytically a general class of nonlinearities; see also [127]. In this regard, the Duffing nonlinear oscillator, with $z(x, \dot{x}) = x^3$ and excited by a time-modulated white noise process with an evolutionary power spectrum $S_w(t) = S_0 F(t)$, is considered in the ensuing analysis. Following [127, 71], a stochastic averaging technique yields the drift and diffusion coefficients given by

$$\begin{cases} m(H) = \frac{S_w(t)}{2} - \beta H \Psi(H) \\ \sigma(H) = \sqrt{S_w(t) H \Psi(H)} \end{cases} \quad (\text{V.4.1})$$

governing the evolution in time of the response potential energy envelope. Related to the above stochastic equation is the Backward-Kolmogorov equation

$$\frac{\partial P}{\partial t} = \left(\frac{S_w(t)}{2} - \beta H \Psi(H) \right) \frac{\partial P}{\partial H} + \frac{S_w(t)}{2} H \Psi(H) \frac{\partial^2 P}{\partial H^2} \quad (\text{V.4.2})$$

with $\Psi(H)$ standing for the nonlinearity and given by

$$\Psi(H) = \frac{4r}{3m^2} \left| (1+r) - 2 \frac{E \left[\frac{r-1}{2r} \right]}{K \left[\frac{r-1}{2r} \right]} \right| ; \quad r^2 = m^2 + 1 ; \quad m = 4\varepsilon H, \quad (\text{V.4.3})$$

where $K[\cdot]$ and $E[\cdot]$ are the complete elliptic integrals of the first and second kind. Defining next $\tau = \beta t$ and $s^2(\tau) = \frac{S_w(\tau)}{2\beta}$, Equation (V.4.2) becomes

$$\frac{\partial P}{\partial \tau} = (s^2(\tau) - H \Psi(H)) \frac{\partial P}{\partial H} + s^2(\tau) H \Psi(H) \frac{\partial^2 P}{\partial H^2}. \quad (\text{V.4.4})$$

Note that for the linear case ($u(x) = \frac{x^2}{2}$) this formulation is identical to the one developed in Section V.3. This is anticipated as the energy definitions (V.2.10) and (V.2.4) coincide in this case and $\Psi = 1$.

Next, the Galerkin projection solution scheme as developed in Section V.3.2 is applied for solving numerically Equation (V.4.4). To this aim, Equation (V.3.14) takes the form

$$\begin{cases} \mathcal{L}_{\text{lin}} \{ \} &= (s^2(\tau) - H) \frac{\partial}{\partial H} + s^2(\tau) H \frac{\partial^2}{\partial H^2} \\ \mathcal{L}_{\text{nl}} \{ \} &= (1 - \Psi(H)) H \frac{\partial}{\partial H} + s^2(\tau) (\Psi(H) - 1) H \frac{\partial^2}{\partial H^2}. \end{cases} \quad (\text{V.4.5})$$

V.4.2 Numerical examples

Duffing oscillator under stationary white noise excitation

A Duffing nonlinear oscillator under Gaussian white noise excitation, i.e., $S_w(t) = S_0$, with parameters values $\beta = 0.02$, $S_0 = 0.1$ and $\varepsilon = 1$ is considered next. In Figure V.7 (left) typical time-histories of both the amplitude-based energy and the potential energy envelopes are plotted for comparison. Figure V.7 (right) shows the time-dependent reliability functions obtained via the Galerkin scheme for both energy envelope definitions and for various nonlinearity magnitude values, i.e., $\varepsilon = 0, 1, 2$ and 3 , while $H_0 = 0$ and $H_c = 1$. It is highlighted that the nonlinearity influences the reliability function in two distinct ways. First, an increase in nonlinearity leads to a stiffer oscillator (see governing Equation (V.2.1)); thus, requiring more time for the system to reach the same amplitude of the displacement x . Second, note that the two definitions of energy envelopes behave in different ways with variations of the value of ε . In the first formulation, the amplitude-based energy of Equation (V.2.4) decreases with increasing ε , so that for the same values of x and \dot{x} , the energy decreases. These two complementary effects, i.e., the oscillator stiffening and the energy decrease, lead to increasing first-passage times, or higher values of the reliability functions. This is observed in Figure V.7 (right - blue color). Also, the difference between the Galerkin approximation (continuous lines) and the Monte Carlo simulations (circles) increases with higher values of ε , or in other words, the accuracy of the Galerkin scheme deteriorates with increasing nonlinearity magnitude. In the second formulation, the potential energy of Equation (V.2.10) increases with ε , so that for the same values of x and \dot{x} , the energy increases. The effects of stiffening of the oscillator and of energy increase apparently balance each other, yielding reliability functions that appear practically insensitive to the nonlinearity degree. This can be readily seen in Figure V.7 (right - red color), where the reliability functions, determined both by Monte Carlo simulations and by the Galerkin scheme, practically coincide for all the chosen nonlinearity magnitude ε values. Thus, it is suggested that the choice of the potential energy over the amplitude-based energy is the preferable one related to a stochastic averaging treatment of the first-passage time problem, as the accuracy degree seems to be insensitive to the nonlinearity level. Note, however, the potential energy definition does not appear as versatile as the amplitude-based definition since it is restricted to time-modulated white noise excitations, and nonlinearities in terms of stiffness, and the available analytical solutions are practically limited to the

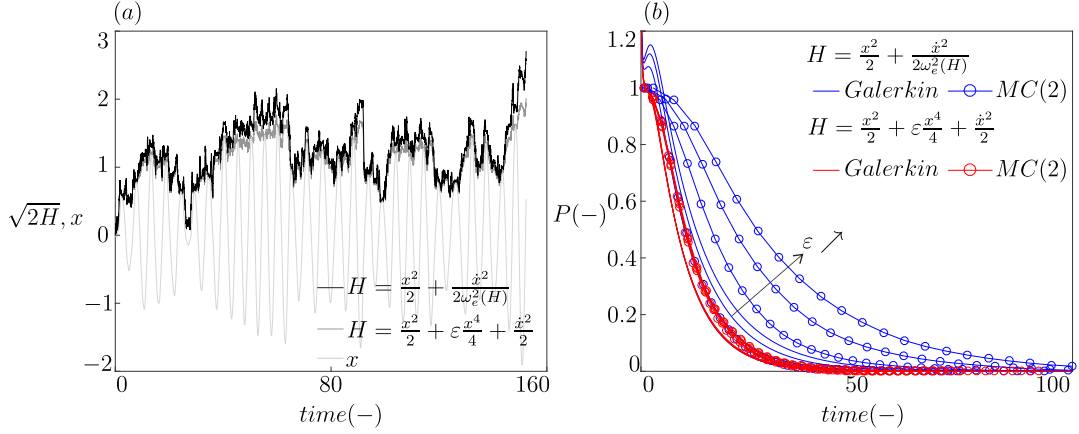


Figure V.7: (a) Time evolution of the potential energy envelope and (b) reliability function of the Duffing oscillator under white noise excitation for $N = 5$ and $\varepsilon = 0, 1, 2$ and 3 ; comparisons with MCS data (10000 realizations).

case of the Duffing oscillator.

Duffing oscillator under evolutionary excitation

For completeness, an additional example is included referring to a Duffing oscillator excited by a time-modulated white noise process compatible with the evolutionary spectrum $S_w(1, t)$ of Equation (V.3.35) with the parameter values given by $c = 0.01$, $H_0 = 0$, $H_c = 0.18$, $\beta = 0.02$, and $S_0 = 0.01$. Figure (V.8) shows the reliability function and corresponding first-passage time distribution obtained by the Galerkin scheme in conjunction with a potential energy envelope definition. Comparisons with Monte Carlo simulation data demonstrate a satisfactory degree of accuracy. The problem is solved, both numerically with the Galerkin scheme and through Monte Carlo simulations, for various nonlinearity magnitudes ($\varepsilon = 0.1, 1, 2$ and 3) and appears insensitive to ε , supporting further the argument made in Section V.4.2 about insensitivity of the potential energy treatment to the nonlinearity magnitude. Numerical results are illustrated for $\varepsilon = 0.1$.

V.5 Conclusion

The approximate semi-analytical technique developed in [71] for determining the response first-passage time distribution of a class of lightly damped nonlinear oscillators has been generalized herein to account for evolutionary stochastic excitation. Specifically, relying on a Markovian approximation of the response energy, and on a stochastic averaging treatment, has yielded a Backward-Kolmogorov equation governing the evolution in time of the oscillator reliability. Then, the

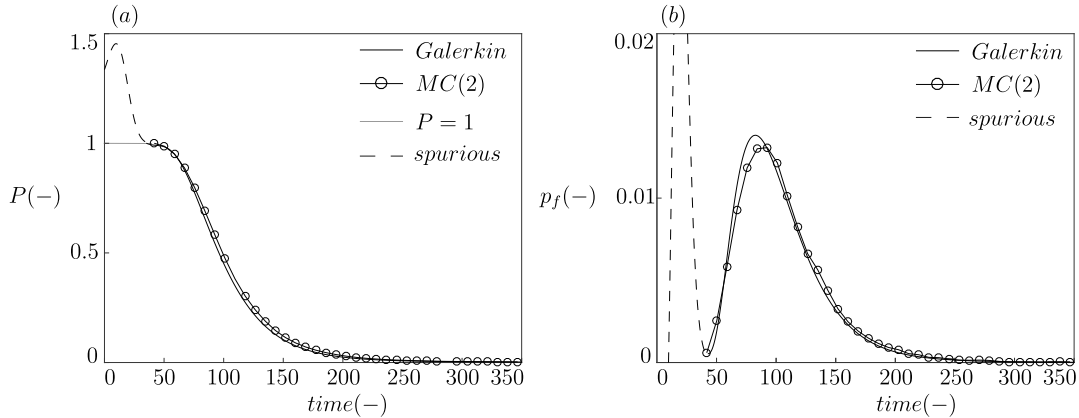


Figure V.8: (a) Reliability function and (b) first-passage time distribution of a Duffing oscillator under evolutionary excitation for $N = 5$ following the potential energy envelope definition.

Backward-Kolmogorov equation has been solved approximately by employing an appropriate orthogonal basis in conjunction with a Galerkin projection scheme. It has been shown that the technique can account for arbitrary evolutionary excitation forms, even of the non-separable type. The special case of an undamped oscillator, for which relevant analytical results exist in the literature, has also been included and studied in detail. The basis of eigenfunctions developed in this case is promising for future developments related to the analysis of lightly damped and nonlinear oscillators. In addition to an amplitude-based energy envelope definition, a potential energy based envelope has been considered as well. In comparison to the conventional amplitude-based energy formulation, the intermediate step of linearizing the nonlinear stiffness element is circumvented; thus, reducing the overall approximation degree of the technique. An additional significant advantage of the potential energy envelope formulation relates to the fact that its degree of accuracy appears rather insensitive to the magnitude of nonlinearity; however, it does not appear as versatile as the amplitude-based definition in handling a wide range of nonlinearity types.

Chapter VI

Conclusion

VI.1 Contributions of this work

VI.2 Limitations of the study and perspectives

VI.1 Contributions of this work

This thesis provides a frame for the use of the first-passage time as an analysis tool for engineering applications. It responds to the need for suitable methods to describe the transient response of systems that spend a lot of time in the transient regime, for example.

A closed form expression for the average first-passage time of an undamped oscillator under white noise excitations has been determined thanks to an asymptotic expansion of the Pontryagin equation. The obtained explicit solution (II.2.22) leads to the definition of the reduced energy H^* so that the first-passage time can now be written as a function of the reduced initial energy and energy increase H_0^* and ΔH^*

$$\mu_f \frac{S_u}{4} = \ln \left(1 + \frac{\Delta H^*}{H_0^* + 1} \right) \quad (\text{VI.1.1})$$

and represented in the universal map of Figure VI.1 (a). Three regimes are identified: the incubation regime (I) in the lower part of the diagram, where the curves of equal first-passage time are equally spaced, the additive regime (A) in the left part of the diagram where the horizontal asymptotes indicate an average first-passage time that is independent on the initial energy H_0^* , and the multiplicative regime (M) in the right part of the diagram, where the unitary slope indicates an average first-passage time depending on the ratio $\Delta H^*/H_0^*$. The representation of the solution as a function of the reduced energy, as well as the three regimes with their features are one important contribution of this work. They are re-used as a frame for the determination of the first-passage time of more complex problems.

Different types of complexities are successively added, such as the average first-passage time of a damped oscillator leading to the map represented in Figure VI.2 by analogy with the undamped case. The three regimes are also identified with a linear behavior in the incubation regime, an independency in H_0^* in the additive regime and oblique asymptotes of equal slope in the multiplicative regime. The slope is not equal to the unit as in the undamped case, but decreases with damping and can even become negative.

Another important contribution is the development of the mean square first-passage time, variance and coefficient of variation for the undamped oscillator. The coefficient of variation is of high interest for the confidence of the evaluation of the first-passage time, combined with its average value. The map of coefficient of variation is represented in Figure VI.1 (b), as a function of the reduced energy once more. Limit cases in the lower left and upper right corners –respectively corresponding to a forced-only and parametric-only oscillator– present a unitary slope of the curves of equal coefficient of variation, so that the curves can be approximated in these areas by diagonal straight lines.

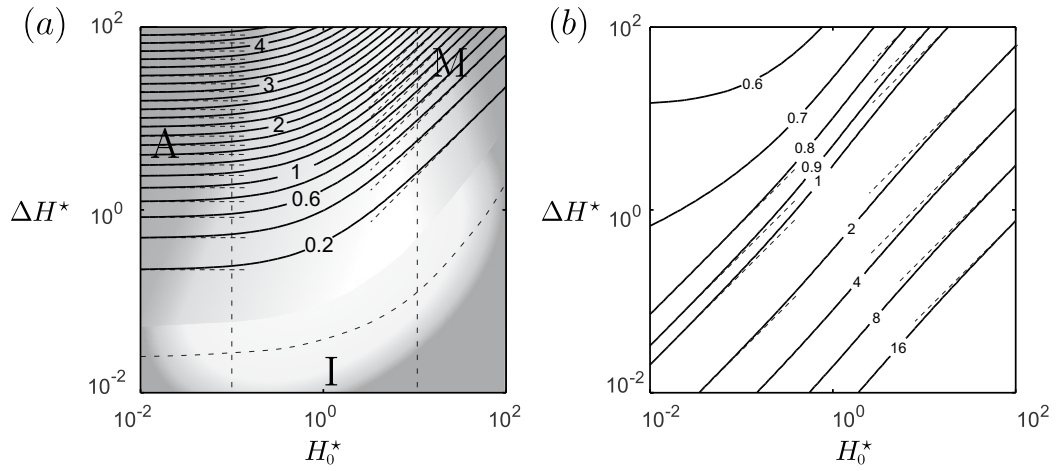


Figure VI.1: Undamped oscillator universal maps (a) Dimensionless first-passage time $\frac{\mu_f S_u}{4}$ and identification of the three regimes (b) Coefficient of variation cv_f and limit cases.

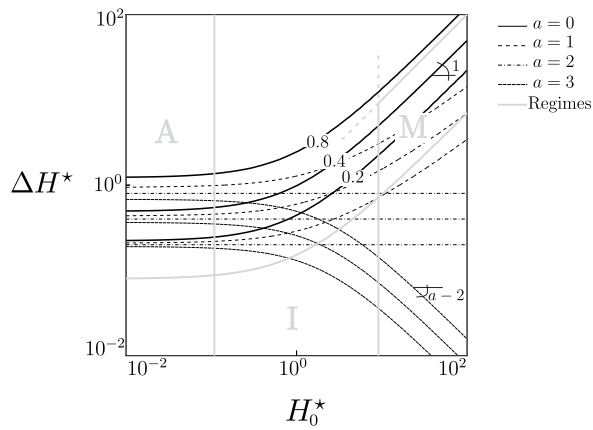


Figure VI.2: Dimensionless first-passage time $\frac{\mu_f S_u}{4}$ and identification of the three regimes for the damped oscillator (various values of $a = 8\xi/S_u$).

Next, the applicability of the first-passage time to real, and thus more complex, engineering applications is demonstrated through some examples, and assessed with a tower crane that is left free to rotate and placed into a turbulent wind velocity field. The free rotative motion of the crane is measured for a long period of time. Based on these time series, the first-passage map is reconstructed thanks to an efficient ad-hoc algorithm. An equivalent Mathieu oscillator is identified so that the tower crane presents the same first-passage maps. Hereby, the behavior of a complex system, with nonlinearities and time- and space-correlated excitations, can be caught and predicted with a simple model, for which analytical results are available.

Finally, a numerical method is developed in order to determine with accuracy the complete distribution of the first-passage time of more complex oscillators. A previously known Galerkin scheme is extended to include both nonlinearities and evolutionary excitations. This tool is seen as complementary to the analytical but approximate approach of the previous developments. It offers the possibility to compute numerical values for the entire distribution of the first-passage time with a good precision and short computation time, without the need for heavy Monte Carlo simulations. Two different definitions of the energy are implemented and it is seen that they have a different sensitivity to the amplitude of the nonlinearity. Finally, a specific scheme with the corresponding basis of eigenfunctions is determined for the undamped oscillator. The lower computational complexity of this new basis presents a particular interest and its use might be extended to slightly damped oscillators, such as those studied in the first part of this work.

The three aspects treated in this thesis –analytical developments, experimental demonstration and numerical method– are complementary and provide a consistent demonstration that the first-passage time might be –should be– used as an efficient tool in the analysis of transient regimes of engineering applications.

VI.2 Limitations of the study and perspectives

The theoretical solutions developed in Chapters II and III present an important level of complexity so that, first, one might expect not to be able to find an analytical solution for more complex systems, and second, the practical interest of a very complex analytical solution is limited for the understanding of the problem. However, the reduced energy, the map and the three regimes provide a frame that can be extended to more complex systems. Indeed, the representation of the results in the map, where the results might be obtained by experiments or numerical simulations, can lead first to a quantitative observation of the map in the three regimes, and then to the determination of an equivalent linear Mathieu oscillator, as it has been done in Chapter IV. In this context, a linear oscillator submitted to colored excitations could be reduced to an equivalent oscillator under white noise excitations. The influence of the spectrum of the colored exci-

tations on the equivalent intensities S_u and S_w would be a significant contribution to the model. Depending on the time scale of the excitation and the period of the oscillator, different behaviors might be observed. Similarly, a modulated white noise excitation might influence the first-passage time in a different way depending on the time scale of the modulating function. From the same point of view, a nonlinear oscillator might be reduced to an equivalent linear Mathieu oscillator. Based on what is known from classical methods of statistical linearization, one expects to find equivalent properties that depend on the level of energy. From a first-passage standpoint, the influence of the nonlinearity might be different in the different corners of the map for example, or for the different regimes. The integration of those levels of complexity into the model would be a great step for the application of the first-passage time of physical systems. An equivalent Mathieu oscillator could not only be identified but also be predicted, depending on the system characteristics.

A second important perspective is the extension of the approach for multi-degree-of-freedom systems. The corresponding challenges are the multimodal response of the system, possible coupling between the modes, and the broadband character of the excitation that will influence different modes. A first perspective is the extension of the model to a 2-degree-of-freedom system, to capture the main behaviour and refinements of the model. Experimental observation of such a system might be done through a double pendulum for example.

A final important perspective of the theoretical approach is the research for approximate solutions of the Backward-Kolmogorov equation (I.6.15) governing the complete distribution of the first-passage time. The topology of the generalized Pontryagin equation (I.6.23) shows recurrence in the definition of the statistical moments. This was confirmed with the analytical solutions of the average and mean square first-passage time, that could be expressed as a function of the reduced initial energy and energy increase, as well as the parameter a for the damping. The three regimes were also observed, with slight modifications, through the different observed cases. Since these typical features are observed for the first two, and expectedly higher, statistical moments, similarities should be observed in the complete distribution. This is an important avenue worth exploring for the resolution of the Backward-Kolmogorv equation.

Finally, a promising perspective is the use of the first-passage time as an identification or monitoring tool for systems properties. The construction of the map based on experimental data only requires time measurement of the system in place. There are two options. Based on the map, the system characteristics like damping, period and excitation intensities, might be identified. Otherwise, a drift in the first-passage map could be used to detect abnormalities or changes in the structural behavior. The advantage is that the method is not based on any model but data-driven only.

Only some examples of engineering applications could be studied in the frame-

work of this thesis. Many more could benefit the use of the first-passage approach for an alternative assessment. For example, it could contribute to questions such as the time it takes for a pollutant to reach a given concentration at a given place, the time required to reach a bridge deck flutter instability in turbulent flows, or even how long does it take for vortex-induced vibrations to develop or to oscillators to synchronize in stochastic conditions, etc. This work constitutes a first analysis with physical and engineering understanding of first-passage times. We hope this work will serve as a solid basis for these suggested investigation tracks.

Bibliography

- [1] H. Vanvinckenroye, V. Denoël, Monte Carlo Simulations of Autorotative Dynamics of a Simple Tower Crane Model, in: Proceedings of the 14th International Conference on Wind Engineering, Porto Alegre, Brazil, 2015.
- [2] Youtube.com, K. Mok, Crane Spinning out of Control (2008).
URL www.youtube.com/watch?v=6h5p9WC6Y7s
- [3] J. F. Eden, A. J. Butler, J. Patient, Wind tunnel tests on model crane structures, *Engineering Structures* 5 (4) (1983) 289–298.
- [4] Z. Sun, N. Hou, H. Xiang, Safety and serviceability assessment for high-rise tower crane to turbulent winds, *Frontiers of Architecture and Civil Engineering in China* 3 (1) (2009) 18–24.
- [5] D. Voisin, Etudes des effets du vent sur les grues à tour, "Wind effects on tower cranes", Ph.D. thesis, Ecole Polytechnique de l'Université de Nantes (2003).
- [6] D. Voisin, G. Grillaud, C. Sollic, A. Beley-Sayettat, J.-L. Berlaud, A. Minton, Wind tunnel test method to study out-of-service tower crane behaviour in storm winds, *Journal of Wind Engineering and Industrial Aerodynamics* 92 (7-8) (2004) 687–697.
- [7] J. Eden, A. Iny, A. Butler, Cranes in storm winds, *Engineering Structures* 3 (3) (1981) 175–180.
- [8] J. Náprstek, C. Fischer, Stability of limit cycles in autonomous nonlinear systems, *Meccanica* 49 (8) (2014) 1929–1943.
- [9] T. K. Caughey, F. Ma, The Steady-State Response of a Class of Dynamical Systems to Stochastic Excitation, *Journal of Applied Mechanics* 49 (3) (1982) 629.
- [10] T. Caughey, F. Ma, The exact steady-state solution of a class of non-linear stochastic systems, *International Journal of Non-Linear Mechanics* 17 (3) (1982) 137–142.

- [11] C. Soize, *The Fokker-Planck Equation for Stochastic Dynamical Systems and Its Explicit Steady State Solutions*, Vol. 17 of Series on Advances in Mathematics for Applied Sciences, World Scientific Publishing, 1994.
- [12] J. Náprstek, Combined analytical and numerical approaches in Dynamic Stability analyses of engineering systems, *Journal of Sound and Vibration* 338 (2015) 2–41.
- [13] Z. Schuss, *Theory and Applications of Stochastic Processes*, Vol. 170 of Applied Mathematical Sciences, Springer New York, New York, NY, 2010.
- [14] A. K. Chopra, *Dynamics of structures : theory and applications to earthquake engineering*, [Pearson Education India], 2007.
- [15] T. Stathopoulos, L. Lazure, P. Saathoff, A. Gupta, The effect of stack height, stack location and rooftop structures on air intake contamination : a laboratory and full-scale study, Tech. rep., IRSST, Quebec (2004).
- [16] W.-W. Li, R. N. Meroney, Gas dispersion near a cubical model building. Part I. Mean concentration measurements, *Journal of Wind Engineering and Industrial Aerodynamics* 12 (1) (1983) 15–33.
- [17] P. Gousseau, B. Blocken, T. Stathopoulos, G. van Heijst, CFD simulation of near-field pollutant dispersion on a high-resolution grid: A case study by LES and RANS for a building group in downtown Montreal, *Atmospheric Environment* 45 (2) (2011) 428–438.
- [18] R. N. Meroney, Ten questions concerning hybrid computational/physical model simulation of wind flow in the built environment, *Building and Environment* 96 (2016) 12–21.
- [19] T. Andrienne, V. de Ville de Goyet, Mitigation of the torsional flutter phenomenon of bridge deck section during a lifting phase, in: *8th International Colloquium on Bluff Body Aerodynamics and Applications*, Northeastern University, Boston, Massachusetts, USA, 2016.
- [20] C.-L. Lee, G. Stell, J. Wang, First-passage time distribution and non-Markovian diffusion dynamics of protein folding, *Journal of Chemical Physics* 118 (2) (2003) 959–968.
- [21] E. d. S. Caetano, Cable vibrations in cable-stayed bridges, in: *I. A. f. B. Engineering, Structural (Eds.)*, Structural Engineering Document, IABSE-AIPC-IVBH, 2007, p. 188.
- [22] A. Najdecka, S. Narayanan, M. Wiercigroch, Rotary motion of the parametric and planar pendulum under stochastic wave excitation, *International Journal of Non-Linear Mechanics* 71 (2015) 30–38.

- [23] D. Yurchenko, P. Alevras, Stochastic Dynamics of a Parametrically base Excited Rotating Pendulum, *Procedia IUTAM* 6 (2013) 160–168.
- [24] P. Alevras, D. Yurchenko, Stochastic rotational response of a parametric pendulum coupled with an SDOF system, *Probabilistic Engineering Mechanics* 37 (0) (2014) 124–131.
- [25] B. W. Horton, M. Wiercigroch, Effects of Heave Excitation on Rotations of a Pendulum for Wave Energy Extraction, in: E. Kreuzer (Ed.), *IUTAM Symposium on Fluid-Structure Interaction in Ocean Engineering*, Vol. 8 of *Iutam Bookseries*, Springer Netherlands, Dordrecht, 2008, pp. 117–128.
- [26] B. Horton, J. Sieber, J. Thompson, M. Wiercigroch, Dynamics of the nearly parametric pendulum, *International Journal of Non-Linear Mechanics* 46 (2) (2011) 436–442.
- [27] N. K. Moshchuk, R. A. Ibrahim, R. Z. Khasminskii, P. L. Chow, Ship capsizing in random sea waves and the mathematical pendulum, *IUTAM Symposium on Advances in Nonlinear Stochastic Mechanics* 47 (1995) 299–309.
- [28] A. W. Troesch, J. M. Falzarano, S. W. Shaw, Application of global methods for analyzing dynamical systems to ship rolling motion and capsizing, *International Journal of Bifurcation and Chaos* 02 (01) (1992) 101–115.
- [29] M. Gitterman, Spring pendulum: Parametric excitation vs an external force, *Physica A: Statistical Mechanics and its Applications* 389 (16) (2010) 3101–3108.
- [30] X. Xu, M. Wiercigroch, M. Cartmell, Rotating orbits of a parametrically-excited pendulum, *Chaos, Solitons & Fractals* 23 (5) (2005) 1537–1548.
- [31] J. Náprstek, C. Fischer, Auto-parametric semi-trivial and post-critical response of a spherical pendulum damper, *Computers & Structures* 87 (19–20) (2009) 1204–1215.
- [32] R. Král, S. Pospíšil, J. Náprstek, Wind tunnel experiments on unstable self-excited vibration of sectional girders, *Journal of Fluids and Structures* 44 (2014) 235–250.
- [33] A. H. Nayfeh, D. T. Mook, *Nonlinear oscillations*, Wiley-VCH, 2004.
- [34] H. K. Khalil, *Nonlinear systems*, Prentice Hall, 2002.
- [35] W. Garira, S. Bishop, Rotating solutions of the parametrically excited pendulum, *Journal of Sound and Vibration* 263 (1) (2003) 233–239.

- [36] S. Bishop, M. Clifford, Zones of chaotic behaviour in the parametrically excited pendulum, *Journal of Sound and Vibration* 189 (1) (1996) 142–147.
- [37] X. Xu, M. Wiercigroch, Approximate analytical solutions for oscillatory and rotational motion of a parametric pendulum, *Nonlinear Dynamics* 47 (1-3) (2006) 311–320.
- [38] F. J. Poulin, G. R. Flierl, The stochastic Mathieu's equation, *Proceedings of the Royal Society A: Mathematical, Physical and Engineering Sciences* 464 (2095) (2008) 1885–1904.
- [39] M. Gitterman, *The Chaotic Pendulum*, World Scientific Publishing, 2010.
- [40] D. Yurchenko, A. Naess, P. Alevras, Pendulum's rotational motion governed by a stochastic Mathieu equation, *Probabilistic Engineering Mechanics* 31 (2013) 12–18.
- [41] P. Alevras, D. Yurchenko, A. Naess, Numerical investigation of the parametric pendulum under filtered random phase excitation, in: V. P. M. Papadrakakis V. Plevris (eds.) (Ed.), *Compdyn 2013*, Kos Island, 2013.
- [42] K. Mallick, P. Marcq, On the stochastic pendulum with Ornstein-Uhlenbeck noise, *Journal of Physics A: Mathematical and General* 37 (17) (2004) 14.
- [43] V. D. Potapov, Stability of elastic systems under a stochastic parametric excitation, *Archive of Applied Mechanics* 78 (11) (2008) 883–894.
- [44] D. Bover, Moment equation methods for nonlinear stochastic systems, *Journal of Mathematical Analysis and Applications* 65 (2) (1978) 306–320.
- [45] I. I. Gihman, A. V. Skorohod, *Stochastic Differential Equations*, Springer, New York, NY, 1979, pp. 113–219.
- [46] S. Ariaratnam, P. Graefe, Linear Systems with Stochastic Coefficients, *International Journal of Control* 1 (3) (1965) 239–250.
- [47] J. Náprstek, Stochastic exponential and asymptotic stability of simple non-linear systems, *International Journal of Non-Linear Mechanics* 31 (5) (1996) 693–705.
- [48] P. E. Kloeden, E. Platen, *Numerical solution of stochastic differential equations*, Springer Verlag, Heidelberg, 1992.

- [49] T. Primožič, Estimating expected first passage times using multilevel Monte Carlo algorithm, MSc in Mathematical and Computational Finance University.
- [50] M. B. Giles, Multilevel Monte Carlo Path Simulation, *Operations Research* 56 (3) (2008) 607–617.
- [51] J. Drugowitsch, Fast and accurate Monte Carlo sampling of first-passage times from Wiener diffusion models, *Scientific Reports* 6 (2016) 20490.
- [52] T. Opperstrup, V. V. Bulatov, A. Donev, M. H. Kalos, G. H. Gilmer, B. Sadigh, First-passage kinetic Monte Carlo method, *Phys. Rev. E* 80 (6) (2009) 66701.
- [53] M. Grigoriu, *Stochastic calculus: applications in science and engineering*, Springer Verlag, Birkhäuser, 2002.
- [54] Y. K. Lin, G. Q. Cai, *Probabilistic Structural Dynamics: Advanced Theory and Applications*, McGraw-Hill, 2004.
- [55] V. V. Bolotin, *Random vibrations of elastic systems*, Vol. 8 of *Mechanics of Elastic Stability*, Springer Netherlands, Dordrecht, 1984.
- [56] R. L. Stratonovic, *Topics in the theory of random noise / 1. General theory of random processes.*, Gordon & Breach, 1963.
- [57] S. Crandall, First-crossing probabilities of the linear oscillator, *Journal of Sound and Vibration* 12 (3) (1970) 285–299.
- [58] J. Yang, M. Shinozuka, First-Passage Time Problem, *The Journal of the Acoustical Society of America* 47 (1B) (1970) 393–394.
- [59] B. Oksendal, *Stochastic Differential Equations: An Introduction with Applications-Fifth Edition*, 2003, pp. 1–5.
- [60] Y. K. Y.-K. Lin, *Probabilistic theory of structural dynamics*, R.E. Krieger Pub. Co, 1976.
- [61] M. C. Wang, G. E. Uhlenbeck, On the Theory of the Brownian Motion II, *Reviews of Modern Physics* 17 (2-3) (1945) 323–342.
- [62] A. Preumont, *Random Vibration and Spectral Analysis*, Kluwer Academic Publishers, 1994.
- [63] L. A. Bergman, J. C. Heinrich, On the moments of time to first passage of the linear oscillator, *Earthquake Engineering & Structural Dynamics* 9 (3) (1981) 197–204.

- [64] W. Li, L. Chen, N. Trisovic, A. Cvetkovic, J. Zhao, First passage of stochastic fractional derivative systems with power-form restoring force, *International Journal of Non-Linear Mechanics* 71 (2015) 83–88.
- [65] V. Palleschi, M. R. Torquati, Mean first-passage time for random-walk span: Comparison between theory and numerical experiment, *Physical Review A* 40 (8) (1989) 4685–4689.
- [66] E. H. Vanmarcke, On the Distribution of the First-Passage Time for Normal Stationary Random Processes, *Journal of Applied Mechanics* 42 (1) (1975) 215.
- [67] S. Englund, R. Rackwitz, C. Lange, Approximations of first-passage times for differentiable processes based on higher-order threshold crossings, *Probabilistic Engineering Mechanics* 10 (1) (1995) 53–60.
- [68] I. A. Kougiumtzoglou, P. D. Spanos, Nonstationary Stochastic Response Determination of Nonlinear Systems: A Wiener Path Integral Formalism, *Journal of Engineering Mechanics* 140 (9).
- [69] I. A. Kougiumtzoglou, P. D. Spanos, Stochastic response analysis of the softening Duffing oscillator and ship capsizing probability determination via a numerical path integral approach, *Probabilistic Engineering Mechanics* 35 (2014) 67–74.
- [70] D. Yurchenko, E. Mo, A. Naess, Reliability of Strongly Nonlinear Single Degree of Freedom Dynamic Systems by the Path Integration Method, *Journal of Applied Mechanics* 75 (6).
- [71] P. D. Spanos, I. A. Kougiumtzoglou, Galerkin scheme based determination of first-passage probability of nonlinear system response, *Structure and Infrastructure Engineering* 10 (10) (2014) 1285–1294.
- [72] P. D. Spanos, A. Di Matteo, Y. Cheng, A. Pirrotta, J. Li, Galerkin Scheme-Based Determination of Survival Probability of Oscillators With Fractional Derivative Elements, *Journal of Applied Mechanics* 83 (12).
- [73] T. Canor, L. Caracoglia, V. Denoël, Perturbation methods in evolutionary spectral analysis for linear dynamics and equivalent statistical linearization, *Probabilistic Engineering Mechanics* 46 (2016) 1–17.
- [74] T. Canor, V. Denoël, Transient Fokker-Planck-Kolmogorov equation solved with smoothed particle hydrodynamics method, *International Journal For Numerical Methods In Engineering* 94 (6) (2013) 535–553.

- [75] J. Náprstek, R. Král, Finite element method analysis of Fokker-Planck equation in stationary and evolutionary versions, *Advances in Engineering Software* 72 (2014) 28–38.
- [76] J. Náprstek, R. Král, Evolutionary analysis of Fokker-Planck equation using multi-dimensional Finite Element Method, *Procedia Engineering* 199 (2017) 735–740.
- [77] M. Deng, W. Zhu, Feedback minimization of first-passage failure of quasi integrable Hamiltonian systems, *Acta Mechanica Sinica* 23 (4) (2007) 437–444.
- [78] W. Q. Zhu, Y. J. Wu, First-Passage Time of Duffing Oscillator under Combined Harmonic and White-Noise Excitations, *Nonlinear Dynamics* 32 (3) (2003) 291–305.
- [79] R. Král, J. Náprstek, Theoretical background and implementation of the finite element method for multi-dimensional Fokker-Planck equation analysis, *Advances in Engineering Software* 113 (2017) 54–75.
- [80] M. Barbato, J. P. Conte, Structural Reliability Applications of Nonstationary Spectral Characteristics, *Journal of Engineering Mechanics* 137 (5) (2011) 371–382.
- [81] P. D. Spanos, I. A. Kougiumtzoglou, Survival Probability Determination of Nonlinear Oscillators Subject to Evolutionary Stochastic Excitation, *Journal of Applied Mechanics* 81 (5) (2014) 051016.
- [82] M. U. Thomas, Some Mean First-Passage Time Approximations for the Ornstein-Uhlenbeck Process, *Journal of Applied Probability* 12 (3) (1975) 600.
- [83] K. P. N. Murthy, K. W. Kehr, Mean first-passage time of random walks on a random lattice, *Physical Review A* 40 (4) (1989) 2082–2087.
- [84] B. Dybiec, E. Gudowska-Nowak, P. Hänggi, Lévy-Brownian motion on finite intervals: Mean first passage time analysis, *Physical Review E - Statistical, Nonlinear, and Soft Matter Physics* 73 (4).
- [85] V. Tejedor, O. Bénichou, R. Voituriez, Global mean first-passage times of random walks on complex networks, *Physical Review E - Statistical, Nonlinear, and Soft Matter Physics* 80 (6).
- [86] G. Chunbiao, X. Bohou, First-passage time of quasi-non-integrable-Hamiltonian system, *Acta Mechanica Sinica* 16 (2) (2000) 183–192.

- [87] H. Risken, *The Fokker-Planck Equation: Methods of Solution and Applications* (1996) 63–95.
- [88] N. Moshchuk, R. Ibrahim, R. Khasminskii, P. Chow, Asymptotic expansion of ship capsizing in random sea waves-I. First-order approximation, *International Journal of Non-Linear Mechanics* 30 (5) (1995) 727–740.
- [89] G.-Q. Cai, W.-Q. Zhu, *Elements of Stochastic Dynamics*, WORLD SCIENTIFIC, 2016.
- [90] W. Eugene, Z. Moshe, On the relation between ordinary and stochastic differential equations, *International Journal of Engineering Science* 3 (2) (1965) 213–229.
- [91] L. Pontryagin, A. Andronov, A. Vitt, Appendix: On the statistical treatment of dynamical systems, in: F. Moss, P. V. E. McClintock (Eds.), *Noise in Nonlinear Dynamical Systems Volume 1. Theory of Continuous Fokker-Planck Systems.*, Cambridge University Press, 1989, pp. 329–348.
- [92] C. W. To, *Nonlinear Random Vibration: Analytical Techniques and Applications*, CRC Press, 2000.
- [93] W.-Y. Liu, W.-Q. Zhu, W. Xu, Stochastic stability of quasi non-integrable Hamiltonian systems under parametric excitations of Gaussian and Poisson white noises, *Probabilistic Engineering Mechanics* 32 (2013) 39–47.
- [94] N. Moshchuk, R. Khasminskii, R. Ibrahim, P. Chow, Asymptotic expansion of ship capsizing in random sea waves-II. Second-order approximation, *International Journal of Non-Linear Mechanics* 30 (5) (1995) 741–757.
- [95] R. Khasminskii, On diffusion processes with small parameter, *Izv. USSR Acad. Sci. Math* 27 (1963) 1281–1300.
- [96] E. J. Hinch, *Perturbation Methods, Vol. 1*, Cambridge University Press, Cambridge, 1991.
- [97] J. J. Roberts, P. P. Spanos, Stochastic averaging: An approximate method of solving random vibration problems, *International Journal of Non-Linear Mechanics* 21 (2) (1986) 111–134.
- [98] S. Howison, *Practical Applied Mathematics: Modelling, Analysis, Approximation*, Cambridge Texts in Applied Mathematics, Cambridge University Press, 2005.
- [99] J. Kevorkian, J. D. Cole, *Multiple Scale and Singular Perturbation Methods*, Springer Verlag, Berlin, 1996.

- [100] V. Denoël, E. Detournay, Multiple Scales Solution for a Beam with a Small Bending Stiffness, *Journal of Engineering Mechanics* 136 (1) (2010) 69–77.
- [101] J. B. Roberts, S. N. Yousri, An Experimental Study of First-Passage Failure of a Randomly Excited Structure, *Journal of Applied Mechanics* 45 (4) (1978) 917.
- [102] P. Spano, A. D’Ottavi, A. Mecozzi, B. Daino, S. Piazzolla, Experimental measurements and theory of first passage time in pulse-modulated semiconductor lasers, *IEEE Journal of Quantum Electronics* 25 (6) (1989) 1440–1449.
- [103] E. Delhez, Experimental and numerical study of first passage time, Ph.D. thesis, University of Liege (2018).
URL <https://orbi.uliege.be/handle/2268/224212>
- [104] K. R. Gurley, M. A. Tognarelli, A. Kareem, Analysis and simulation tools for wind engineering, *Probabilistic Engineering Mechanics* 12 (1) (1997) 9–31.
- [105] A. Pinto da Costa, J. Martins, F. Branco, J.-L. Lilien, *Journal of engineering mechanics.*, Vol. 122, American Society of Civil Engineers, 1983.
- [106] E. Delhez, H. Vanvinckenroye, J.-C. Golinval, V. Denoël, Numerical and experimental study of first passage time of a steel strip subjected to forced and parametric excitations, in: *Proceedings of the 28th International Conference on Noise and Vibration Engineering*, 2018.
URL <https://orbi.uliege.be/handle/2268/218221>
- [107] S. Downing, D. Socie, Simple rainflow counting algorithms, *International Journal of Fatigue* 4 (1) (1982) 31–40.
- [108] H. Vanvinckenroye, Algorithm for the determination of the first passage time chart (2017).
URL <https://orbi.ulg.ac.be/handle/2268/215378>
- [109] C. Dyrbye, S. O. Hansen, *Wind loads on structures*, John Wiley & Sons, 1997.
- [110] Y. C. Y.-c. Fung, *An introduction to the theory of aeroelasticity*, Dover Publications, 2002.
- [111] Borri Claudio, Costa Carlotta, Quasi-steady analysis of a two-dimensional bridge deck element, *Computers & Structures* 82 (13-14) (2004) 993–1006.

- [112] Costa Carlotta, Borri Claudio, Application of indicial functions in bridge deck aeroelasticity, *Journal of Wind Engineering and Industrial Aerodynamics* 94 (11) (2006) 859–881.
- [113] A. G. Davenport, Buffeting of a suspension bridge by storm winds, *Journal of the Structural Division ASCE* (88) (1962) 233–264.
- [114] Roach P.E., The generation of nearly isotropic turbulence by means of grids, *International Journal of Heat and Fluid Flow* 8 (2) (1987) 82–92.
- [115] H. Vanvinckenroye, V. Denoël, Second-order moment of the first passage time of a quasi-Hamiltonian oscillator with stochastic parametric and forcing excitations, *Journal of Sound and Vibration* 427 (2018) 178–187.
- [116] H. Vanvinckenroye, V. Denoël, Average first-passage time of a quasi-Hamiltonian Mathieu oscillator with parametric and forcing excitations, *Journal of Sound and Vibration* 406 (2017) 328–345.
- [117] A. Kovaleva, An exact solution of the first-exit time problem for a class of structural systems, *Probabilistic Engineering Mechanics* 24 (3) (2009) 463–466.
- [118] A. Naess, O. Gaidai, Monte Carlo Methods for Estimating the Extreme Response of Dynamical Systems, *Journal of Engineering Mechanics* 134 (8) (2008) 628–636.
- [119] S.-K. Au, Y. Wang, *Engineering risk assessment and design with subset simulation*, 2014.
- [120] I. A. Kougioumtzoglou, Y. Zhang, M. Beer, Softening Duffing Oscillator Reliability Assessment Subject to Evolutionary Stochastic Excitation, *ASCE-ASME Journal of Risk and Uncertainty in Engineering Systems, Part A: Civil Engineering* 2 (2) (2016) C4015001.
- [121] J. J. Coleman, *Reliability of Aircraft Structures in Resisting Chance Failure* (1959).
- [122] I. A. Kougioumtzoglou, P. D. Spanos, Response and First-Passage Statistics of Nonlinear Oscillators via a Numerical Path Integral Approach, *Journal of Engineering Mechanics* 139 (9) (2013) 1207–1217.
- [123] Y. Zhang, I. A. Kougioumtzoglou, Nonlinear Oscillator Stochastic Response and Survival Probability Determination via the Wiener Path Integral, *ASCE-ASME J. Risk and Uncert. in Engrg. Sys., Part B: Mech. Engrg.* 1 (2) (2015) 021005.
- [124] J. Li, J. Chen, *Stochastic dynamics of structures*, Wiley, 2009.

- [125] I. Kougioumtzoglou, P. Spanos, An approximate approach for nonlinear system response determination under evolutionary stochastic excitation, *Current Science* 97 (2009) 1203–1211.
- [126] Y. Lin, G. Cai, Some thoughts on averaging techniques in stochastic dynamics, *Probabilistic Engineering Mechanics* 15 (1) (2000) 7–14.
- [127] J. Red-Horse, P. Spanos, A generalization to stochastic averaging in random vibration, *International Journal of Non-Linear Mechanics* 27 (1) (1992) 85–101.
- [128] W. Q. Zhu, *Stochastic Averaging Methods in Random Vibration*, *Applied Mechanics Reviews* 41 (5) (1988) 189.
- [129] C. Proppe, H. Pradlwarter, G. Schuëller, Equivalent linearization and Monte Carlo simulation in stochastic dynamics, *Probabilistic Engineering Mechanics* 18 (1) (2003) 1–15.
- [130] L. Socha, *Linearization Methods for Stochastic Dynamic Systems*, Springer Berlin Heidelberg, Berlin, Heidelberg, 2008, pp. 1–5.
- [131] J. B. Roberts, P. D. Spanos, *Random vibration and statistical linearization*, Dover Publications, 2003.
- [132] P.-T. D. Spanos, Numerics for Common First-Passage Problem, *Journal of the Engineering Mechanics Division* 108 (5) (1982) 864–882.
- [133] A. Di Matteo, P. Spanos, A. Pirrotta, Approximate survival probability determination of hysteretic systems with fractional derivative elements (In Press), *Probabilistic Engineering Mechanics*.
- [134] P. Spanos, G. P. Solomos, Barrier Crossing Due to Transient Excitation, *Journal of Engineering Mechanics* 110 (1) (1984) 20–36.
- [135] P. D. Spanos, J. R. Red-Horse, Nonstationary Solution in Nonlinear Random Vibration, *Journal of Engineering Mechanics* 114 (11) (1988) 1929–1943.
- [136] P. D. Spanos, I. A. Kougioumtzoglou, K. R. M. dos Santos, A. T. Beck, Stochastic Averaging of Nonlinear Oscillators: Hilbert Transform Perspective, *Journal of Engineering Mechanics* 144 (2) (2018) 04017173.
- [137] J. Liang, S. R. Chaudhuri, M. Shinozuka, Simulation of Nonstationary Stochastic Processes by Spectral Representation, *Journal of Engineering Mechanics* 133 (6) (2007) 616–627.

Appendix A

List of Publications

- [1] Delhez E., Vanvinckenroye H., Golinval J.-C. and Denoël V. (2018) ‘Numerical and experimental study of first passage time of a steel strip subjected to forced and parametric excitations’, in Proceedings of the 28th International Conference on Noise and Vibration Engineering.
- [2] Vanvinckenroye H., Kougioumtzoglou I.A. and Denoël V. (2018, Under review) ‘Reliability function determination of nonlinear oscillators under evolutionary stochastic excitation via a Galerkin projection technique’, *Nonlinear Dynamics*.
- [3] Vanvinckenroye H., Andrianne T. and Denoël V. (2018) ‘First passage time as an analysis tool in experimental wind engineering’, *Journal of Wind Engineering & Industrial Aerodynamics*. 177, pp. 366–375.
- [4] Vanvinckenroye H. and Denoël V. (2018) ‘Second-order moment of the first passage time of a quasi-Hamiltonian oscillator with stochastic parametric and forcing excitations’, *Journal of Sound and Vibration*. 427, pp. 178–187.
- [5] Vanvinckenroye H. and Denoël V. (2017) ‘Average first-passage time of a quasi-Hamiltonian Mathieu oscillator with parametric and forcing excitations’, *Journal of Sound and Vibration*, 406, pp. 328–345.
- [6] Demonceau J.-F., Vanvinckenroye H., D’Antimo M. et al. (2017) ‘Beam-to-column joints, column bases and joint components under impact loading’, in Proceeding of Eurosteel 2017 conference. Ernst & Sohn.
- [7] Vanvinckenroye H. and Denoël V. (2016) ‘Stochastic rotational stability of tower cranes under gusty winds’, in 6th International Confer-

- ence on Structural Engineering, Mechanics and Computation. Cape Town, South Africa.
- [8] Vanvinckenroye H., Andrianne T. and Denoël V. (2017) ‘Stochastic stability of a tower crane under gusty winds’, in Proceedings of the 7th European-African Conference on Wind Engineering.
- [9] Hoffmann N., Kuhlmann U., Vanvinckenroye H. et al. (2016) Verification of analytical and numerical tools - Deliverable D.5b - Robustimpact. RFCS.
- [10] Hoffmann N., Kuhlmann U., Vanvinckenroye H. et al. (2016) Detailed results of the experimental tests - Deliverable D.5a - Robustimpact. RFCS.
- [11] Vanvinckenroye H. and Denoël V. (2016) ‘Stochastic stability of a rotational oscillator under gusty winds’, in Proceedings of the XIV Conference of the Italian Association for Wind Engineering.
- [12] Vanvinckenroye H. and Denoël V. (2015) ‘Monte Carlo Simulations of Autorotative Dynamics of a Simple Tower Crane Model’, in Proceedings of the 14th International Conference on Wind Engineering. Porto Alegre, Brazil.
- [13] Vanvinckenroye H. (2014) Étude du mouvement autorotatif des grues sous vent turbulent. Université de Liège, Liège, Belgique.

Appendix B

Second order and boundary layer solutions

The Itô formulation (II.2.2) corresponding to the energy-phase variables k and θ reads

$$d\tilde{\mathbf{x}} = \tilde{\mathbf{a}}(\tilde{\mathbf{x}}, t)dt + \tilde{\mathbf{b}}(\tilde{\mathbf{x}}, t)d\mathbf{B}, \quad (\text{B.0.1})$$

where $\tilde{\mathbf{x}} = \begin{bmatrix} k \\ \theta \end{bmatrix}$, $\tilde{\mathbf{a}} = \begin{bmatrix} \gamma_1 \\ 1 + \gamma_2 \end{bmatrix}$ and $\tilde{\mathbf{b}} = \begin{bmatrix} -k \cos \theta \sin \theta & \frac{\cos \theta}{2} \\ \sin^2 \theta & -\frac{\sin \theta}{2k} \end{bmatrix}$ and where the Wong-Zakai correction terms are given, according to (I.6.7), by

$$\gamma = \sum_{j=1}^2 \sum_{k=1}^2 \frac{1}{2} J_{ij} \frac{\partial^2 \tilde{\mathbf{x}}}{\partial x_i \partial x_j} = \varepsilon (\nu_w - 4k\nu_{uw} \sin \theta + 4k^2\nu_u \sin^2 \theta) \begin{bmatrix} \frac{\sin^2 \theta}{\cos \theta} \\ \frac{8k \sin \theta}{4k^2} \end{bmatrix}. \quad (\text{B.0.2})$$

From this transformation follows that

$$\begin{aligned} \tilde{\mathbf{J}} &= \varepsilon \tilde{\mathbf{b}}(\tilde{\mathbf{x}}, t) \nu \tilde{\mathbf{b}}^T(\tilde{\mathbf{x}}, t) & (\text{B.0.3}) \\ &= \varepsilon \begin{bmatrix} k^2 \nu_u \cos^2 \theta \sin^2 \theta - k \nu_{uw} \cos^2 \theta \sin \theta + \nu_w \frac{\cos^2 \theta}{4} & -k \nu_u \cos \theta \sin^3 \theta + \nu_{uw} \cos \theta \sin^2 \theta - \nu_w \frac{\cos \theta \sin \theta}{4k} \\ -k \nu_u \cos \theta \sin^3 \theta + \nu_{uw} \cos \theta \sin^2 \theta - \nu_w \frac{\cos \theta \sin \theta}{4k} & \nu_u \sin^4 \theta - \nu_{uw} \frac{\sin^3 \theta}{k} + \nu_w \frac{\sin^2 \theta}{4k^2} \end{bmatrix}. \end{aligned}$$

The invariant operators \mathcal{L}_1 and \mathcal{L}_2 become

$$\mathcal{L}_1 \{ \cdot \} = \frac{\partial \cdot}{\partial \theta} \quad ; \quad \mathcal{L}_2 \{ \cdot \} = \gamma_1 \frac{\partial \cdot}{\partial k} + \gamma_2 \frac{\partial \cdot}{\partial \theta} + \frac{1}{2} \tilde{J}_{11} \frac{\partial^2 \cdot}{\partial k^2} + \frac{1}{2} \tilde{J}_{22} \frac{\partial^2 \cdot}{\partial \theta^2} + \tilde{J}_{12} \frac{\partial^2 \cdot}{\partial k \partial \theta}. \quad (\text{B.0.4})$$

Equation (II.2.12) provides the following expression :

$$\begin{aligned}
\mathcal{L}_1 \{u_1\} &= \frac{\partial u_1}{\partial \theta} = -1 - \mathcal{L}_2 \{u_0\} = \langle \mathcal{L}_2 \{u_0\} \rangle - \mathcal{L}_2 \{u_0\} \\
&= [k^2 \nu_u \cos 2\theta + 2\nu_{uw} \cos \theta] \frac{\partial u_0}{\partial H} \\
&\quad + k^2 (k^2 \nu_u \cos 4\theta + 8k\nu_{uw} \cos^2 \theta \sin \theta - \nu_w \cos 2\theta) \frac{\partial^2 u_0}{\partial H^2}
\end{aligned} \tag{B.0.5}$$

Integration of expression (B.0.5) with respect to θ provides a decomposition of u_1 into two components with the constant of integration $u_{12}(k)$:

$$u_1(k, \theta) = u_{11}(k, \theta) + u_{12}(k), \tag{B.0.6}$$

with

$$\begin{aligned}
u_{11}(k, \theta) &= \frac{k^2 \nu_u \sin 2\theta}{2(k^2 \nu_u + \nu_w)^2} [(\cos 2\theta - 2)k^2 \nu_u - 3\nu_w \\
&\quad + \frac{8 \sin^2 \frac{\theta}{2}}{3k \sin 2\theta} \nu_{uw} \left(2k^2 (2 \cos \theta + \cos 2\theta) - 6 \frac{\nu_w}{\nu_u} \right)] \\
&= \frac{k^2 S_u \sin 2\theta}{2(k^2 S_u + S_w)^2} [(\cos 2\theta - 2)k^2 S_u - 3S_w \\
&\quad + \frac{8 \sin^2 \frac{\theta}{2}}{3k \sin 2\theta} S_{uw} \left(2k^2 (2 \cos \theta + \cos 2\theta) - 6 \frac{S_w}{S_u} \right)].
\end{aligned} \tag{B.0.7}$$

Provided u_{12} is dependent on the Hamiltonian only, the averaging of Equation (II.2.13) over one period of the unperturbed motion gives:

$$\begin{aligned}
\langle \mathcal{L}_2 \{u_{12}\} \rangle &= \left(\frac{H}{2} \nu_u + \frac{1}{2} \nu_w \right) \frac{\partial u_{12}}{\partial H} + \left(\frac{H^2}{4} \nu_u + \frac{H}{2} \nu_w \right) \frac{\partial^2 u_{12}}{\partial H^2} \\
&= -\langle \mathcal{L}_2 \{u_{11}\} \rangle = -\frac{\nu_{uw} (k^6 \nu_u^3 - k^4 \nu_u^2 \nu_w + 27k^2 \nu_u \nu_w^2 - 3\nu_w^3)}{12k (k^2 \nu_u + \nu_w)^3}
\end{aligned} \tag{B.0.8}$$

The resolution of Equation (B.0.8) provides:

$$u_{12}(k) = \frac{4k\nu_{uw} (k^2 \nu_u + 3\nu_w)}{3 (k^2 \nu_u + \nu_w)^2} + \frac{C_1}{\nu_w} \ln \left(\frac{k^2}{k^2 \nu_u + \nu_w} \right) + C_2. \tag{B.0.9}$$

The first constant of integration C_1 is equal to zero in order to respect the solvability condition $|U(0)| < \infty$. The second constant C_2 will be determined together with the boundary layer solution in order to respect the boundary condition $U(H_c) = 0$.

The boundary layer solution is the solution of $\mathcal{L}^* \{G_n\} = 0$. The coordinate stretching is classical in the boundary layers problems [100]. Therefore, the boundary layer solution G_n is written as a function of the stretched coordinate $\zeta = \frac{H-H_c}{\sqrt{\varepsilon}}$

$$G_n(\zeta, \theta) = g_1(\zeta, \theta) + \sqrt{\varepsilon}g_2(\zeta, \theta) + \cdots + \varepsilon^{\frac{n-1}{2}}g_n(\zeta, \theta). \quad (\text{B.0.10})$$

Similarly, the operator \mathcal{L}^* is transformed via the asymptotic expansion of the functions \tilde{J}_{ij} and δ_i in the neighborhood of $H = H_c$:

$$\tilde{J}_{ij}(H, \theta) = \tilde{J}_{ij}(H_c, \theta) + \sqrt{\varepsilon}\zeta\tilde{J}_{ij}^{(1)}(H_c, \theta) + \dots \quad (\text{B.0.11})$$

$$\delta_i(H, \theta) = \delta_i(H_c, \theta) + \sqrt{\varepsilon}\zeta\delta_i^{(1)}(H_c, \theta) + \dots \quad (\text{B.0.12})$$

Taking into account $\frac{\partial \cdot}{\partial k} = \frac{4k}{\sqrt{\varepsilon}}\frac{\partial \cdot}{\partial \zeta}$ and $\frac{\partial^2 \cdot}{\partial k^2} = \frac{4}{\sqrt{\varepsilon}}\frac{\partial \cdot}{\partial \zeta} + \frac{16k^2}{\varepsilon}\frac{\partial^2 \cdot}{\partial \zeta^2}$, the Backward-Kolmogorov operator becomes

$$\begin{aligned} \mathcal{L}^* \{ \cdot \} &= \frac{\partial \cdot}{\partial \theta} + 4H_c\tilde{J}_{11}(H_c, \theta)\frac{\partial^2 \cdot}{\partial \zeta^2} \\ &+ \sqrt{\varepsilon} \left[2\sqrt{2H_c}\delta_1(H_c, \theta) + 2\tilde{J}_{11}(H_c, \theta)\frac{\partial \cdot}{\partial \zeta} \right] \\ &+ \dots \\ &= \Lambda_0 \{ \cdot \} + \sqrt{\varepsilon}\Lambda_1 \{ \cdot \} + \varepsilon\Lambda_2 \{ \cdot \} + \dots \end{aligned} \quad (\text{B.0.13})$$

so that the governing equation becomes

$$\begin{aligned} LG_n &= (\Lambda_0 + \sqrt{\varepsilon}\Lambda_1 + \varepsilon\Lambda_2 + \dots) \{g_1 + \sqrt{\varepsilon}g_2 + \cdots\} \\ &= \Lambda_0 \{g_1\} + \sqrt{\varepsilon}[\Lambda_0 \{g_2\} + \Lambda_1 \{g_2\}] + \cdots = 0 \end{aligned} \quad (\text{B.0.14})$$

Balancing again the similar powers of ε provides the expression of the functions $g_i(\zeta, \theta)$. In particular, the first order solution $g_1(\zeta, \theta)$ is the solution of the following diffusion equation

$$\Lambda_0 \{g_1\} = \frac{\partial g_1}{\partial \theta} + 4H_c\tilde{J}_{11}(H_c, \theta)\frac{\partial^2 g_1}{\partial \zeta^2} = 0 \quad (\text{B.0.15})$$

with the boundary conditions $g_1(0, \theta) = -u_1(H_c, \theta)$ and $g_1(\zeta, \theta) \rightarrow 0$ when $\zeta \rightarrow -\infty$. The solution of this equation is given by

$$\begin{aligned} g_1(\zeta, \theta) &= b_0 + \sum_{n=1}^{\infty} b_n e^{\sqrt{\frac{nc_1}{2}}\zeta} \cos \left(n\alpha(\theta) - \sqrt{\frac{nc_1}{2}}\zeta \right) \\ &+ \sum_{n=1}^{\infty} a_n e^{\sqrt{\frac{nc_1}{2}}\zeta} \sin \left(n\alpha(\theta) - \sqrt{\frac{nc_1}{2}}\zeta \right) \end{aligned} \quad (\text{B.0.16})$$

with

$$\begin{aligned}
c_1 &= 2\pi / \int_0^T 4H_c \tilde{J}_{11}(H_c, s) ds \\
\alpha(\theta) &= c_1 \int_0^\theta 4H_c \tilde{J}_{11}(H_c, s) ds \\
b_0 &= -\frac{1}{2\pi} \int_0^{2\pi} u_1(H_c, \theta(\alpha)) d\alpha \\
b_n &= -\frac{1}{\pi} \int_0^{2\pi} u_1(H_c, \theta(\alpha)) \cos(n\alpha) d\alpha \\
a_n &= -\frac{1}{\pi} \int_0^{2\pi} u_1(H_c, \theta(\alpha)) \sin(n\alpha) d\alpha
\end{aligned} \tag{B.0.17}$$

Because of the second boundary condition, it follows that

$$b_0 = -\frac{1}{2\pi} \int_0^{2\pi} u_1(H_c, \theta(\alpha)) d\alpha = 0. \tag{B.0.18}$$

Finally, averaging (B.0.6) with respect to variable α and accounting that $b_0 = 0$, the constant of integration C_2 is obtained:

$$\begin{aligned}
-\frac{1}{2\pi} \int_0^{2\pi} u_{12}(k_c) d\alpha &= \frac{4k_c \nu_{uw}}{3} \frac{(k_c^2 \nu_u + 3\nu_w)}{(k_c^2 \nu_u + \nu_w)^2} + C_2 \\
&= \frac{1}{2\pi} \int_0^{2\pi} u_{11}(k_c, \theta(\alpha)) d\alpha = \frac{4k \nu_{uw}}{3} \frac{(k^2 \nu_u + 3\nu_w)}{(k^2 \nu_u + \nu_w)^2}.
\end{aligned} \tag{B.0.19}$$

It finally follows from (B.0.19) that the second constant of equation is equal to zero.

Adapted to relation (B.0.17) and provided the expected parity of the boundary layer with respect to θ , only the even coefficients a_n are non-zero and can be obtained via numerical integration.

Appendix C

Damped oscillator

The mean first-passage time of the damped oscillator governed by Equation (III.2.1) is obtained following the same methodology. The Itô formulation of the differential equation now reads

$$d\mathbf{x} = \mathbf{a}(\mathbf{x}, t)dt + \mathbf{b}(\mathbf{x}, t)d\mathbf{B}, \quad (\text{C.0.1})$$

where $\mathbf{x} = \begin{bmatrix} q \\ p \end{bmatrix}$, $\mathbf{a} = \begin{bmatrix} p \\ -q - 2\varepsilon\nu_\xi p \end{bmatrix}$, $\mathbf{b} = \begin{bmatrix} 0 & 0 \\ -q & -1 \end{bmatrix}$.

The Backward-Kolmogorov operator \mathcal{L}^* is now defined by

$$\mathcal{L}^* \{ \cdot \} = \mathcal{L}_1 \{ \cdot \} + \varepsilon \mathcal{L}_2 \{ \cdot \}, \quad (\text{C.0.2})$$

where

$$\begin{cases} \mathcal{L}_1 \{ \cdot \} = p \frac{\partial \cdot}{\partial q} - q \frac{\partial \cdot}{\partial p} \\ \mathcal{L}_2 \{ \cdot \} = \frac{1}{2} (q^2 \nu_u + \nu_w - 2q\nu_{uw}) \frac{\partial^2 \cdot}{\partial p^2} - 2\nu_\xi p \frac{\partial \cdot}{\partial p} \end{cases} \quad (\text{C.0.3})$$

The first operator $\mathcal{L}_1 \{ \cdot \}$ is independent of the damping and Equation (II.2.11) still provides the information that the first order solution u_0 is a function of the Hamiltonian only.

Averaging Equation (II.2.12) assuming transformation (II.2.17) successively provides:

$$\begin{aligned} \langle \mathcal{L}_2 \{ u_0 \} \rangle &= -1, \\ \left[\frac{H}{2} \nu_u + \frac{1}{2} \nu_w - 2H\nu_\xi \right] \frac{du_0}{dH} + \left[\frac{H^2}{4} \nu_u + \frac{H}{2} \nu_w \right] \frac{d^2 u_0}{dH^2} &= -1, \\ \frac{1}{\varepsilon} \left(m(H) \frac{du_0}{dH} + \frac{\sigma^2(H)}{2} \frac{d^2 u_0}{dH^2} \right) &= -1 \end{aligned} \quad (\text{C.0.4})$$

with $m(H) = \frac{H}{2}S_u + \frac{1}{2}S_w - 2H\xi$ and $\sigma(H) = \sqrt{\frac{H^2S_u}{2} + HS_w}$. Similarly to the undamped oscillator, the governing equation is independent of the correlation between the parametric and forced excitations.

A first integration provides

$$\frac{du_0}{dH} = -e^{c(H)} \int_0^H \frac{2\varepsilon}{\sigma^2(y)} e^{c(y)} dy + C_1 e^{-c(H)}. \quad (\text{C.0.5})$$

with

$$c(H) = \int \frac{2m(H)}{\sigma^2(H)} dH = \ln(H) + \left(1 - \frac{8\nu_\xi}{\nu_u}\right) \ln(H\nu_u + 2\nu_w) \quad (\text{C.0.6})$$

The solvability condition implies $C_1 = 0$ so that

$$\frac{du_0}{dH} = \frac{2}{\nu_w} \frac{(1 + H^*)^{a-1} - 1}{H^*(1 - a)}, \quad (\text{C.0.7})$$

with $a = \frac{8\nu_\xi}{\nu_u} = \frac{8\xi}{S_u}$ and $H^* = \frac{H\nu_u}{2\nu_w} = \frac{HS_u}{2S_w}$. A second integration accounting for $u_0(H_c) = 0$ provides

$$u_0(H_0) = \int_0^H \frac{du_0}{dH} dH + C_2$$

$$= \frac{4}{\nu_u(1-a)} \left[\ln\left(1 + \frac{\Delta H^*}{H_0^*}\right) + \frac{(1 + H_0^* + \Delta H^*)^a - (1 + H_0^*)^a}{a} \right] \quad (\text{C.0.8})$$

$$- \int_{H_0^*}^{H_0^* + \Delta H^*} \frac{(1+t)^a}{t} dt \quad (\text{C.0.9})$$

so that the first-order mean first-passage time U_0 is finally given by

$$U_0(H_0) = \frac{4}{S_u(1-a)} \left[\ln\left(1 + \frac{\Delta H^*}{H_0^*}\right) + \frac{(1 + H_0^* + \Delta H^*)^a - (1 + H_0^*)^a}{a} \right] \quad (\text{C.0.10})$$

$$- \int_{H_0^*}^{H_0^* + \Delta H^*} \frac{(1+t)^a}{t} dt \quad (\text{C.0.11})$$

Appendix D

Pseudo-code for the computation of the average first-passage times map

Algorithm 1 Construction of the average first-passage times map

Require: $\tilde{H}(t)$

Ensure: FPT , the matrix of average first-passage times as a function of \tilde{H}_0 and $\Delta\tilde{H}$

Characterization of the time series

```

1: for t in time vector do
2:   if  $\tilde{H}(t)$  is a minimum or increases in t then
3:      $type(t) = 1$ 
4:      $nexttime(t) =$  time of the next maximum
5:   else
6:      $type(t) = 2$ 
7:      $nexttime(t) =$  time of the next higher value of  $\tilde{H}$ 
8:   end if
9: end for

```

Construction of the main envelope

```

10:  $t_0 = 0$ ;  $\tilde{H}_0 = \tilde{H}(t_0)$ 
11:  $t_{local} = t_0$ 
12: while  $t_{local} < t_{end}$  do
13:    $[\tilde{H}_{local}(t); nexttime] = \mathbf{local}(t_{local})$ 
14:    $\tilde{H}_c(t) = [\tilde{H}_c(t) \ \tilde{H}_{local}(t)]$ 
15:    $t_{local} = nexttime$ 
16: end while
17:  $\tilde{H}_c^{main}(t) = \tilde{H}_c(t)$ 
18:  $\Delta\tilde{H}(t) = \tilde{H}_c(t) - \tilde{H}_0$ 
19:  $FPT(\tilde{H}_0, \Delta\tilde{H}(t)) = FPT(\tilde{H}_0, \Delta\tilde{H}(t)) + t$ 
20:  $Counter(\tilde{H}_0, \Delta\tilde{H}(t)) = Counter(\tilde{H}_0, \Delta\tilde{H}(t)) + 1$ 

```

Construction of the partial envelopes

```

21: for  $t_0 = \Delta t : t_{end}$  do
22:    $t_{local} = t_0$ 
23:    $\tilde{H}_0 = \tilde{H}(t_0)$ 
24:   while  $t_{local} < t_{end}$  do
25:     if  $t_{local}$  not in main envelope then
26:        $[\tilde{H}_{local}(t); nexttime] = local(t_{local})$ 
27:        $\tilde{H}_c(t) = [\tilde{H}_c(t) \ \tilde{H}_{local}(t)]$ 
28:        $t_{local} = nexttime$ 
29:     else
30:        $\tilde{H}_c(t) = [\tilde{H}_c(t) \ \tilde{H}_c^{main}(t_{local} : t_{end})]$ 
31:        $t_{local} = t_{end}$ 
32:     end if
33:   end while
34:    $\Delta\tilde{H}(t) = \tilde{H}_c(t) - \tilde{H}_0$ 
35:    $t = t - t_0$ 
36:    $FPT(\tilde{H}_0, \Delta\tilde{H}(t)) = FPT(\tilde{H}_0, \Delta\tilde{H}(t)) +$ 
37:    $Counter(\tilde{H}_0, \Delta\tilde{H}(t)) = Counter(\tilde{H}_0, \Delta\tilde{H}(t)) + 1$ 
38: end for
39:  $FPT = FPT./Counter$ 

```

Nested function - local(t_{local})

```

Require:  $t_{local}$ 
Ensure:  $\tilde{H}_{local}(t), nexttime$ 
40: if  $type(t_{local}) = 1$  then
41:    $\tilde{H}_{local}(t) = \tilde{H}(t_{local} : nexttime(t_{local}))$ 
42: else
43:    $\tilde{H}_{local}(t) = \tilde{H}(nexttime(t_{local}))$ 
44: end if

```

Appendix E

Comparison between Galerkin scheme and analytical expressions for the average and mean square first-passage times

Considering a linear undamped oscillator under white noise excitation ($S_w(\omega, t) = S_0$), since $\dot{T}_i(t) = -\frac{\lambda_i S_0}{2} T_i(t)$ and $\dot{c}_i(t) = 0$, Equation (V.3.31) becomes

$$\begin{cases} \mathcal{E} \{t_f\} = \sum_i A_i \Phi_i(H) & \text{with } A_i = \frac{2}{\lambda_i S_0} \frac{F_{1,i}}{F_{2,i}} \\ \mathcal{E} \{t_f^2\} = \sum_i B_i \Phi_i(H) & \text{with } B_i = \frac{8}{\lambda_i^2 S_0^2} \frac{F_{1,i}}{F_{2,i}} \end{cases} \quad (\text{E.0.1})$$

Analytical results are derived for this particular case in Sections II.3 and III.1 for the mean and mean square first-passage times $\mathcal{E} \{t_f\}$ and $\mathcal{E} \{t_f^2\}$ based on a stochastic averaging treatment and are given by

$$\begin{cases} \mathcal{E} \{t_f\} = \frac{2}{S_0} \Delta H \\ \mathcal{E} \{t_f^2\} = \frac{4}{S_0^2} \Delta H \left(H + \frac{3}{2} \Delta H \right) \end{cases} \quad (\text{E.0.2})$$

where $\Delta H = H_c - H$ is the energy increase. The equalities to be proved are

$$\frac{2}{S_0} \sum_i \frac{1}{\lambda_i} \frac{F_{1,i}}{F_{2,i}} \Phi_i(H) = \frac{2}{S_0} \Delta H \quad (\text{E.0.3})$$

for the average first-passage time, and

$$\frac{8}{S_0^2} \sum_i \frac{1}{\lambda_i^2} \frac{F_{1,i}}{F_{2,i}} \Phi_i(H) = \frac{4}{S_0^2} \Delta H \left(H + \frac{3}{2} \Delta H \right) \quad (\text{E.0.4})$$

for the mean square first-passage time. The lemmas (E.0.3) and (E.0.4) are demonstrated by projection of the two sides of the equations on the basis of

eigenfunctions $\Phi_j(H)$. Equality is proved by showing that these projections are identical for all $\Phi_j(H)$.

First, Equation (E.0.3) is proved. Then, the second demonstration for Equation (E.0.4) results in a similar way from the first one.

Invoking the orthogonality property (V.3.8) with $f(H) = 1$, the projection of Equation (E.0.3) on the eigenfunctions $\Phi_j(H)$ yields

$$\frac{2}{S_0} \int_0^{H_c} \left(\sum_i \frac{1}{\lambda_i} \frac{F_{1,i}}{F_{2,i}} \Phi_i(H) \right) \Phi_j(H) dH = \frac{2F_{1,j}}{\lambda_j S_0} = \frac{2}{S_0} \int_0^{H_c} (H_c - H) \Phi_j(H) dH \quad (\text{E.0.5})$$

that can be rewritten, according to (V.3.11), as

$$\int_0^{H_c} \Phi_j(H) dH = \int_0^{H_c} \lambda_j \Phi_j(H) (H_c - H) dH. \quad (\text{E.0.6})$$

Considering the definition of the Bessel function (V.3.25), one finds

$$\begin{aligned} \int_0^{H_c} \Phi_j(H) dH &= - \int_0^{H_c} (H \Phi_j''(H) + \Phi_j'(H)) (H_c - H) dH \\ &= - \int_0^{H_c} (H \Phi_j'(H))' (H_c - H) dH. \end{aligned} \quad (\text{E.0.7})$$

Integration by parts of (E.0.7) leads to

$$\int_0^{H_c} \Phi_j(H) dH = [(H \Phi_j'(H)) (H_c - H)]_0^{H_c} - \int_0^{H_c} H \Phi_j'(H) dH. \quad (\text{E.0.8})$$

The first term in the right-hand side is trivially equal to zero while a second integration by parts of the second term leads to

$$\int_0^{H_c} \Phi_j(H) dH = - [H \Phi_j(H)]_0^{H_c} + \int_0^{H_c} \Phi_j(H) dH. \quad (\text{E.0.9})$$

Accounting for the boundary condition $\text{BesselJ}(0, \sqrt{4\lambda_i H_c}) = 0$ (V.3.9), equality is proved.

The demonstration is similarly done for the mean square first-passage time. After projection on the eigenfunction $\Phi_j(H)$, Equation (E.0.4) yields

$$\int_0^{H_c} \Phi_j(H) dH = \frac{1}{4} \int_0^{H_c} (H_c - H) (3H_c - H) \lambda_j^2 \Phi_j(H) dH. \quad (\text{E.0.10})$$

Considering the definition of the Bessel function (V.3.25), one finds

$$\int_0^{H_c} \Phi_j(H) dH = -\frac{1}{4} \int_0^{H_c} (H_c - H)(3H_c - H) \lambda_j (H\Phi_j''(H) + \Phi_j'(H)) dH. \quad (\text{E.0.11})$$

A first integration by parts leads to

$$\int_0^{H_c} \Phi_j(H) dH = -\frac{1}{2} \lambda_j [H\Phi_j'(H)(H_c - H)(3H_c - H)]_0^{H_c} - \frac{\lambda_j}{2} \int_0^{H_c} (H - 2H_c) H\Phi_j'(H) dH. \quad (\text{E.0.12})$$

The first term in the right-hand side is equal to zero, while the second one can be developed using (V.3.25) and a second integration by parts and yields

$$\int_0^{H_c} \Phi_j(H) dH = [H\Phi_j'(H)(H - H_c)]_0^{H_c} - \int_0^{H_c} H\Phi_j'(H) dH, \quad (\text{E.0.13})$$

which proves equality.